Graduate School Form 30
(Revised 08/14)

PURDUE UNIVERSITY
GRADUATE SCHOOL
Thesis/Dissertation Acceptance

This is to certify that the thesis/dissertation prepared

By Uttam Kumar Majumder

Entitled
Nearly Orthogonal, Doppler Tolerant Waveforms and Signal Processing for Multi-mode Radar Applications

For the degree of Doctor of Philosophy

Is approved by the final examining committee:

MARK R. BELL

DAVID J. LOVE

MICHAEL D. ZOLTOWSKI

MURALIDHAR RANGASWAMY

To the best of my knowledge and as understood by the student in the Thesis/Dissertation Agreement, Publication Delay, and Certification/Disclaimer (Graduate School Form 32), this thesis/dissertation adheres to the provisions of Purdue University's "Policy on Integrity in Research" and the use of copyrighted material.

Approved by Major Professor(s): MARK R. BELL

Approved by: M. R. Melloch 12/03/2014

Head of the Department Graduate Program Date

NEARLY ORTHOGONAL, DOPPLER TOLERANT WAVEFORMS AND SIGNAL PROCESSING FOR MULTI-MODE RADAR APPLICATIONS

A Dissertation

Submitted to the Faculty

of

Purdue University

by

Uttam Kumar Majumder

In Partial Fulfillment of the

Requirements for the Degree

of

Doctor of Philosophy

December 2014

Purdue University

West Lafayette, Indiana

To My Beloved Parents, Mr. Ranajit and Mrs. Mamata Majumder

and

My Aunt Mrs. Sharoj Deb.

ACKNOWLEDGMENTS

First of all, I would like to express my deepest gratitude to my dissertation research advisor Professor Mark R. Bell. Professor Bell's patience, guidance, and immense knowledge in radar systems kept my research focused and on schedule. I could not think of having a better research supervisor and mentor for my doctoral study.

I also wish to thank Professors Michael D. Zoltowski, David J. Love, and Dr. Muralidhar Rangaswamy for taking the time to serve in my committee. I am thankful to the Air Force Office of Scientific Research (AFOSR) for supporting my research through the prestigious STAR Team award. Dr. Rangaswamy helped me align my research proposal with this AFOSR research project, and this focused the project work towards my thesis research.

I really appreciate the staff of the Graduate Program Office of Electrical and Computer Engineering Department at Purdue University. Mr. Matt Golden provides exceptional services to ensure that students succeed at graduate school.

I am grateful to Air Force Research Laboratory Sensors Directorate to sponsor my study at Purdue University. I thank RYA Division Chief Mr. Christopher Ristich, RYA Technical Advisor Ms. Lori Westerkamp, RYAS Branch Chief Mr. Martin Justice, RYAP Branch Chief Dr. Jeffrey Sanders, and RYAA Branch Chief Ms. Christina Schutte who all supported my long-term full-time (LTFT) study with funding and encouragement. The AFOSR STAR team members Mr. Aaron Jones, Dr. Pawan Setlur, Dr. Sandeep Gogineni, and Dr. Tariq Qureshi provided helpful suggestions upon reading several sections of my thesis. I am grateful to them for this review. I would like to thank Dr. Mir Mahmood, Mr. Abdur Rahman, Mr. Wenwei Zhou, and Mr. I-Fan Lin for having fruitful technical discussions during our meetings at Radar Research Laboratory, Purdue University. I appreciate all the supports provided by AFRL/RY finance and training personnel Mr. Steven Sawtelle, Ms. Dena Duncan, Ms. Elizabeth Etter, Ms. Sheela Padmaja, and Ms. Edith Bunch. I also would like to acknowledge the support of my colleagues Ms. Patti Ryan, Dr. John Malas, Mr. Ed Zelnio, and Dr. Mike Minardi.

Finally, I thank my wife Moumita, our daughter Tanishee, my parents, and my brothers for their love and encouragement while I pursued this research.

TABLE OF CONTENTS

Page

LIST OF TABLES

LIST OF FIGURES

Figure Page

Figure Page

Figure Page

Figure Page

ABBREVIATIONS

RADAR	RAdio Detection And Ranging
MIMO	Multiple-Input Multiple-Output
SNR	Signal-to-Noise-Ratio
OW	Orthogonal Waveform
LFM	Linear Frequency Modulation
DSSS	Direct Sequence Spread Spectrum
SSCL	Spread Spectrum Coded LFM
AAF	Auto-Ambiguity Function
CAF	Cross-Ambiguity Function
PN	Pseudonoise
CDMA	Code Division Multiple Access
RCS	Radar Cross Section
ATR	Automatic Target Recognition
SAR	Synthetic Aperture Radar
GMTI	Ground Moving Target Indication

ABSTRACT

Majumder, Uttam Kumar Ph.D., Purdue University, December 2014. Nearly Orthogonal, Doppler Tolerant Waveforms and Signal Processing for Multi-Mode Radar Applications. Major Professor: Mark R. Bell.

In this research, we investigate the design and analysis of nearly orthogonal, Doppler tolerant waveforms for diversity waveform radar applications. We then present a signal processing framework for joint synthetic aperture radar (SAR) and ground moving target indication (GMTI) processing that is built upon our proposed waveforms.

To design nearly orthogonal and Doppler tolerant waveforms, we applied direct sequence spread spectrum (DSSS) coding techniques to linear frequency modulated (LFM) signals. The resulting transmitted waveforms are rendered orthogonal using a unique spread spectrum code. At the receiver, the echo signal can be decoded using its spreading code. In this manner, transmit orthogonal waveforms can be matched filtered only with the intended receive signals.

Our proposed waveforms enable efficient SAR and GMTI processing concurrently without reconfiguring a radar system. Usually, SAR processing requires transmit waveforms with a low pulse repetition frequency (PRF) rate to reduce range ambiguity; on the other hand, GMTI processing requires a high PRF rate to avoid Doppler aliasing and ambiguity. These competing requirements can be tackled by employing some waveforms (with low PRF) for the SAR mission and other waveforms (with high PRF) for the GMTI mission. Since the proposed waveforms allow separation of individual waveforms at the receiver, we can accomplish both SAR and GMTI processing jointly.

1. INTRODUCTION

Transmit waveforms play a key role on exploitation capabilities of a radar system. Hence, transmit waveforms are often designed based on operational goal of a radar platform. Certain characteristics of waveforms are desired for radars operating in different environments (e.g. air, ground, or sea). For example, radar operating from air to ground where heavy clutter and different classes (high RCS and low RCS) of moving objects can be found, transmit waveforms should be designed to provide high resolution and Doppler tolerance capabilities. The pivot of this research is designing almost orthogonal, Doppler tolerant waveforms to satisfy multiple functionalities of a radar system.

1.1 Research Problem

The design of nearly orthogonal (on both transmit and receive), Doppler tolerant waveforms for waveform-agile radar (e.g. MIMO radar) applications is a longstanding research problem. Hence, the focus of this research is to design and analyze a pragmatic solution to this crucial problem. We then apply these waveforms to develop a novel signal processing scheme that solves another critical technical problem in radar signal processing namely "joint SAR and GMTI processing". Unlike current techniques, our approach does not require switching radar operations either in SAR or GMTI processing mode to accomplish both tasks simultaneously.

1.2 Merits of Diverse, Nearly Orthogonal, and Doppler Tolerant Waveforms

Our proposed waveforms allow a novel way of designing radar systems that would solve more complex problems and extend current capabilities. Traditional radar systems and the associated signal processing techniques have evolved for decades without significant changes to the design pertaining to transmit and receive waveforms. The exploitation techniques surrounding traditional radar concepts also have been explored at a level that it has reached a limit. In addition, traditional waveform design is ill-suited to the challenges imposed difficult targets and a rapidly shrinking electromagnetic spectrum for the users.

A key beneficiary of our proposed waveforms is multi-mode/multi-function radar systems. Traditional multi-mode radar systems require setting operational parameters (such as bandwidth, pulse repetition frequency) based on the mission (e.g. imaging of a scene or target detection). This requires a radar operator's involvement to switch from one mode to the other mode of operation. Designing a radar system that can operate in multiple sensor modes without operator's engagement reduces complexity of radar operations but achieves multiple exploitation capabilities. We found that diverse, nearly orthogonal, and Doppler tolerant waveforms allows this agility to operate a radar system in multi-mode.

A second beneficiary of our proposed waveforms is multiple-input multiple-output (MIMO) radar. As an emerging technology, MIMO radar promises to deliver "the next generation" radar systems for the users. MIMO radar could be vital for addressing the onerous challenges imposed by complex and contested environments [1] [2]. First of all, in MIMO radar settings, we can transmit diverse, nearly orthogonal waveforms. In our proposed transmit waveform design, the received waveforms can be nearly orthogonal; hence we can separate them to be matched filter correctly. This allows processing diversity gains for MIMO radar over the conventional radar systems.

Lastly, a third beneficiary of our proposed waveform is fully adaptive radar (FAR) system. Adaptive radar can be viewed as transmitting diverse waveforms (and from various angles) and adaptively processing the received waveforms to optimize functionalities (such as detection, classification, and tracking). Researchers also used the terms *Cognitive Radar*, *Knowledge-Aided Radar* to describe fully adaptive radar [3]. Because of various diversities (chirp, code, frequency) encapsulated in our waveforms, we can adapt our waveforms based on environments. For example, just changing the code lengths, we can gain different bandwidths as needed to achieve better resolution for target identification.

1.3 Significance of This Dissertation Research

This dissertation research investigated and developed theoretical solutions to two problems in radar signal processing that is original and not available in published literature (by other researchers).

1.3.1 Design and Analysis of Radar Waveforms to Satisfy Nearly Orthogonal on Transmit and Receive

In most MIMO radar settings, it is assumed that waveforms should remain orthogonal on both transmit and receive. However, because of unknown Doppler shifts and delays caused by targets' motion, receive waveforms don't stay nearly orthogonal. Researchers are aware of this critical issue. To solve this problem, engineers developed methods to optimize receive waveforms instead of designing waveforms that should remain nearly orthogonal on both transmit and receive. *This research provides a solution to designing waveforms that should remain approximately orthogonal on both transmit and receive.*

1.3.2 Joint SAR and GMTI Processing

Concurrent processing of SAR and GMTI is an important research problem. Principal technical issue on this problem is that waveforms characteristics for SAR and GMTI are different. Hence, a radar has to be operated in different modes to accomplish SAR or GMTI mission. We investigated this problem and developed an innovative solution to accomplish SAR and GMTI simultaneously. *Our diverse waveforms allow transmitting some waveforms (with high bandwidth) for SAR mission and the others (with low bandwidth) for GMTI mission in different PRF rates. Nearly orthogonal feature of these waveforms permit us separating them at the receiver and develop SAR and GMTI products in parallel.*

1.4 Outline of This Dissertation

The rest of the dissertation is organized as follows. In Chapter 2, we introduce the ideas and tools used to describe radar target resolution, radar waveform Doppler tolerance, and the orthogonality—or approximate orthogonality—of radar waveforms. We also present closed-form expressions for simple rectangular pulse and linear frequency modulated (LFM) pulse waveforms. Understanding of the LFM waveform's ambiguity function is essential as this provides us insight into our proposed waveform design. In Chapter 3, we present our approach to designing waveforms that are nearly orthogonal on both transmit and receive. We use cross-ambiguity function as a measure to determine orthogonality of two waveforms. We observe that orthogonality of two waveforms improve by increasing code length. However, increased code length also expands bandwidth of the waveforms. In Chapter 4, we present the high resolution imaging capability of our proposed waveforms and discuss a bandwidth reduction scheme by using biorthogonal codes. In Chapter 5, we present a review of SAR signal processing and modeling moving target signatures. A basic understanding of SAR signals is necessary to apply our proposed waveforms for the joint SAR and GMTI processing. In Chapter 6, we present how our proposed diverse, orthogonal waveforms can be used to process SAR and GMTI concurrently. We develop a signal processing framework that enables SAR imaging, fast moving target detection, and slow moving target detection simultaneously without switching the radar modes either for SAR or GMTI. Finally, in Chapters 7 and 8, we summarize our research and provide future research directions.

2. THE RADAR AMBIGUITY FUNCTION, ORTHOGONAL WAVEFORM, TARGET RESOLUTION, AND DOPPLER TOLERANCE

2.1 Introduction

In this chapter, we will introduce the ideas and tools used to describe radar target resolution, radar waveform Doppler tolerance, and the orthogonality—or approximate orthogonality—of radar waveforms. As we will see, all of these ideas can be described in terms of ambiguity functions and cross-ambiguity functions in the case of a matched-filter radar.

First, we will consider the response of a matched-filter radar when the matched filter is mismatched to the radar return in both delay and Doppler shift. We derive the expression for the mismatched target response and show that the mismatched response can be written in terms of the ambiguity function of the transmitted waveform. We then formally define the ambiguity function and cross ambiguity function and then review the properties of the ambiguity function that are relevant to our work.

Next, we use the cross-ambiguity function to characterize the orthogonality or approximate orthogonality of two radar waveforms. The idea of using orthogonal—or nearly orthogonal—waveforms is the basis for Code-Division Multiple Access (CDMA) communications systems, and is widely employed in more general spread-spectrum communications systems as well. Here, the key idea is that the separation of orthogonal waveforms is straightforward. However, even in CDMA communication systems, the waveforms used are often not truly orthogonal, but are actually only approximately orthogonal. However, even approximate orthogonality allows for approximate separation of the nearly orthogonal waveforms by treating them as if they are orthogonal. While there may be some residual interference between the waveforms in this case (e.g., the well known "near-far" problem in CDMA communication systems), these nearly orthogonal waveforms are still useful for code-division multiple access. However, in radar systems that attempt to use code-division multiple access separation of waveforms, the situation is complicated by the fact that radar signal returns can have arbitrary delays and Doppler frequency shifts in them. Two orthogonal waveforms $s_1(t)$ and $s_2(t)$ which are arbitrarily delayed to produce $s_1(t-\tau_1)$ and $s_2(t-\tau_2)$ are in general no longer orthogonal, just as two orthogonal waveforms $s_1(t)$ and $s_2(t)$ which have arbitrary frequency shifts applied to them to produce $s_1(t)e^{i2\pi\nu_1 t}$ and $s_2(t)e^{i2\pi\nu_2 t}$ are in general no longer orthogonal. It goes without saying then that if $s_1(t)$ and $s_2(t)$ are two orthogonal waveforms, the two arbitrarily delayed and frequency shifted waveforms

$$r_1(t) = s_1(t-\tau_1)e^{i2\pi\nu_1 t}$$

and

$$r_2(t) = s_2(t-\tau_2)e^{i2\pi\nu_2 t}$$

will not in general be orthogonal. That is, even though

$$\int_{-\infty}^{\infty} s_1(t)s_2^*(t)\,dt = 0,$$

in general, for arbitrary real numbers τ_1, τ_2, ν_1 and ν_2,

$$\int_{-\infty}^{\infty} s_1(t-\tau_1)e^{i2\pi\nu_1 t}s_2^*(t-\tau_2)e^{-i2\pi\nu_2 t}\,dt \neq 0. \tag{2.1}$$

However, because in general a matched-filter radar matched to a waveform $s_1(t-\tau_1)e^{i2\pi\nu_1 t}$ will process returns of the form $s_2(t-\tau_2)e^{i2\pi\nu_2 t}$ if waveform $s_2(t)$ is transmitted as well, we will want the integral of Eq. (2.1) to be small even if it is not zero. This will lead us to introduce the notion of *ϵ-orthogonal* waveforms, which will be defined in terms of the cross-ambiguity function of $s_1(t)$ and $s_2(t)$.

Next, we will review the role of the ambiguity function in characterizing the resolution of two radar targets close together in delay and Doppler. In particular, we will how the problem of target resolution follows from the delay-Doppler mismatch response of the matched filter. This leads to the well-known imaging interpretation of the target resolution problem in matched-filter radar, where the ambiguity function effectively plays the role of an imaging point-spread function.

Finally, we investigate the notion of *Doppler tolerance* of a waveform in a matched-filter radar. Doppler tolerance measures the ability of a waveform to be used to detect a radar target even if there is a significant Doppler shift in the radar return that has not been accounted for in the matched-filter of the radar receiver. The canonical example of a Doppler tolerant waveform is a linear FM chirp, which can be detected using the matched filter matched to the stationary transmitted waveform even when there is a significant Doppler shift that is not accounted for in the receiver matched filter. This is in stark contrast to many phase coded waveforms, which cannot be reliably detected without taking the Doppler shift into account explicitly through the use of a Doppler filter bank or Doppler compensation. The Doppler tolerance of a particular waveform with matched filter processing can be determined from its ambiguity function, and we introduce a new analytical measure of Doppler tolerance based on the ambiguity function.

2.2 Mismatched Filters and The Ambiguity Function

Consider, a radar system transmits a signal $s(t)$. Then the received signal resulting from the radar return from a moving point target can be written as

$$r(t) = (ae^{i\phi})s(t - \tau_0)e^{i2\pi\nu_0 t}, \tag{2.2}$$

where τ_0 is the time delay due to propagation of the signal to and from the target, ν_0 is Doppler shift resulting from the radial motion of the target with respect to the radar, and $ae^{i\phi}$ is the complex amplitude of a point scatterer.

Assume we process with a matched filter (MF) matched to $s(t)$ with delay τ and Doppler shift ν. If we sample at $t = T$, then,

$$\begin{aligned} h_{\tau\nu}(t) &= \mathrm{MF}_T \left\{ s(t-\tau)e^{i2\pi\nu t} \right\} \\ &= s^*(T - t - \tau)e^{-i2\pi\nu_0(t-T)}. \end{aligned} \tag{2.3}$$

The output of the matched filter sampled at time $t = T$ can be written as

$$\begin{aligned}
\mathrm{O}_T(\tau,\nu) &= r(t) * h_{\tau\nu}(t)|_{t=T} \\
&= ae^{i\phi}\int_{-\infty}^{\infty} s(t-\tau_0)\, e^{i2\pi\nu_0 t} s^*(t-\tau) e^{-i2\pi\nu t} dt \\
&= ae^{i\phi}\int_{-\infty}^{\infty} s(t-\tau_0)\, s^*(t-\tau)\, e^{-i2\pi(\nu-\nu_0)t} dt.
\end{aligned} \tag{2.4}$$

Making the substitution $p = t - \tau_0$, from which it follows that $t = p + \tau_0$ and $dt = dp$. Then we can write,

$$\begin{aligned}
\mathrm{O}_T(\tau,\nu) = ae^{i\phi}&\int_{-\infty}^{\infty} s(p)\, s^*(p-(\tau-\tau_0))\, e^{-i2\pi(\nu-\nu_0)(p+\tau_0)} dp \\
&= ae^{i\phi} e^{-i2\pi(\nu-\nu_0)\tau_0}\int_{-\infty}^{\infty} s(p)\, s^*(p-(\tau-\tau_0))\, e^{-i2\pi(\nu-\nu_0)p} dp \\
&= ae^{i\phi} e^{-i2\pi(\nu-\nu_0)\tau_0}\beta_s(\tau-\tau_0, \nu-\nu_0)
\end{aligned} \tag{2.5}$$

where

$$\beta_s(\tau,\nu) := \int_{-\infty}^{\infty} s(t)s^*(t-\tau)e^{-i2\pi\nu t}dt = \chi_s(\tau,-\nu)$$

and

$$\chi_s(\tau,\nu) := \int_{-\infty}^{\infty} s(t)s^*(t-\tau)e^{+i2\pi\nu t}dt$$

If we think of a radar as an imaging system, then the ambiguity function is the point spread function or impulse response of the system. To obtain high-resolution images, we will require sharp ambiguity functions. Then one might say that the radar target resolution research primarily becomes a radar waveform design problem.

2.3 Radar Ambiguity Function Terminology, Properties, and Examples

As we saw in the previous section, the ambiguity function $\chi_s(\tau,\nu)$ specifies the mismatched delay-Doppler response of a matched filter radar. As we will see in section 6, the ambiguity function also specifies the target resolution characteristics of a radar waveform processed using matched filter processing. We will also see the role of the ambiguity function in determining a waveform's Doppler tolerance when processed using a matched filter in section 9. For these reasons, we now define various terms associated with ambiguity function and several important properties.

Definition 2.3.1 (Asymmetric ambiguity function) *The asymmetric ambiguity function of a finite energy signal $s(t)$ is defined as*

$$\chi(\tau, \nu) = \int_{-\infty}^{\infty} s(t)s^*(t-\tau)e^{+i2\pi\nu t}dt. \tag{2.6}$$

Definition 2.3.2 (Symmetric ambiguity function) *The symmetric ambiguity function of a finite energy signal $s(t)$ is defined as*

$$\Gamma(\tau, \nu) = \int_{-\infty}^{\infty} s(t+\tau/2)s^*(t-\tau/2)e^{-i2\pi\nu t}dt. \tag{2.7}$$

By a simple change of variable, it can be shown that

$$\Gamma(\tau, \upsilon) = e^{i\pi\upsilon\tau}\chi(\tau, -\upsilon)$$
$$\chi(\tau, \upsilon) = e^{i\pi\upsilon\tau}\Gamma(\tau, -\upsilon)$$

Historically, asymmetric form of the ambiguity function was first introduced by P.M. Woodward [4]. We will use either of the two forms of the ambiguity function to demonstrate the basic properties or applications since moving between them is easy.

Definition 2.3.3 (Ambiguity surface) *The modulus of either of the above ambiguity functions is called the ambiguity surface.*

When we wish to see the behavior of the ambiguity function, we will typically plot the ambiguity surface $|\chi(\tau, \nu)|$.

The ambiguity function defined in (2.6) is one of the several forms found in literature. It depicts matched filter output response when input signal is mismatched due to time delay (τ) and Doppler shift (ν). Various authors' definition of ambiguity function differs with regard to using sign to represent Doppler shifts (ν) for a closing vs. opening target and time delays (τ).

The following is the definition of ambiguity function presented by P.M. Woodward:

$$\chi(\tau, \upsilon) = \int_{-\infty}^{\infty} s(t)s^*(t+\tau)e^{-i2\pi\upsilon t}dt \tag{2.8}$$

From Woodward's book, it is understood that he meant a positive Doppler frequency shift occurs when a target moves away from the radar. In other words, ν is positive for negative Doppler frequency shift. Sinsky and Wang proposed "Standardization of the Definition of the Radar Ambiguity Function" for the radar researchers. Following is their definition

$$|\chi(\tau,\upsilon)|^2 = \left|\int_{-\infty}^{\infty} s(t)s^*(t+\tau)e^{i2\pi\upsilon t}dt\right|^2 \tag{2.9}$$

In this definition, a target located at a distant point from the reference position of the radar (i.e. $\tau = 0$) corresponds to a positive τ and a target moving toward the radar corresponds to a positive ν. In this thesis, we will primarily use the form of the ambiguity function given in Eq. (2.6).

2.3.1 Important Properties of Radar Ambiguity Function

Property 1: The largest value of the ambiguity function, $|\chi(\tau,\upsilon)|$ **always occurs at the origin i.e.** $|\chi(\tau,\upsilon)| \leq |\chi(0,0)| = E_s$. Here E_s represents energy in the signal $s(t)$.

Proof: By applying Schwarz inequality, we can write

$$\begin{aligned}
|\chi(\tau,\upsilon)|^2 &= \left|\int_{-\infty}^{\infty} s(t)s^*(t-\tau)e^{i2\pi\upsilon t}dt\right|^2 \\
&\leq \int_{-\infty}^{\infty} |s(t)|^2\, dt \int_{-\infty}^{\infty} \left|s^*(t-\tau)e^{i2\pi\upsilon t}\right|^2 dt \\
&\leq \int_{-\infty}^{\infty} |s(t)|^2\, dt \int_{-\infty}^{\infty} |s^*(t-\tau)|^2\, dt = E_s \cdot E_s = E_s^2
\end{aligned} \tag{2.10}$$

The conditions for equality occurs when $(\tau,\upsilon) = (0,0)$

Property 2: The total volume under the square of ambiguity surface is constant.

Proof: We can express the symmetric ambiguity function $\Gamma(\tau,\upsilon)$in the following two ways:

$$\Gamma(\tau,\upsilon) = e^{i\pi\tau\upsilon}\int_{-\infty}^{\infty} s(t)s^*(t-\tau)e^{-i2\pi\upsilon t}dt$$

$$\Gamma(\tau,\upsilon) = e^{i\pi\tau\upsilon}\int_{-\infty}^{\infty} S(f+\upsilon)s^*(f)e^{-i2\pi f\tau}df$$

Thus

$$\int_{-\infty}^{\infty}\int_{-\infty}^{\infty}|\Gamma(\tau,\upsilon)|^2\,d\tau d\upsilon = \int_{-\infty}^{\infty}\int_{-\infty}^{\infty}\Gamma(\tau,\upsilon)\Gamma^*(\tau,\upsilon)d\tau d\upsilon$$
$$= \int_{-\infty}^{\infty}\int_{-\infty}^{\infty}\int_{-\infty}^{\infty}\int_{-\infty}^{\infty} s(t)s^*(t-\tau)S^*(f)S(f+\upsilon)dtdfd\tau d\upsilon \tag{2.11}$$

By interchanging the order of integration and identifying terms with Fourier transforms

$$\begin{aligned}\int_{-\infty}^{\infty} s^*(t-\tau)e^{-i2\pi f\tau}d\tau = S^*(f)e^{-i2\pi ft}\\ \int_{-\infty}^{\infty} S(f+\upsilon)S^*(f)e^{i2\pi\upsilon t}d\upsilon = s^*(t)e^{i2\pi ft}\end{aligned} \tag{2.12}$$

We get

$$\int_{-\infty}^{\infty}\int_{-\infty}^{\infty}|\Gamma(\tau,\upsilon)|^2\,d\tau d\upsilon = \int_{-\infty}^{\infty}\int_{-\infty}^{\infty}|s(t)|^2\,|S(f)|^2\,dtdf = E_s\cdot E_s = E_s^2$$

This property is known as ***the law of the conservation of ambiguity***; also called ***radar uncertainty principle***. This property state that the volume under the surface must equal the square of the maximum. Any attempt to increase the peak height of the ambiguity function will result in increase in volume under the ambiguity surface.

Furthermore, according to *The Uncertainty Principle of Fourier Transform*, for a given signal $s(t)$, the product of the mean square duration $(\Delta t)^2$and the mean-square bandwidth $(\Delta f)^2$ must satisfy

$$\left(\Delta t^2\right)\left(\Delta f^2\right) \geq 1/\left(4\pi\right)^2. \tag{2.13}$$

This imposes the restriction that simultaneous discrimination in delay and Doppler is unachievable.

Property 3: Ambiguity function is symmetric with respect to the origin i.e. $|\chi(-\tau,-\upsilon)| = |\chi(\tau,\upsilon)|$**.**

Proof: This proof is trivial. By setting $\tau = -\tau$ and $\upsilon = -\upsilon$ in equation (2.6) we can easily find that $\chi(-\tau,-\upsilon)=e^{i2\pi\upsilon\tau}\chi^*(\tau,\upsilon)$. Therefore, $|\chi(-\tau,-\upsilon)|=|\chi(\tau,\upsilon)|$.

Property 4: Consider a linear frequency modulated (LFM) signal $\psi(t)=e^{i\pi\alpha t^2}$. Then LFM to a signal $s(t)$ shears the ambiguity function of the signal i.e. $|\Gamma_\psi(\tau,\upsilon)|=|\Gamma(\tau,\upsilon+\alpha\tau)|$. This is also known as quadratic phase-shift property.

Proof: The asymmetric ambiguity function for $\psi(t)$ can be written as

$$\begin{aligned}\chi_\psi(\tau,\upsilon)&=\int_{-\infty}^{\infty}\psi(t)\psi^*(t-\tau)e^{i2\pi\upsilon t}dt\\&=\int_{-\infty}^{\infty}s(t)e^{i\pi\alpha t^2}s^*(t-\tau)e^{-i\pi\alpha(t-\tau)^2}e^{i2\pi\upsilon t}dt\\&=e^{-i\pi\alpha t^2}\int_{-\infty}^{\infty}s(t)s^*(t-\tau)e^{i2\pi(\upsilon+\alpha\tau)t}dt\\&=e^{-i\pi\alpha t^2}\chi(\tau,\upsilon+\alpha\tau).\end{aligned}\tag{2.14}$$

By taking absolute value, we get

$$|\chi_\psi(\tau,\upsilon)|=|\chi(\tau,\upsilon+\alpha\tau|\,.$$

2.3.2 Ambiguity Function of Two Common Waveforms

In this section we will illustrate ambiguity function of two common waveforms. Simple derivation of these two waveforms' ambiguity functions will guide us developing orthogonal waveforms to be presented next chapter.

2.3.3 Rectangular Pulse and Ambiguity Function

Consider a rectangular pulse,

$$s(t)=\mathrm{rect}\left(\frac{t}{T}\right),\tag{2.15}$$

where

$$\mathrm{rect}(x)=\begin{cases}1,\ 0\le x\le 1,\\ 0,\mathrm{otherwise.}\end{cases}$$

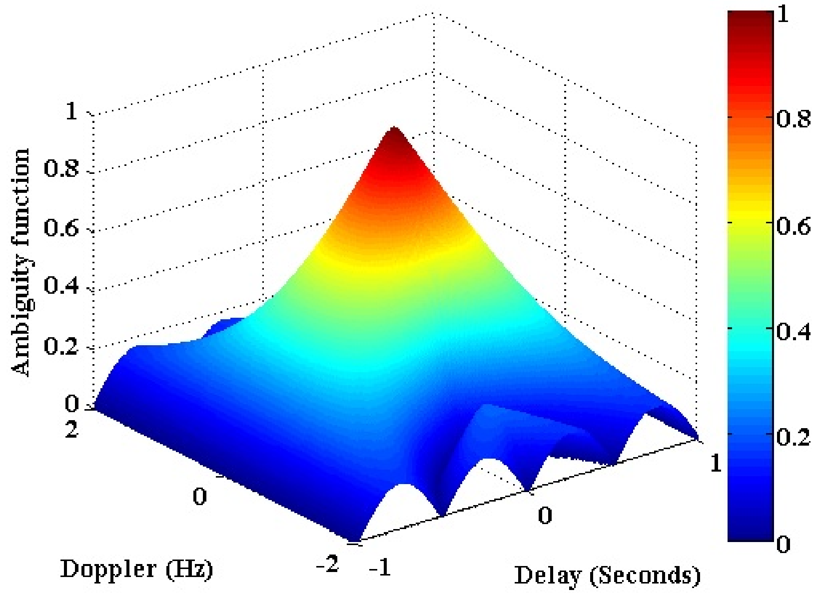

Fig. 2.1. 3D ambiguity function of a rectangular pulse

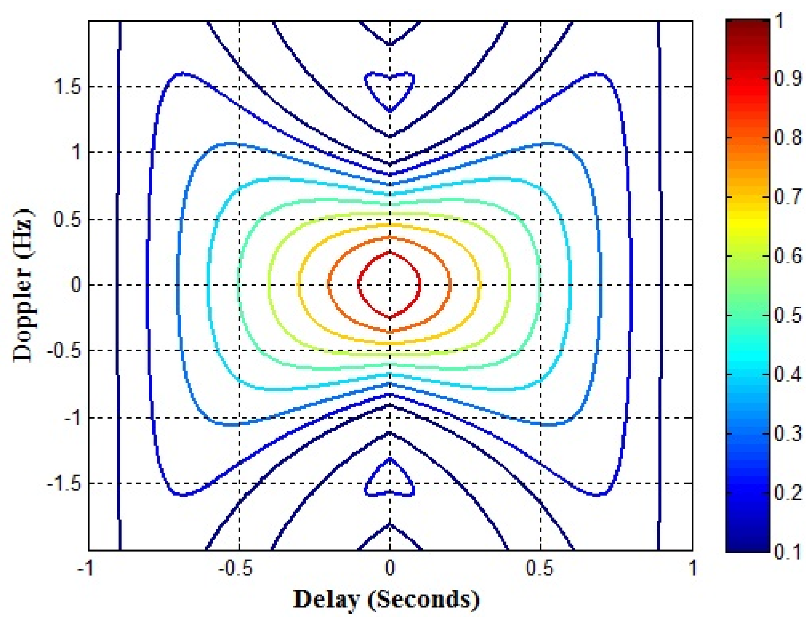

Fig. 2.2. Contour plot of the ambiguity function of a rectangular pulse

Then the ambiguity function (or auto-ambiguity function) of the above signal is defined as

$$\chi_s(\tau,\nu) = \int_{-\infty}^{\infty} s(t)s^*(t-\tau)\exp(i2\pi\nu t)dt. \tag{2.16}$$

Substituting the rectangular pulse for $s(t)$, we get

$$\chi_s(\tau,\nu) = \int_{-\infty}^{\infty} \mathrm{rect}(\frac{t}{T})\mathrm{rect}(\frac{t-\tau}{T})\exp(i2\pi\nu t)dt. \tag{2.17}$$

To evaluate the integral presented in (2.17), we need to consider following cases:

Case 1: For $\tau < 0$, limits of integration are $0 \le t \le T + t$, and $|\tau| = -\tau$. Therefore, we can write

$$\begin{aligned} \chi_s(\tau,\nu) &= \int_0^{T+\tau} e^{i2\pi\nu t}dt \\ &= \frac{e^{i2\pi\nu(T+\tau)}-1}{i2\pi\nu}. \end{aligned}$$

After simplifying the above expression, we get

$$\chi_s(\tau,\nu) = (T-|\tau|)\mathrm{sinc}(\nu(T-|\tau|))\cdot e^{i\pi\nu(T+\tau)}.$$

Case 2: For $\tau \ge 0$, limits of integration are $\tau \le t \le T$, and $|\tau| = \tau$

Therefore, we can write

$$\begin{aligned} \chi_s(\tau,\nu) &= \int_\tau^{T} e^{i2\pi\nu t}dt \\ &= \frac{e^{i2\pi\nu T}-e^{i2\pi\nu\tau}}{i2\pi\nu}. \end{aligned}$$

After simplifying the above expression, we get

$$\chi_s(\tau,\nu) = (T-|\tau|)\mathrm{sinc}(\nu(T-|\tau|))\cdot e^{i\pi\nu(T+\tau)}.$$

By combining above two cases, we can finally write the closed-form expression for ambiguity function of a simple rectangular pulse as follows:

$$\chi_s(\tau,\upsilon) = \begin{cases} (T-|\tau|)\mathrm{sinc}(\upsilon(T-|\tau|)).e^{i\pi\upsilon(T+\tau)}, -T \le \tau \le T \\ 0, \text{ elsewhere.} \end{cases} \tag{2.18}$$

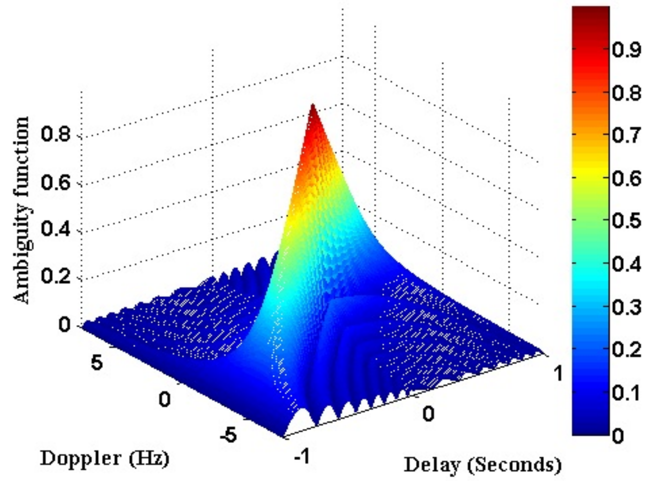

Fig. 2.3. Linear frequency modulated (LFM) waveform ambiguity function in 3D. The waveform has been created with an up-chirp signal.

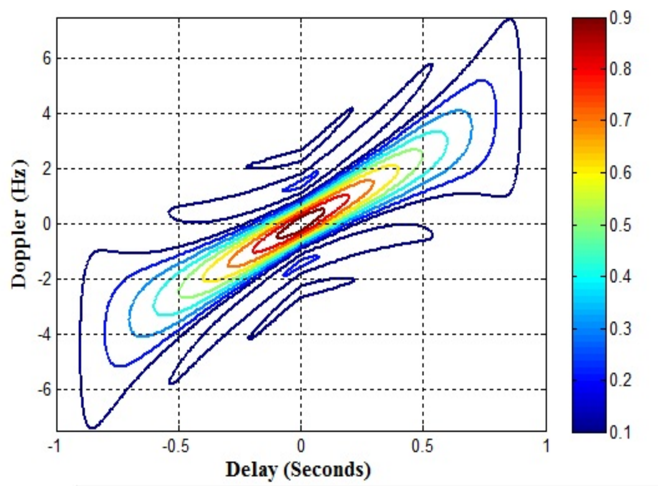

Fig. 2.4. Linear frequency modulated (LFM) waveform ambiguity function in 2D. The waveform has been created with an up-chirp signal.

2.3.4 Linear Frequency Modulated (LFM) Signal and Ambiguity Function

Consider an LFM signal be

$$\begin{aligned} s\left(t\right) &= \mathrm{rect}\left(\frac{t}{T}\right)\exp\left[i2\pi(f_0 t + \frac{1}{2}\alpha t^2)\right] \\ &= \mathrm{rect}\left(\frac{t}{T}\right)\exp(i\pi\alpha t^2)\exp(i2\pi f_0 t) \end{aligned}$$

Therefore,

$$s(t) = u(t)\exp(i2\pi f_0 t) \tag{2.19}$$

where

$$\begin{aligned} f_0 &= \text{carrier frequency} \\ \alpha &= \text{chirp rate} \\ T &= \text{pulse width} \\ u(t) &= \mathrm{rect}\left(\frac{t}{T}\right)\exp(i\pi\alpha t^2), \quad \text{is the complex envelope.} \end{aligned}$$

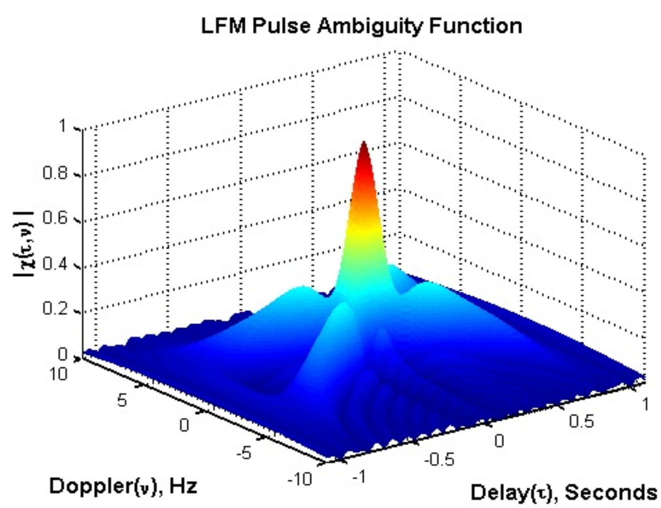

Fig. 2.5. Linear frequency modulated (LFM) waveform ambiguity function. The waveform has been created by combining an up-chirp and a down-chirp signal.

Now, the ambiguity function of the above LFM signal can be defined as

$$\begin{aligned}
\chi_s(\tau,\nu) &= \int_{-\infty}^{\infty} s(t)s^*(t-\tau)e^{i2\pi\nu t}dt \\
&= \int_{-\infty}^{\infty} \text{rect}\left(\frac{t}{T}\right) e^{i\pi\alpha t^2} \text{rect}\left(\frac{t-\tau}{T}\right) e^{-i\pi\alpha(t-\tau)^2}\cdot e^{i2\pi\nu t}dt \\
&= e^{-i\pi\alpha\tau^2}\int_{-\infty}^{\infty} \text{rect}\left(\frac{t}{T}\right) \text{rect}\left(\frac{t-\tau}{T}\right)\cdot e^{i2\pi(\nu+\alpha\tau)t}dt
\end{aligned}$$

Using the similar mathematical derivations as the rectangular pulse, we can show the following:

Case 1: For $\tau < 0$, limits of integration are $0 \le t \le T + t$, and $|\tau| = -\tau$

$$\begin{aligned}
\chi_s(\tau,\nu) &= e^{-i\pi\alpha\tau^2}\int_{0}^{T+\tau} e^{i2\pi(\nu+\alpha\tau)t}dt \\
&= e^{-i\pi\alpha\tau^2}\cdot\frac{[e^{i2\pi(\nu+\alpha\tau)(T+\tau)}-1]}{i2\pi(\nu+\alpha\tau)}.
\end{aligned}$$

After simplifying the above expression, we get

$$\chi_s(\tau,\nu) = (T-|\tau|)\text{sinc}[(\nu+\alpha\tau)(T-|\tau|)]e^{i\pi\nu\tau}e^{i\pi(\nu+\alpha\tau)T}.$$

Case 2: For $\tau \ge 0$, limits of integration are $\tau \le t \le T$, and $|\tau| = \tau$

$$\begin{aligned}
\chi_s(\tau,\nu) &= e^{-i\pi\alpha\tau^2}\int_{\tau}^{T} e^{i2\pi(\nu+\alpha\tau)t}dt \\
&= e^{-i\pi\alpha\tau^2}\frac{[e^{i2\pi(\nu+\alpha\tau)(T)}-e^{i2\pi(\nu+\alpha\tau)(\tau)}]}{i2\pi(\nu+\alpha\tau)}.
\end{aligned}$$

After simplifying the above expression, we get

$$\chi_s(\tau,\nu) = (T-|\tau|)\text{sinc}[(\nu+\alpha\tau)(T-|\tau|)]e^{i\pi\nu\tau}e^{i\pi(\nu+\alpha\tau)T}.$$

By combining above two cases, we can finally write the closed-form expression for ambiguity function of a linear frequency modulated (LFM) signal as follows

$$\chi_s(\tau,\upsilon) = \begin{cases} (T-|\tau|)\text{sinc}[(\upsilon+\alpha\tau)(T-|\tau|)].e^{i\pi\upsilon\tau}e^{i\pi(\upsilon+\alpha\tau)T}, -T\le\tau\le T \\ 0, \quad \text{elsewhere.} \end{cases} \tag{2.20}$$

2.4 The Cross-ambiguity Function

The cross-ambiguity function (CAF) of two finite energy signals $s_1(t)$ and $s_2(t)$ is defined as

$$\chi_{s_1,s_2}(\tau,\nu) = \int_{-\infty}^{\infty} s_1(t)s_2^*(t-\tau)e^{i2\pi\nu t}dt. \tag{2.21}$$

From (2.21), when $s_1(t) = s_2(t)$ we see that cross-ambiguity function (CAF) becomes the auto-ambiguity function (AAF), and mathematical expression for the AAF is same as (2.6).

The ability to distinguish a signal $s_1(t)$ from a time-delayed, Doppler-shifted version of a signal $s_2(t)$ is given by the metric

$$\begin{aligned} d_{\tau,\upsilon}\left(s_1(t), s_2(t)\right) &= \int_{-\infty}^{\infty} \left|s_1(t) - s_2(t-\tau)e^{-i2\pi\upsilon t}\right|^2 dt \\ &= E_{s_1} + E_{s_2} - 2\mathrm{Re}\left\{\chi_{s_1 s_2}(\tau,\upsilon)\right\}. \end{aligned}$$

From above expression, we can say that two signals can be separated easily when cross-ambiguity (cross-correlation) between them is small and this will happen when signals are orthogonal or nearly orthogonal.

We also note that the short-time Fourier transform (STFT) has a similar mathematical expression like the cross-ambiguity function. The STFT is defined as

$$s(\tau,\upsilon) = \int_{-\infty}^{\infty} s(t)g(t-\tau)e^{-i2\pi\upsilon t}dt.$$

So the cross-ambiguity function of two signals $s_1(t)$ and $s_2(t)$ can be viewed as a short-time Fourier transform, where $s_1(t)$ is the signal to be analyzed and $s_2(t)$ plays the role of the window function. This viewpoint allows the properties of the STFT to be applied to cross-ambiguity function.

2.5 Measuring The Approximate Orthogonality of Waveforms Using The Cross-Ambiguity Function

In theory, when two signals are orthogonal to each other, their inner product is zero. This is equivalent to their time cross-correlation function being equal to zero

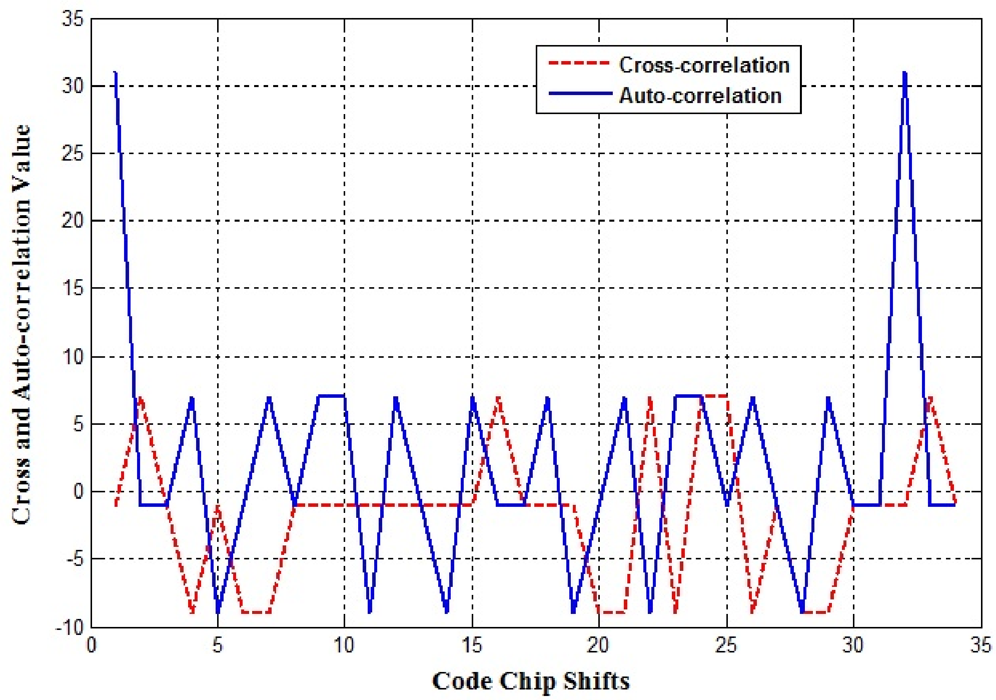

Fig. 2.6. Cross and auto-correlation of length 31 Gold codes when synchronization mismatch occurs. In perfect synchronization (i.e. when transmit and receive codes are completely orthogonal), autocorrelation should exhibit highest peak value at the middle and zero everywhere; similarly, cross-correlation should exhibit zero everywhere. However, often perfect synchronization is unachievable.

at lag $\tau = 0$. However, in practice, cross-correlation may only be nearly zero (but still behave as being practically orthogonal for operational requirements). Even in spread spectrum communication systems with zero Doppler, the correlation is not generally zero for all delays, but for well-designed signals it is small (i.e. almost orthogonal). In code division multiple access communication system, each user's signals are designed to be orthogonal to those of other users so that interference (i.e. cross-correlation) caused by each other is minimal (i.e. bit error probability due to multi-user interference is very low). In a radar system, due to target's motion, receive signals do not stay fully orthogonal. Hence, cross-correlation between two orthogonal signals is expected to be non-zero. Thus if cross-ambiguity between a transmit and receive signal fall below certain threshold, we can declare these signals are orthogonal. In this research, we define two waveforms are nearly orthogonal or ε-*orthogonal* when following criteria is met:

$$\frac{|\text{Cross} - \text{ambiguity of signal } s_1 \text{ and signal } s_2|^2}{(\text{Energy of signal } s_1).(\text{Energy of signal } s_2)} \leq \varepsilon$$

or

$$\max_{\tau,\upsilon} \frac{|\chi_{s_1 s_2}(\tau,\upsilon)|^2}{E_1 E_2} \leq \varepsilon,$$

or equivalently,

$$\max_{\tau,\upsilon} \frac{\left|\int_{-\infty}^{\infty} s_1(t) s_2(t-\tau) e^{i2\pi\upsilon t} dt\right|^2}{E_1 E_2} \leq \varepsilon,$$

where E_1 is the energy in signal $s_1(t)$ and E_2 is the energy in signal $s_2(t)$.
Often the threshold value (i.e. ε) is specified in dB appropriate for operating conditions. Effectively, ε-orthogonality implies that the interference resulting from $s_2(t)$ does not significantly affect the output of a matched-filter for $s_1(t)$, in the presence of all possible delay and Doppler shifts, at least for ε sufficiently small.

2.5.1 Orthogonal Spreading Codes and Cross-correlation

Orthogonal codes such as the Walsh-Hadamard code and Gold code are used in multi-user CDMA communication systems. Orthogonal codes allow minimum interference among users. Hence, codes are choosen so that cross-correlation between two users signals should be close to zero. Figure 2.6 shows cross and auto-correlation of length 31 Gold codes when synchronization mismatch occurs. As mentioned earlier, synchronization mismatch or interference occurs while operating a communication system. Thus signals may not stay perfectly orthogonal. However, if two signals stay orthogonal to a certain extent so that cross-correlation falls below threshold and minimize the interference, we can call these signals nearly orthogonal or ε-orthogonal for a sufficiently small ε.

2.6 The Ambiguity Function and Delay-Doppler Resolution of Matched Filter Radar

In its simple definition, radar target resolution is the ability to determine the presence of a second target in the presence of a target. From a processing view point, two criteria must be satisfied to resolve a target from radar measurement: (i) a target's signature output peak should be as narrow as possible in delay-Doppler because wider output peak will increase uncertainty by adding closely-spaced targets signature and (ii) target's signature should not be obscured by clutter or other interference sources.

The ambiguity function (AF) depicts matched-filter response of a transmit waveform that is mismatched in delay and Doppler. The AF can be used to analyze delay-Doppler resolution of matched filter radar. Intuitively, if an AF exhibits a sharp peak at the origin of the delay-Doppler plane and almost zero everywhere else, then we should be able to resolve a target because this will guarantee above two criteria for target resolvability. However, such an ideal AF cannot be generated in practice. Although we may design radar waveforms that may exhibit reasonably narrow main lobe target response, this may not guarantee resolving multiple targets unambiguously in delay and Doppler. This is due to the fact that sidelobe of these waveforms can obscure presence of a nearby weak target.

The AF can guide us designing waveforms to demonstrate a reasonably narrow main lobe target response and low sidelobe levels, and thus resolving multiple targets both in delay and Doppler. Consider a stationary point target is located at the origin of the interrogated scene. For a given waveform (with narrow main lobe, low sidelobe characteristic) we can generate an ambiguity function for this target with various mismatched delay and Doppler measurements. Similarly, we can generate additional AFs for targets in various locations at the interrogated scene. All of the AFs then can be superimposed to obtain combined receiver response for all the targets. The critical observation here is that narrow main lobe will ensure individual targets signature will remain within a few nearby delay-Doppler bins and low sidelobe will ensure nearby targets will not be masked. As result, by examining combined ambiguity function response, we can have a resolution map for all the targets of an interrogated scene.

Consider two targets with responses, delays, and Dopplers represented by $(a_1, \tau_1, \upsilon_1)$, and $(a_2, \tau_2, \upsilon_2)$ respectively. Now, the combined matched filter output for these two targets can be expressed as:

$$O_T(\tau, \upsilon) = a_1 e^{i\phi_1} \cdot e^{-i2\pi(\upsilon-\upsilon_1)\tau_1} \beta_s(\tau-\tau_1, \upsilon-\upsilon_1) + a_2 e^{i\phi_2} \cdot e^{-i2\pi(\upsilon-\upsilon_2)\tau_2} \beta_s(\tau-\tau_2, \upsilon-\upsilon_2)$$

$$= a_1 e^{i\phi_1} \cdot e^{-i2\pi(\upsilon-\upsilon_1)\tau_1} \chi_s(\tau-\tau_1, -(\upsilon-\upsilon_1)) + a_2 \cdot e^{i\phi_2} \cdot e^{-i2\pi(\upsilon-\upsilon_2)\tau_2} \chi_s(\tau-\tau_2, -(\upsilon-\upsilon_2))$$

We can see the role of the ambiguity function $\chi_s(\tau, \upsilon)$ in determining the signal $s(t)$'s ability to resolve targets with matched filter processing.

2.6.1 Illustration of Ambiguity Function to Resolve Two Closely-spaced Targets

The Figures 2.7 - 2.10 demonstrate how ambiguity function can be useful for designing waveforms to resolve two closely-spaced targets. These figures show the delay-Doppler response of a radar to two targets. In Figure 2.7, there is a strong target at

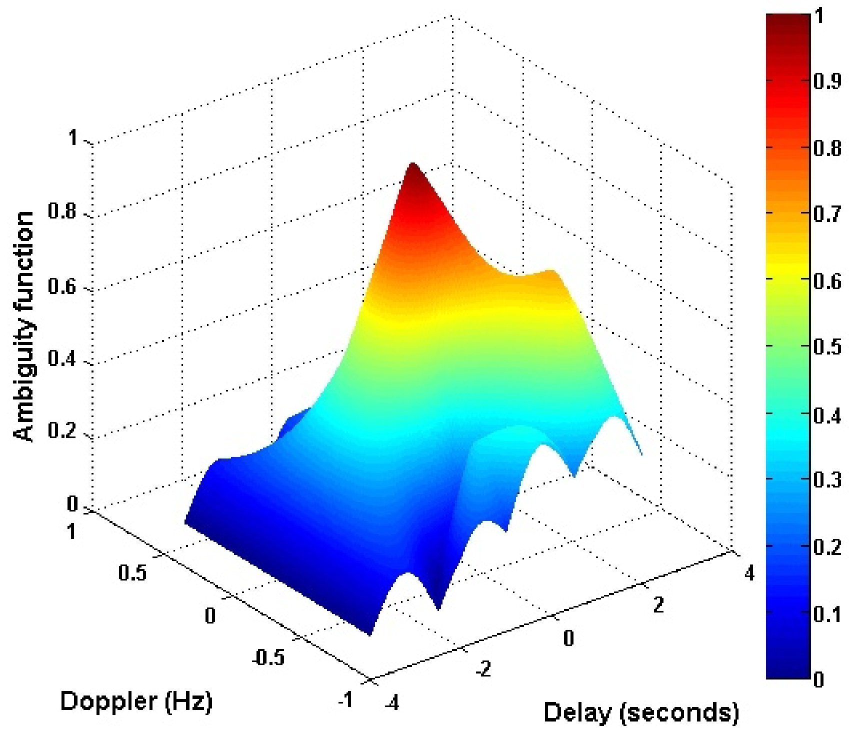

Fig. 2.7. 3D delay-Doppler response of two targets close to each other

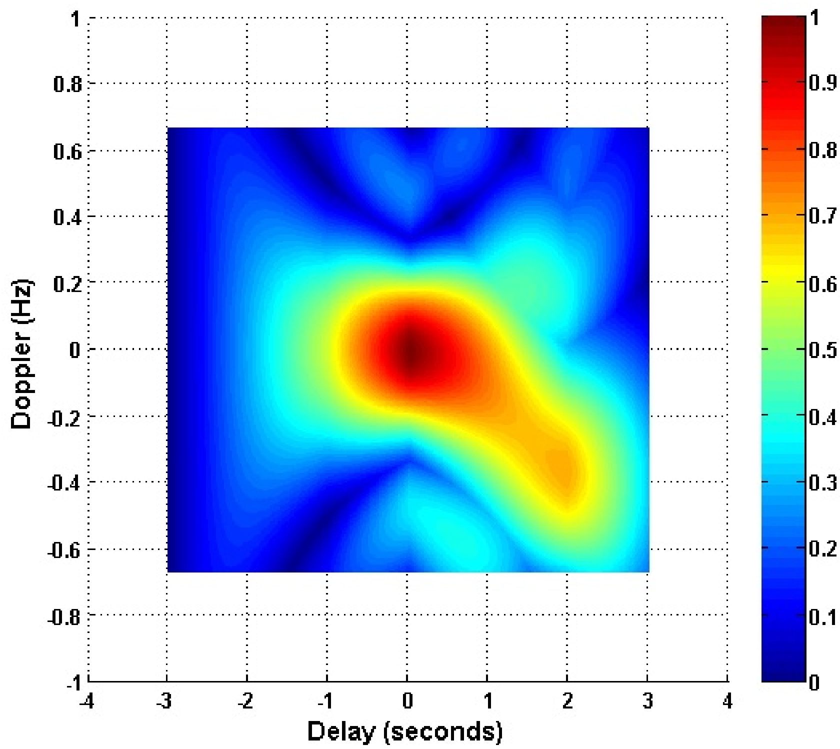

Fig. 2.8. 2D view of the delay-Doppler response presented in Figure 2.7

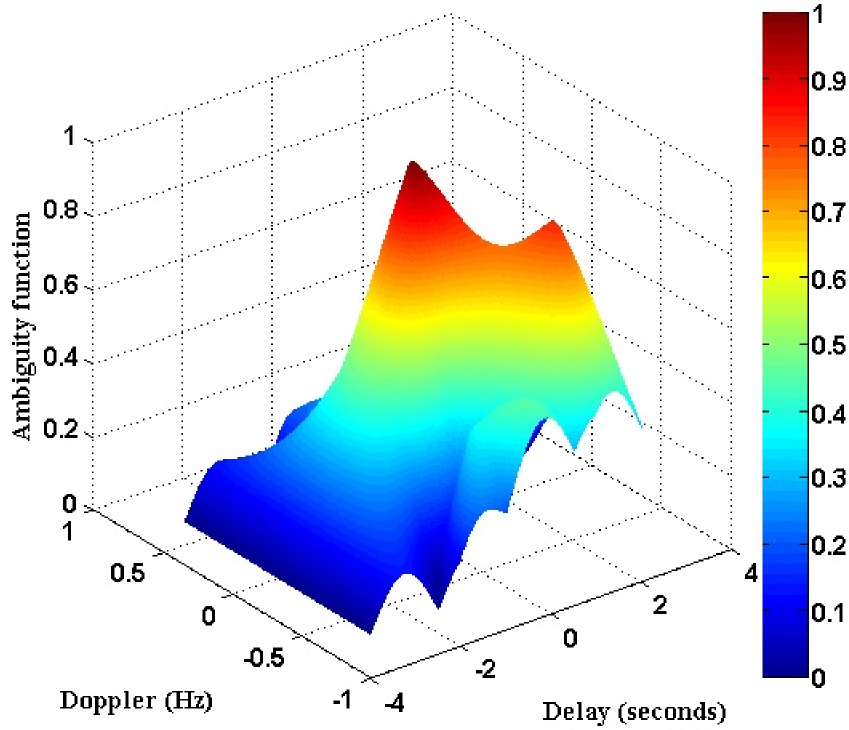

Fig. 2.9. 3D delay-Doppler response of two targets close to each other after redesigning the waveforms to provide better resolution. Both targets are now more resolvable.

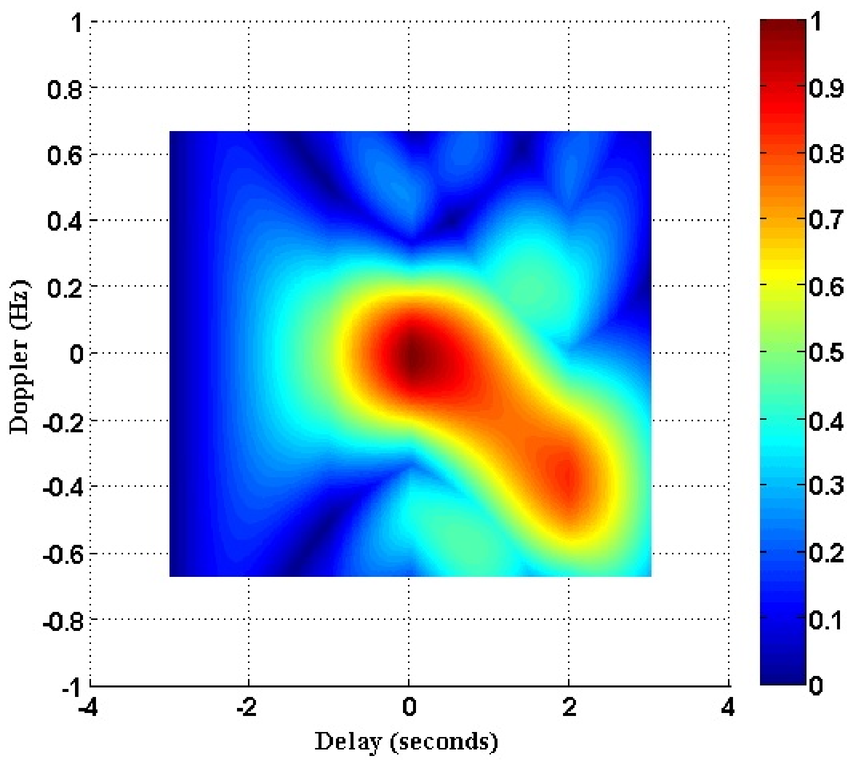

Fig. 2.10. 2D delay-Doppler response presented in Figure 2.9

the center of the interrogated scene and a weak target nearby. AF shows combined response of these two targets in delay and Doppler. Figure 2.8 shows 2D view of two targets presented in Figure 2.7. By examining AF, one may try to re-design the waveforms with extra bandwidth. By increasing bandwidth, we may increase resolution so that the weak target will be more visible/detectable. Figure 2.9 demonstrate that by redesigning the waveforms weak target's resolution can be improved.

2.7 The Role of Diverse, Orthogonal Waveforms for Target Information

Let $\chi_{s_1}(\tau, \upsilon)$ and $\chi_{s_2}(\tau, \upsilon)$ denotes ambiguity functions of two signals $s_1(t)$ and $s_2(t)$, respectively. Then the distance between these two ambiguity functions can be defined by the ℓ_2 norm as

$$d\left(\chi_{s_1}, \chi_{s_2}\right) = \int_{-\infty}^{\infty} \left|\chi_{s_1}(\tau, \upsilon) - \chi_{s_1}(\tau, \upsilon)\right|^2 d\tau d\upsilon$$

$$= \int_{-\infty}^{\infty} \left|\chi_{s_1}(\tau, \upsilon)\right|^2 d\tau d\upsilon + \int_{-\infty}^{\infty} \left|\chi_{s_2}(\tau, \upsilon)\right|^2 d\tau d\upsilon - 2\mathrm{Re}\left\{\int_{-\infty}^{\infty} \chi_{s_1}(\tau, \upsilon)\chi_{s_2}^{*}(\tau, \upsilon) d\tau d\upsilon\right\}$$

$$= E_{s_1}^2 + E_{s_2}^2 - 2\left|\int_{-\infty}^{\infty} s_1(t) s_2^{*}(t) dt\right|^2 .$$

Clearly, $d\left(\chi_{s_1}, \chi_{s_2}\right)$ is maximized when $s_1(t)$ and $s_2(t)$ are orthogonal. It was shown in the paper by Guey and Bell [5] that by selecting diverse and orthogonal waveforms, more information can be obtained through the difference in the matched filter ambiguity responses.

2.8 Pulse Compression Waveform

To detect targets at long range, very long pulses are needed. However, a long pulse provides poor range resolution. Then one might ask why don't we use short pulse? The answer to this question is that there are limitations to use short pulse. First of all, bandwidth (BW) of a short pulse is large. However, large BW can increase system complexity, signal processing burden, and vulnerable to interference. Secondly, high peak power is required for short pulse if it is to achieve significant total energy and these high instantaneous powers make transmitter design difficult.

To mitigate this problem, a frequency or phase modulated signal is transmitted by the radar systems. This is known as ***pulse compression technique***. Pulse compression enables obtaining high range resolution of a short pulse while using a long pulse. In many applications, resolutions provided by the unmodulated signals are not sufficient for desired resolution.

Linear frequency modulation (LFM) pulse compression enables high range resolution capability by using an appropriate time-bandwidth product. LFM signals also exhibit the Doppler tolerant property that will be discussed next section.

2.9 The Ambiguity Function and Doppler Tolerant Waveforms

In the radar literature [6], a waveform is considered to have *Doppler tolerance* if transmit and receive signal mismatch do not degrade performance of the radar system significantly. This is due to the fact that a special structure of some waveforms permits nearly optimal detection performance in the presence of relatively large Doppler shifts which many other waveforms cannot provide. As a result, these Doppler tolerant waveforms do not require as complex processing procedure at the receiver to obtain expected performance because they do not need as many Doppler filters to cover the range of expected Dopplers and still yield reasonable detection performance . Hence, Doppler tolerance waveforms are often used when moving target detection is involved.

We need to mention that a waveform may not be Doppler tolerant to extremely large Doppler shifts caused by extremely fast moving objects. However, Doppler shifts due to many of the ordinary moving objects such as cars, trucks can be accommodated by the Doppler tolerance criteria. Hence, Doppler tolerance should be taken as how a waveform performs compared to others when moderate to large Doppler shifts are expected. In other words, how quickly performance of a waveform degrade as targets moves faster causing moderate to large Doppler shifts. Next section we will define, a metric for measuring the Doppler tolerance of a waveform.

2.9.1 Measuring Doppler Tolerance

We know that the amplitude of the matched-filter output for a received signal mismatched on delay (τ) and Doppler (υ) is given by $|\chi_s(\tau, \upsilon)|$. Figure 2.11 visualizes the $|\chi_s(\tau, \upsilon)|$ of a linear frequency modulated waveform.

The peak value, which occurs at $(\tau, \upsilon) = (0, 0)$ is E_s that is the energy in the signal $s(t)$. We define two planes at the ambiguity surface as follows

$$p_1(\tau, \upsilon) = E_s(1 - \delta_1)$$

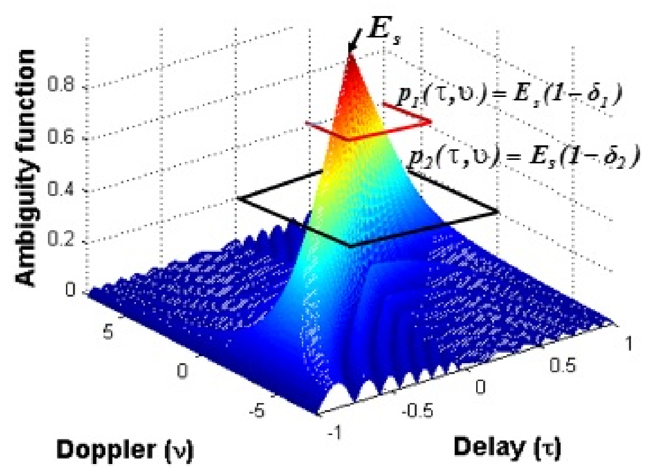

Fig. 2.11. Two planes p_1 and p_2 cut through the ambiguity function of an LFM waveform

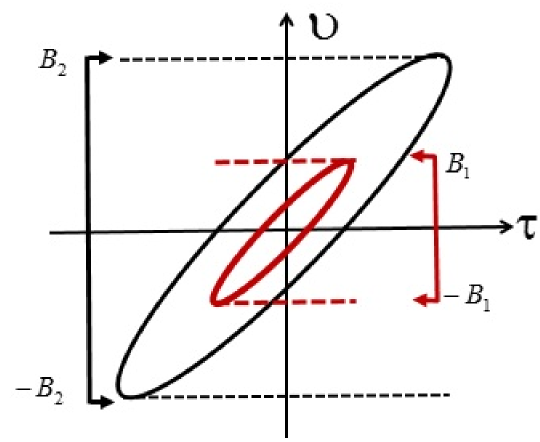

Fig. 2.12. Level sets for two planes cut through the ambiguity function of an LFM waveform. Here, B_1 and B_2 are bandwidths and $B_1 < B_2$.

and

$$p_2(\tau, \upsilon) = E_s(1 - \delta_2)$$

Note that these planes are constant planes that are not a function of (τ, υ). Also, δ_1 and δ_2 control the amplitude level at which the planes intersect the ambiguity function and we assume that $\delta_1 < \delta_2$.

If we look at where the intersection of these planes with $|\chi_s(\tau, \upsilon)|$ we get the level sets (i.e., points that are at level $E_s(1 - \delta_k)$, $k = 1, 2$ on the function $|\chi_s(\tau, \upsilon)|$) depicted in Figure 2.12.

Now if the return signal has a Doppler shift $\upsilon \in [-B_1, B_1]$, then the matched filter's amplitude output (matched to the original non-Doppler shifted signal $s(t)$) will be greater than or equal to $E_s(1 - \delta_1)$. Similarly, if $\upsilon \in [-B_2, B_2]$, we know that the absolute value of the matched filter output will be greater or equal to $E_s(1 - \delta_2)$.

Let, B_δ be the bandwidth over which the matched filter output is greater than or equal to $E_s(1 - \delta)$. We can say in general, as δ grows greater (i.e., if we allow a lower matched filter magnitude output) B_δ will grow bigger. The rate of this growth will depend on the waveform. The LFM waveform has a significant matched filter

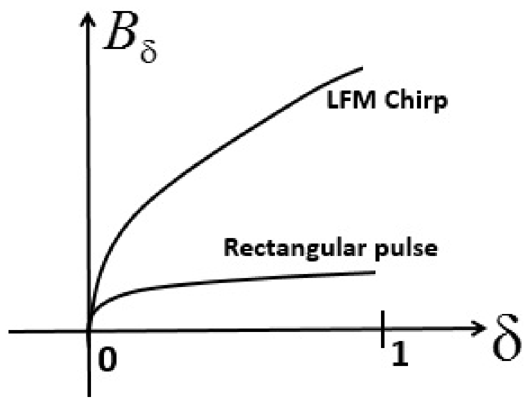

Fig. 2.13. Comparison of LFM and rectangular waveforms for B_δ growth rate when δ gets bigger. B_δ is bandwidth over which the matched filter output is greater than or equal to $E_s(1-\delta)$.

response over a broad range of Doppler frequencies $[-B_\delta, B_\delta]$, whereas for the non-Doppler tolerant waveform ,the range $[-B_\delta, B_\delta]$ will be much smaller. Figure 2.13

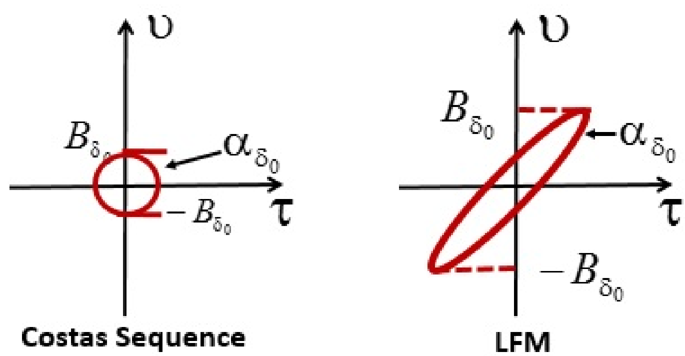

Fig. 2.14. Typical level set surrounding the origin for LFM and Costas sequence. Shear property of LFM covers more frequency and hence Doppler tolerant

shows that by observing the ambiguity functions, we can compare LFM waveform's B_δ with rectangular or other waveforms' B_δ as δ varies from 0 to 1.

Definition 2.9.1 (Doppler Tolerance) *Let $|\chi_s(\tau, \upsilon)|$ be the absolute value of the ambiguity function of the signal s(t). Let α_δ be the innermost connected level set corresponding to amplitude $E_s(1-\delta)$ out of the matched filter. Then we say that $s(t)$ is B_δ Doppler tolerant, and its Doppler tolerance is characterized by the curve (δ, B_δ)as δ varies from 0 to 1.*

We are interested in the closest level set surrounding the origin $(\tau, \upsilon) = (0, 0)$. At this location the waveform that covers more frequency bandwidth, it can accommodate more Doppler frequency shift for good output performance and hence more Doppler tolerant. Figure 2.14 shows typical curves of LFM and Costas waveforms for B_{δ_0} Doppler tolerant at location α_{δ_0} (i.e. closest to the origin).

2.9.2 Range (Delay)-Doppler Coupling

Unfortunately, LFM signal's improved range resolution and Doppler tolerance capabilities introduce range measurement inaccuracy of moving targets. This phenomena is known as range-Doppler coupling or delay-Doppler coupling. When this phenomena happens, a target's range is biased from the true range of the target. The peak response appears slightly off from the actual delay-Doppler location. It also decreases the height of the peak. Fortunately, Doppler frequency shift usually is very small compare to the signal frequency bandwidth and hence peak height reduction of the ambiguity function is not significant to impact the overall performance of a radar system. Similarly, a biased in range measurement error is acceptable in many applications. In applications where range measurement accuracy is extremely important (and LFM waveform has been transmitted) following technique is used. First, make measurements with an up-chirp LFM signal and then with a down-chirp LFM signal. These two measurements will introduce positive and negative range errors. Then average these two measurements to compute the actual range.

2.9.3 A Numerical Example to Illustrate Doppler Tolerance

Let, ν be Doppler frequency, B be bandwidth. For an LFM signal to become 0.3 Doppler tolerant, it has be matched with 30% of the operating bandwidth. Hence following relation needs to be satisfied:

$$|\Delta\nu| \leq (0.3) \cdot \mathrm{B}. \tag{2.22}$$

Now, a target's Doppler frequency shift is given by the following equation [7]:

$$\Delta\nu = \frac{2r' f_c}{c} \tag{2.23}$$

where, r' is range rate, f_c is carrier frequency, and c is the speed of light.
Then, from (2.22) and (2.23) above, we get

$$\frac{2r' f_c}{c} = (0.3)\mathrm{B} \tag{2.24}$$

and,

$$r' = \frac{(0.3)\mathrm{B}\cdot c}{2f_c}. \tag{2.25}$$

Example: Assume $f_c = 10^9 Hz$, and B = (600).(10) ^{6} Hz, and $c = (3).(10)^8 m/\sec$
Then,

$$r' = \frac{(0.3)\mathrm{B}.c}{2\nu_c} = \frac{(0.3).(600).(10)^6.(3).(10)^8}{(2).(10)^9}$$

$$= \frac{(180).(3).(10)^5}{2} = (270).(10)^5 m/\sec = 27,000 km/\sec$$

Now, let's consider performance of a coded waveform with LFM signal. In this case, assume 360 degree Doppler shift in T seconds. Let, T be 10μsec and $f_c = 10^9 Hz$. Then, we get

$$\frac{2r^{'} f_c}{c} = \frac{1}{T}, \tag{2.26}$$

and thus,

$$r^{'} = \frac{c}{2T f_c}. \tag{2.27}$$

Putting the value for T, f_c, and c, we get,

$$r^{'} = \frac{(3).(10)^8}{(2).(10)^9.(10).(10)^{-6}} = \frac{30000}{2} = 15km/\sec.$$

Clearly, LFM waveform provides better range rate than coded waveforms even when Doppler shift has been expected.

2.10 Conclusion

As a building block for later chapters, this chapter reviews the fundamental concepts of radar ambiguity function, cross-ambiguity, target resolution, and Doppler tolerance. Among several important properties of the ambiguity function, we discussed constant volume property; also known as **radar uncertainty principle**. Radar waveform's uncertainty principle presented here is analogous to the uncertainty principle of Fourier transform. The essence of this property is that there is a constraint on achieving the best possible resolution in delay and Doppler simultaneously by a particular waveform. We then established a formula to measure degree of orthogonality of two waveforms. We also presented waveform's role for resolving targets. In particulr we illustrated how ambiguity function helps designing waveforms for resolving closely-spaced targets. This chapter ends with defining Doppler tolerance of a waveform. We hope that the fundamental concepts presented in this chapter will be useful for the reader to understand orthogonal waveforms design and processing techniques to be presented next chapters.

3. TRANSMIT AND RECEIVE ORTHOGONAL WAVEFORMS DESIGN

3.1 Introduction

In recent years, waveform-agile sensing has gained interest among radar researchers [8]. Waveform-agility is defined as the ability of a radar system to adapt and change its waveforms while operating. Waveform-agility often provides improved performance over non-adaptive waveforms radar systems in a dynamic or heterogenious environment. The reason is that waveform-agile radar systems can change various radar operating parameters, including frequency, pulse repetition frequency (PRF), polarization, and bandwidth based on operating conditions of the environment. For example, to detect fast moving targets, a radar system has to operate in high PRF mode. By contrast, a low PRF rate is necessary to detect slow moving targets, as will be discussed in Chapter 6.

This chapter presents the design of orthogonal, Doppler tolerant waveforms for waveform-agile radar (e.g. MIMO radar) applications. Previous work has given limited consideration to the design of radar waveforms that remain orthogonal when they are received; however, this is essential if orthogonality is going to be used to separate the signals after they are received. Our research is focused on: (1) developing sets of waveforms that are orthogonal on both transmit and receive, and (2) ensuring that these waveforms are Doppler tolerant when properly processed.

3.1.1 Contributions and Chapter Organization

We design orthogonal waveforms by combining linear frequency modulated waveforms with a direct sequence spread spectrum coding technique. Designing transmit orthogonal waveforms is straightforward. However, designing waveforms that will remain at least approximately orthogonal on receive is a complex problem. A solution to this problem has significant impact to waveform-agile radar research. Our research addresses this critial problem. Major contributions of this research are:

1. Researchers presented MIMO radar benefits based on the *assumptation* that received waveforms also remain orthogonal [1]. However, other than our investigation, no published literature can be found on waveforms that explain how to maintain orthogonality of the received waveforms. Thus, our work opens new research opportunities for true evaluation of MIMO radar benefits over a traditional phased-array radar system.

2. Often researchers design waveforms that perform well (in theory) for specific applications. However, in practice, these wavefroms are very hard to generate in radar hardware. Considering practical hardware implementation, we have choosen LFM waveforms with spread spectrum coding. Our waveforms can be generated using existing hardware.

3. Our proposed waveforms inherit multiple attributes (e.g. chirp diversity, code diversity, frequency diversity) of diverse waveforms that can be exploited in multi-static radar systems.

4. Our waveforms also satisfy constant modulus property and inherit Doppler tolerant property of the LFM waveforms.

The rest of the chapter is organized as follows. In the next section, we provide a literature review on orthogonal waveforms design. This guides us to adopt a unique method for orthogonal waveform design. We also identified the limitations of other approaches used for orthogonal waveforms design. We then introduce our method for transmit and receive orthogonal waveforms design in section 3.3. We explained our rationale for the selection of LFM waveforms with spread spectrum coding technique to design orthogonal waveforms. The intuition is that LFM waveforms are Doppler tolerant and easy to generate in radar hardware. In addition, LFM waveforms also satisfy constant modulus constraint and provide reasonable sidelobe levels and resolution to detect targets. To make our waveforms orthogonal, we consider the direct sequence spread spectrum (DSSS) technique. The rationale behind this selection is that DSSS technique allows multiple signals to work in an orthogonal fashion. Thus unlike other waveforms, our waveforms, which are based on LFM waveforms and DSSS technique, can remain approximately orthogonal on both transmit and receive. DSSS is widely used by the communication engineers. To understand our waveform design, it is important to know the basic concept of DSSS. Hence, in section 3.4 we provide a brief description on DSSS technique.

How do we measure the orthogonality of the waveforms? In Chapter 2, we provided definition of ε-*orthogonality* of two waveforms. We adopt cross-ambiguity as the measure to evaluate orthogonality of our proposed waveforms. In section 3.5, we developed an analytical expression to quantify cross-ambiguity between two waveforms. The lower the value of the cross-ambiguity, the more orthogonal two signals become. Section 3.6 provides experimental parameters used for numerical evaluation of cross-ambiguity between two waveforms. Finally, in section 3.7, we provide results and analysis of our orthogonal waveforms. We observed that with increased code length, waveforms become more orthogonal (i.e. cross-ambiguity becomes smaller).

3.2 An Overview on Orthogonal Waveforms Design for Diversity Radar Applications

In orthogonal waveforms design for MIMO radar applications, consideration must be given so that not only the transmit waveforms are orthogonal but also receive waveforms remain orthogonal. This is due to the fact if the receive waveforms remain orthogonal, it makes separation of the responses of different transmitted waveforms straightforward (to develop detection or other exploitation algorithms). In fact, orthogonality on receive is actually more important than orthogonality on transmit, as it is after the signal is received then orthogonality is exploited for signal separation. To address the MIMO radar waveforms design issue, researchers attempted techniques such as employing polarization diverse waveforms, frequency diverse waveforms, coded waveforms, and combination of these methods [4], [9], [10], [11], [12], [13], [14], [15]. Moran *et.al.* [16] presented polarization diverse waveforms on multiple channels for MIMO radar. Principal advantages claimed by this approach are it enables detection of smaller radar cross section (RCS) targets and diversity gains. However, this research did not address whether waveforms will remain orthogonal on receive. Gladkova *et.al.* described a family of stepped frequency waveforms to attain high range resolution [17]. This paper demonstrated that a suitable choice of waveform's parameters leads to the essential suppression of its autocorrelation function (ACF) sidelobes. Similarly, Zoltowski *et.al.* [18], and Nehorai [19] also illustrated methods to exploit waveforms for MIMO radar applications.

Other approaches researchers have considered include separating the waveforms into disjoint frequency sub-bands that will not overlap even under the maximum expected Doppler shifts. In this case, the waveforms will remain orthogonal under arbitrary delays and Doppler shifts, but in general the Doppler shifts for a given target velocity and geometry will be different because of the different carrier (center) frequency of each sub-band (e.g., [20]).

3.3 Our Approach for Orthogonal MIMO Radar Waveform Design

When designing radar waveforms, good resolution and Doppler tolerance are two important criteria. Additionally, waveforms should satisfy the constant modulus constraint and have low side lobe levels. Unfortunately, for a given waveform, Doppler tolerance and resolution cannot be obtained simultaneously because these lead to competing design requirements as described in Chapter 2. Thus a waveform's superior Doppler tolerance characteristics imply resolution degradation. Fortunately, for many practical radar systems, LFM waveform has been proven to provide reasonably good Doppler tolerance and resolution at the same time, with the main loss in resolution occuring only along the high delay-Doppler ridge of the LFM ambiguity function. Most other waveforms, unlike LFM, can provide either extremely good resolution or extremely good Doppler tolerance, but not both. Further, LFM waveforms also satisfy constant modulus constraint and provide reasonably good side lobe levels. Hence, as a component of our proposed waveform, our selection for LFM waveform was to satisfy important characteristics that a waveform should possess such as good resolution, Doppler tolerance, constant modulus constraint, and low side lobe levels. By Doppler tolerance, we mean that with relatively high target motion this waveform still allow reasonable detection capability than other waveforms without significant modification to the processing algorithms (e.g. using a bank of Doppler filters). In Chapter 2, we provided a detailed description of the Doppler tolerance waveform.

As mentioned earlier, our goal is designing a practial set of transmit orthogonal waveforms that are Doppler tolerant and remain orthogonal (or nearly orthogonal) on receive. Hence, we choose LFM waveforms to satisfy good Doppler tolerance criteria. To fulfill the need for orthogonality on receive, we consider coding each of the transmited waveforms with a unique phase code, and each of these codes should be orthogonal to each other. This concept is familiar in communications and this is known as direct sequence spread spectrum. Thus, we consider blending LFM waveforms with the spread spectrum technique to achieve a Doppler tolerant, orthogonal (or near orthogonal) waveform design for MIMO radar. In communication, chirp modulated spread spectrum combined with antipodal signaling has been utilized to reduce bit error rate [21]. In the radar literature, coded waveforms have been utilized to reduce sidelobes and provide high resolution in delay and Doppler [9], but here we are combining these two types of waveform modulation in a unique way to generate multiple access radar waveforms to make the equivalent of two simultaneous non-interfering LFM measurements that can exploit the difference in the two different LFM ambiguity functions.

3.4 Direct Sequence Spread Spectrum Technique

Spread spectrum is a widely implemented technique in modern CDMA (code division multiple access) wireless communication. Spread spectrum (SS) signaling performs very well in high interference environments. Among different types of spectrum spreading techniques, such as direct sequence, frequency hopping, or hybrid combinations, we found direct sequence is better suited to design our waveforms. In this section, we provide a brief description of the direct sequence spread spectrum (DSSS) technique. The presentation provided here closely follows the texts by Proakis [22] and Simon [23]. Using standard spread spectrum signal notation, the information signal to be modulated can be expressed

$$A(t) = \sum_{n=-\infty}^{\infty} a_n P_{T_b}(t - nT_b), \tag{3.1}$$

where

$$a_n \quad = \quad \pm 1$$

and

$$P_{T_b}(t) \quad = \quad \text{rectangular pulse of duration } T_b.$$

Now, $A(t)$ is multiplied by the coded signal

$$C(t) = \sum_{n=-\infty}^{\infty} c_n P_{T_c}(t - nT_c) \tag{3.2}$$

to produce the product or spreaded signal

$$B(t) = A(t) \cdot C(t), \tag{3.3}$$

where

$$c_n \quad = \quad \text{binary, pseudo} - \text{noise(PN) code of } \pm 1's,$$

and

$$P_{T_c}(t) \quad = \quad \text{rectangular pulse of duration } T_c.$$

The product signal is then used to modulate the carrier signal and transmitted. So, the transmitted signal becomes:

$$T_x(t) = A(t)C(t) \cdot \cos(2\pi f_c t). \tag{3.4}$$

The received signal is the transmitted signal $T_x(t)$ and the interfering signal, $I(t)$, i.e.

$$R_x(t) = A(t)C(t)\cos(2\pi f_c t) + I(t). \tag{3.5}$$

In the demodulation process, the received signal $R_x(t)$ is multiplied by the coded waveform $C(t)$, yielding

$$D_x(t) = R_x(t)C(t). \tag{3.6}$$

This process is also known as spectrum despreading. The output of the despreading process is the original information signal (after low-pass filtering), i.e.

$$D_x(t) = A(t). \tag{3.7}$$

In equation (3.1) the information rate is $1/T_b$, which is the bandwidth R of the information-bearing baseband signal. In equation (3.2), the rectangular pulse $P_{T_c}(t)$ and T_c are known as *chip waveform* and *chip interval*, respectively. Also, $1/T_C$ is known as *chip rate* and this is approximately the bandwidth, W, of the transmitted signal (i.e. spreaded signal). The processing gain of a DSSS signal is defined as

$$L_C = \frac{T_b}{T_c} = \frac{W}{R}. \tag{3.8}$$

In a DSSS signal, L_C represents number of chips used in the pseudo noise (PN) code per information symbol. This is also known as bandwidth expansion factor, and it represents reduction in power in the interfering signal. In our waveform, the bandwidth expansion factor is determined by code length. Figure 3.1 presents a simple block diagram of the DSSS system.

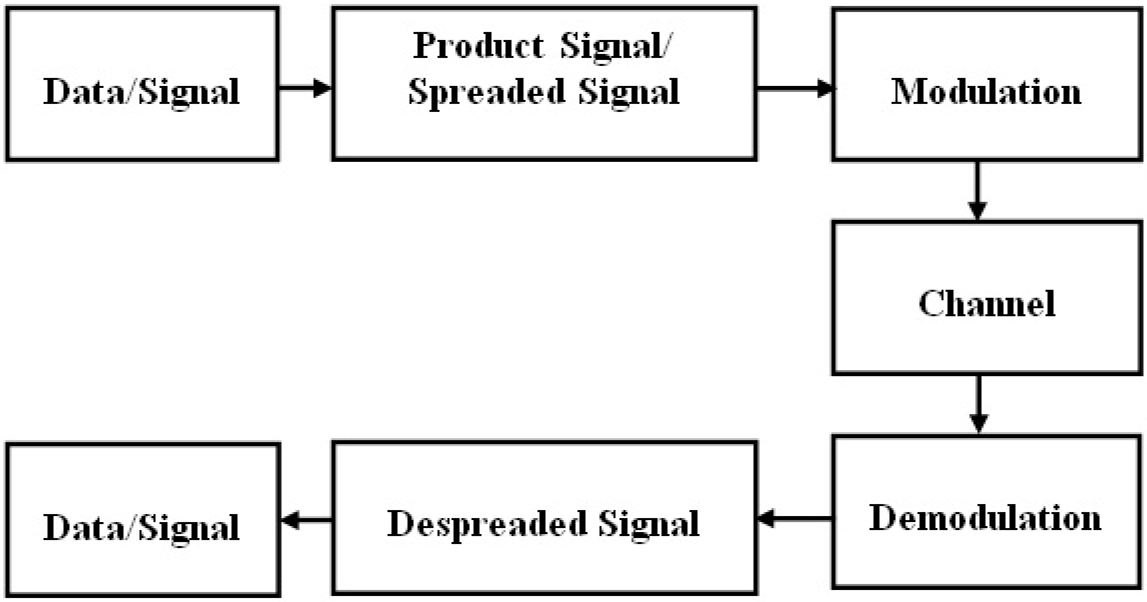

Fig. 3.1. Block Diagram of a Direct Sequence Spread Spectrum System

3.5 Cross-ambiguity Function for Spread Spectrum Coded LFM Waveforms

In previous chapter (i.e. Chapter 2), we derived closed-form mathematical expression for an LFM signal's ambiguity function. We have also presented algorithmic steps for direct sequence spread spectrum concept in previous section. In this section, we develop an expression for cross-ambiguity function of direct sequence spread spectrum modulated LFM waveforms.

Define the indicator function as

$$1_{[0,\ \mathrm{T}]}(t) = \begin{cases} 1 & 0 \leq t \leq \mathrm{T}, \\ 0 & \text{otherwise.} \end{cases} \tag{3.9}$$

Let, an LFM signal be

$$s(t) = e^{i\pi\alpha t^2} \cdot 1_{[0,T]}(t)$$

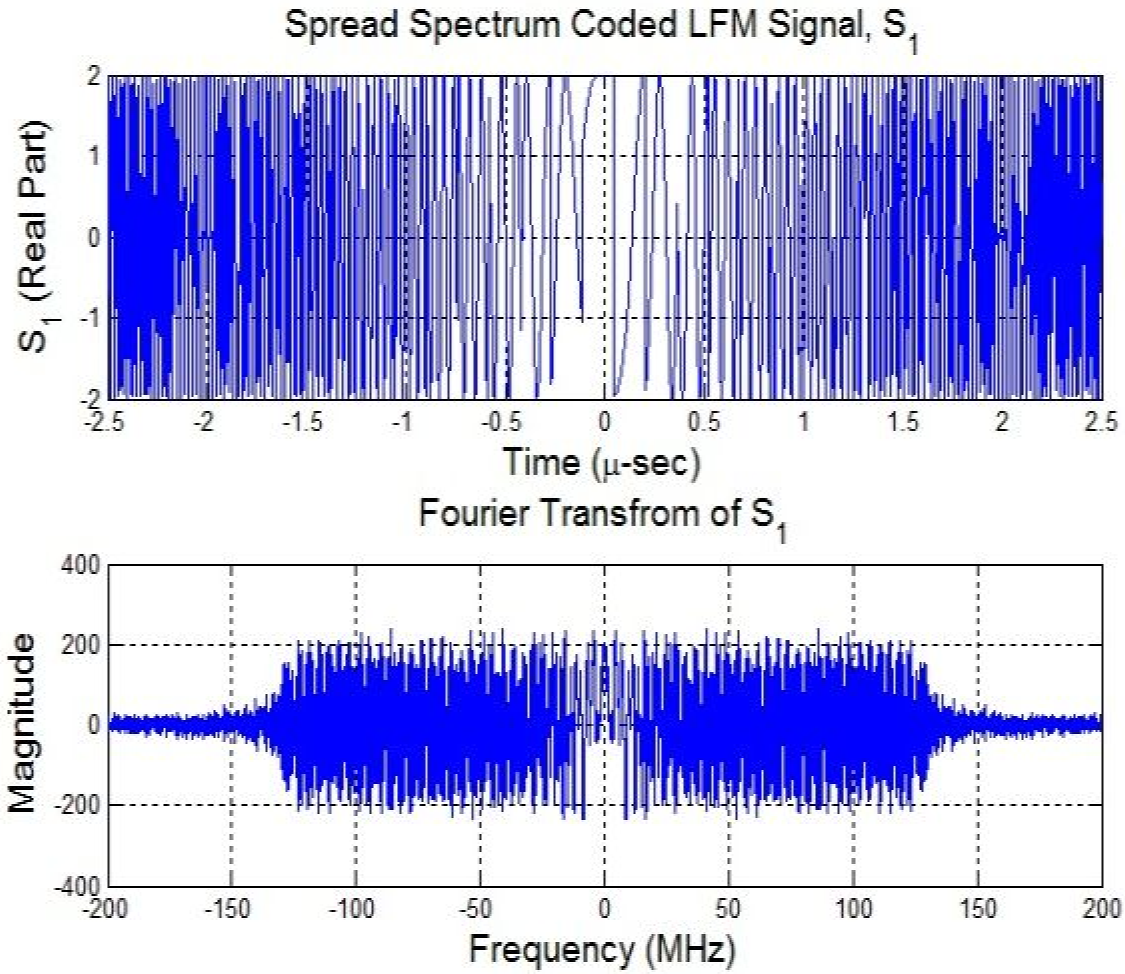

Fig. 3.2. Spread spectrum coded LFM signal s_1 and corresponding Fourier transform. Chirp rates used were, $\alpha_1 = (B)/TP_1$ and $\alpha_2 = (-B)/TP_1$, where B is the bandwidth of the LFM signal after applying spread spectrum code, TP_1 is duration of the signal. Walsh-Hadamard code of length 64 has been used to spread the LFM signal.

Now define two direct sequence spread spectrum coded LFM (SSCL) signals as follows

$$s_1(t) = \sum_{m}^{M-1} C_m P(t - mT_C) e^{i\pi\alpha_1 t^2}, \tag{3.10}$$

and

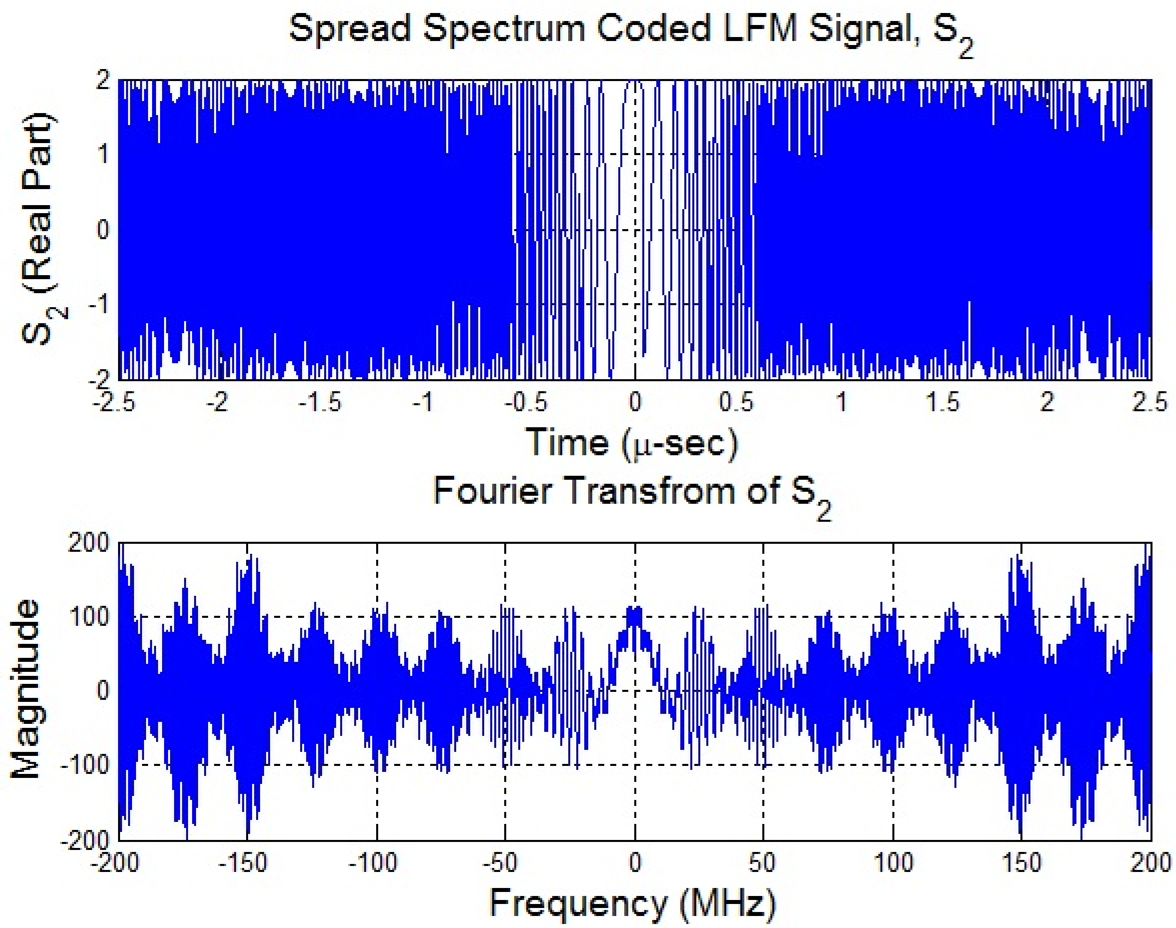

Fig. 3.3. Spread spectrum coded LFM signal s_2 and corresponding Fourier transform. Chirp rates used were, $\alpha_1 = (2B)/TP_2$ and $\alpha_2 = (-2B)/TP_2$, where B is the bandwidth of the LFM signal after applying spread spectrum code, TP_2 is duration of the signal. Walsh-Hadamard code of length 64 has been used to spread the LFM signal.

$$s_2(t) = \sum_{n}^{M-1} D_n P(t - nT_C) e^{i\pi\alpha_2 t^2}, \tag{3.11}$$

where

$$\begin{aligned} C_m &= \text{first code sequence,} \\ D_n &= \text{second code sequence (different from } C_m\text{),} \\ T_C &= \text{chip time,} \\ P(t) &= \text{rectangular pulse,} \\ \alpha_1,\ \alpha_2 &= \text{LFM chirp rates of s}_1\text{(t) and s}_2\text{(t)} \end{aligned}$$

Then, the cross-ambiguity function of $s_1(t)$ and $s_2(t)$ can be expressed as

$$\chi_{s_1,s_2}(\tau,\nu) = \int_R s_1(t)s_2^*(t-\tau)e^{i2\pi\nu t}dt$$

$$= \int_R \left(\sum_{m=0}^{M-1} C_m P(t-mT_C).e^{i\pi\alpha_1 t^2}\right) \cdot \left(\sum_{n=0}^{M-1} D_n P(t-nT_c-\tau).e^{i\pi\alpha_2(t-\tau)^2}\right)^* e^{i2\pi\nu t}dt$$

$$= \sum_{m=0}^{M-1}\sum_{n=0}^{M-1} C_m D_n^*. \int_R P(t-mT_C)P^*(t-nT_C-\tau).e^{i\pi[\alpha_1 t^2-\alpha_2(t-\tau)^2]}e^{i2\pi\nu t}dt$$

Let,

$$f(m,n,\tau,\nu) := \int_R P(t-mT_C)P^*(t-nT_C-\tau).e^{i\pi[\alpha_1 t^2-\alpha_2(t-\tau)^2]}e^{i2\pi\nu t}dt$$

Therefore,

$$\chi_{s_1,s_2}(\tau,\nu) = \sum_{m=0}^{M-1}\sum_{n=0}^{M-1} C_m D_n^* f(m,n,\tau,\nu). \tag{3.12}$$

In Chapter 2, we defined ε-*orthogonality* of two signals by measuring cross-ambiguity i.e.

$$\max_{\tau,\upsilon} \frac{\int_{-\infty}^{\infty} s_1(t)s_2(t-\tau)e^{i2\pi\upsilon t}dt}{E_1E_2} \leq \varepsilon,$$

where E_1 is the energy in signal $s_1(t)$ and E_2 is the energy in signal $s_2(t)$, and ε is the threshold.

Equation (3.12) above represents the fundamental equation of a *Spread Spectrum Coded LFM (SSCL)* signaling. In particular, it represents the output of the matched-filter of $s_1(t)$ to a delayed and Doppler shifted version of $s_2(t)$. As described in Chapter 2, this allow us to measure the approximate orthogonality (ε-*orthogonal*) of $s_1(t)$ and

$s_2(t)$. This is fundamental because it represents overlap between two spread spectrum modulated LFM signals when processed by matched filter. More specifically, if two signals s_1 and s_2 are different (i.e. orthogonal), the cross-ambiguity between them will be low; on the other hand, if they are the same signals, then the cross-ambiguity (i.e. auto-ambiguity) between them will be high. From equations (3.10) or (3.11), we can see that the diversity features of our proposed waveforms include chirp rate, type of code, length of code, and frequency. Some important properties of the SSCL signaling have been listed below. The proofs for these properties are straightforward.

1. ***Cross-Ambiguity property of SSCL signaling:*** When the codes C_m and D_n are orthogonal, $\chi_{s_1,s_2}(\tau,\nu) \cong 0$. This property implies that matched filter response of a transmitted signal s_1 with a received signal s_2 will be small if s_2 does not have the same code as the s_1 (i.e. cross-ambiguity function will be almost zero when C_m and D_n are orthogonal).

2. ***Auto-Ambiguity property of SSCL signaling:*** When codes C_m and D_n are the same, $\chi_{s_1,s_2}(\tau,\nu)$ will provide the highest return. This property implies that matched filter response of a transmitted signal s_1 with a received signal s_2 will be the highest if s_2 has the same code as the s_1 (this also implies that $s_1 = s_2$).

3. ***Code property of SSCL signaling:*** The type of code used, such as Walsh-Hadamard, Gold, Kasami codes, will influence the cross-ambiguity or auto-ambiguity response (i.e. degree of orthogonality of the received signal).

4. ***Code length property of SSCL signaling:*** The length of code, such as 8, 16, 32 or 512, will also determine degree of orthogonality of the received signal. Furthermore, the length of code will also determine bandwidth expansion of the SSCL signaling and hence increased range resolution (of the coded signal).

5. ***Time bandwidth property of SSCL signaling:*** Increased time-bandwidth product can be achieved by SSCL signaling. Bandwidth expansion provides the

unique capability of this SSCL signaling. First of all, after dispreading the code, we can get our original LFM signal back and get our usual LFM signal resolution (Doppler tolerant). Secondly, by processing the coded signal we can get ultra-high resolution to separate closely spaced targets.

6. ***Bandwidth reduction property of SSCL signaling:*** We can use biorthogonal (i.e. "two sets of orthogonal codes in which each codeword in one set has its antipodal codeword in the other set" [24]) codes to reduce the bandwidth (by a factor of half) requirement of SSCL signaling. This does not affect the performance of SSCL signaling significantly.

3.6 Experiments on SSCL Signaling for Auto and Cross-ambiguity Response

We set up experiments for SSCL signaling presented in equation (3.12) and examined the auto and cross-ambiguity responses. Table 6.1 presents key parameters choosen to evaluate the auto and cross-ambiguity function of the SSCL signalinging. In terms of transmit orthogonal code selection, we used a Walsh-Hadamard code (we selected this code arbitrarily; other codes can be used as well).

We used different bandwidths for the LFM (chirp) signals that correspond to the length of the codes. Our initial bandwidth of 4 MHz has been used for the code length of 1. This is the scenario of just using a LFM signal without any spread spectrum coding. From this signal we expect to get an ambiguity response as shown in Figure 1. Then we used a bandwidth of 36 MHz that corresponds to code length 8. The new bandwidth has been calculated using the following formula (as a result of spread spectrum coding):

$$B = \left(\frac{1}{TC_1} + \frac{1}{TP_1}\right), \tag{3.13}$$

where, $TC_1 = TP_1/NC_1$ and assume that $NC_1 = NC_2$.

Similarly, we have calculated and used bandwidths of 260 MHz and 1000 MHz which corresponds to the code lengths of 64 and 256 respectively. In addition, we

Table 3.1
Experimental parameters used to examine SSCL waveform presented in equation (3.12).

Parameters	Values
Bandwidth (B)	4,36,130,260,1000 MHz
First Pulse Duration(TP_1)	10 μsec
Second Pulse Duration (TP_2)	10 μsec
First Pulse Chirp Rate(α_1)	$(B)/TP_1$
Second Pulse Chirp Rate (α_2)	$(-2B)/TP_2$
First Pulse Code Length (NC_1)	1,8,32,64,256
Second Pulse Code Length (NC_2)	1,8,32,64,256

used a bandwidth of 130 MHz which corresponds to a code length of 32 to experiment with a biorthogonal code. The length 32 biorthogonal code has been generated using a length 64 Walsh-Hadamard code.

3.7 Results and Analysis

To reiterate our research problem, we want to design waveforms for diversity radar that should remain orthogonal both on transmit and receive and should be Doppler tolerant. The chief benefit of the waveforms that remain orthogonal on receive is that we can separate them to be matched filter with their corresponding transmitted waveforms. The cross-ambiguity function can be used as a measure of the orthogonality of one signal, $s_1(t)$, and a time-delayed Doppler shifted version of another signal, $s_2(t-\tau)e^{i2\pi\nu t}$. In particular, cross-ambiguity provides the response of a matched filter matched to the first signal when excited by the second signal.

Table II presents key results (auto- and cross-ambiguity) obtained from our waveforms (i.e. SSCL signaling) presented in equations (3.10) and (3.11). Intuitively, for

Table 3.2
SSCL signaling Performance Analysis. In this table, B is the Bandwidth, Max. AAF is the Maximum Auto-Ambiguity Function, Max. CAF is maximum cross-ambiguity function.

Code Type	Code Length	Bandwidth (MHz)	Max. AAF (dB)	Max. CAF (dB)
-	1	4	0	-5
Walsh-Hadamard	8	36	0	-9
Walsh-Hadamard	64	260	0	-14
Walsh-Hadamard	256	1000	0	-16
Biorthogonal	32	130	0	-13.5

a given code, the longer it is, the better cross-ambiguity response we expect. From Table II, we can see that with code length of 1, maximum cross-ambiguity response observed was about -5 dB. This case is just using LFM signal with chirp diversity; no influence from spread spectrum code. With code length of 8, maximum cross-ambiguity response observed was about -9 dB. In this case, we started to see the influence of spread spectrum code. Similarly, using the code length of 64 and 256, we have observed improved cross-ambiguity response.

Figure 3.4 shows auto-ambiguity response of the signal s_1. The code used was Walsh-Hadamard of length 64. This is the case, where $s_1 = s_2$ and $C_m = D_n$. As expected, the auto-ambiguity function takes the shape of the LFM signal presented in Figure 1.

Figure 3.7 shows cross-ambiguity response of the signals s_1 and s_2. Two orthogonal codes used were Walsh-Hadamard sequences of length 64. We also applied two different chirp rates for each signals. The key attribute of Figure 3.7 is that we don't

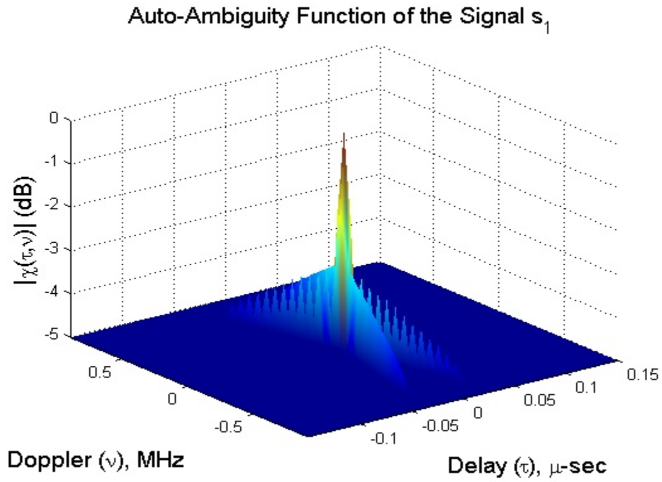

Fig. 3.4. Auto-ambiguity function (AAF) of the LFM signal s_1. First, we generated s_1 using an up-chirp rate, $\alpha_1 = (B)/TP_1$ and down-chirp rate, $\alpha_2 = (-B)/TP_1$. Then this signal was spreaded with Walsh-Hadamard code of length 64. The AAF has been evaluated on the spreaded signal.

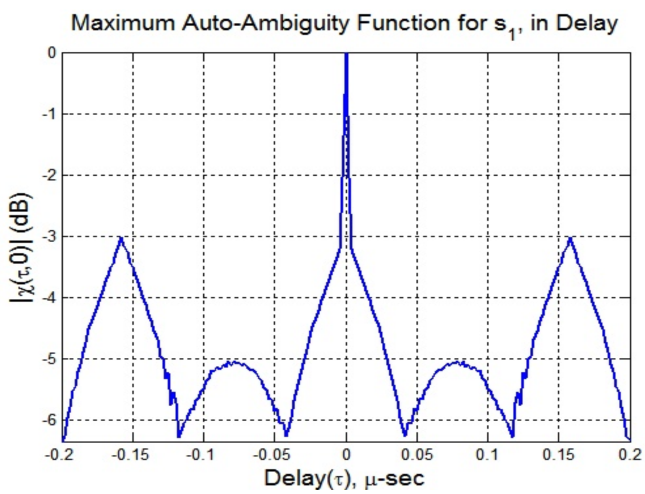

Fig. 3.5. Zero-Doppler cut (i.e. when $\nu = 0$) of the auto-ambiguity function (AAF) presented in Fig. 3.4 for signal s_1.

see the shape of LFM signal ambiguity response anymore. This is due to the fact that

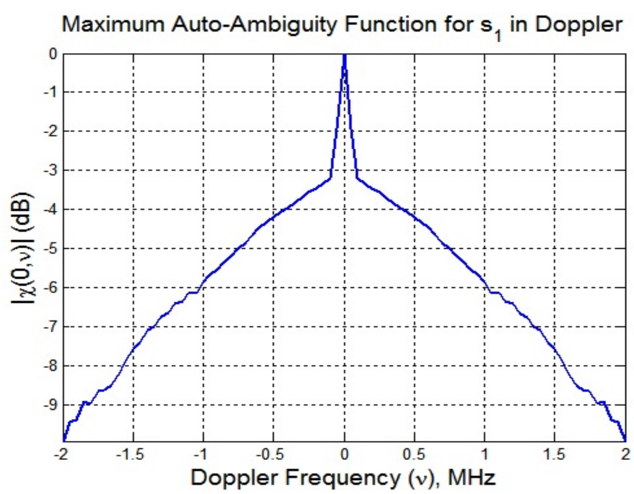

Fig. 3.6. Zero-delay cut (i.e. when $\tau = 0$) of the auto-ambiguity function (AAF) presented in Fig. 3.4 for signal s_1.

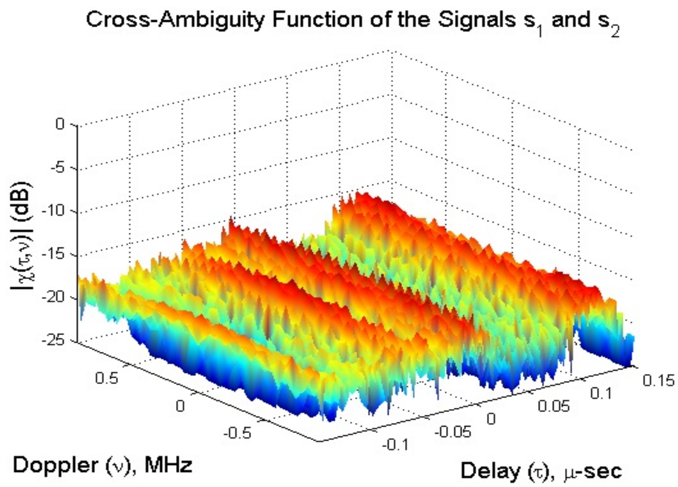

Fig. 3.7. Cross-ambiguity function (CAF) of two LFM signals s_1 and s_2. First, we generated s_1 using an up-chirp rate, $\alpha_1 = (B)/TP_1$ and down-chirp rate, $\alpha_2 = (-B)/TP_1$. Second, we generated S_2 using an up-chirp rate, $\alpha_1 = (2B)/TP_1$ and down-chirp rate, $\alpha_2 = (-2B)/TP_1$. Then this signals were spreaded with Walsh-Hadamard code of length 64. The key attribute of this figure is that maximum cross-ambiguity becomes about -14dB.

signals s_1 and s_2 were multiplied by orthogonal codes. We observe that the maximum cross-ambiguity response is approximately -14 dB.

From Table II, we can see that by increasing the code length, we can achieve lower cross-ambiguity and hence nearer orthogonality of the received signals. However, the longer the code, the greater the bandwidth expansion. In practical applications, we know that bandwidth is a scarce resource. In particular, using a bandwidth greater than 1 GHz could be very expensive for various reasons. In such a scenario, we can use biorthogonal coding to reduce the bandwidth requirements of the SSCL signaling by a factor of one-half. In Table II, we see that by using a biorthogonal code of length 32 our waveform achieves a cross-ambiguity response of about - 13.5 dB, which almost comparable (-14 dB) to using Walsh-Hadamard code of length 64. However, the biorthogonal code reduces the bandwidth by a factor of one-half.

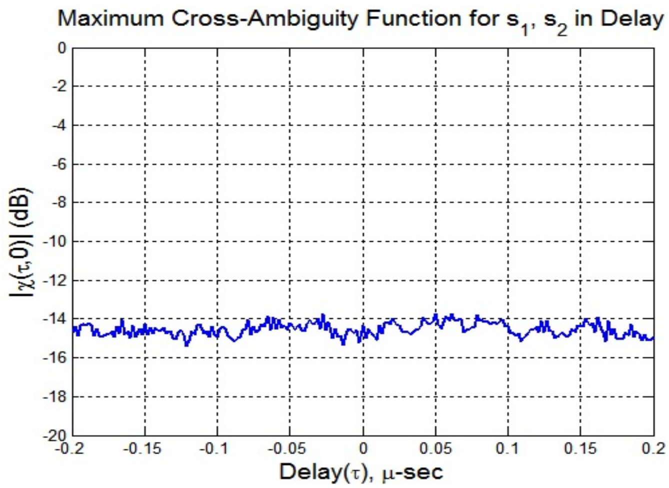

Fig. 3.8. Zero-Doppler cut (i.e. when $\nu = 0$) of the cross-ambiguity function (CAF) presented in Fig. 3.7 for signals s_1 and s_2.

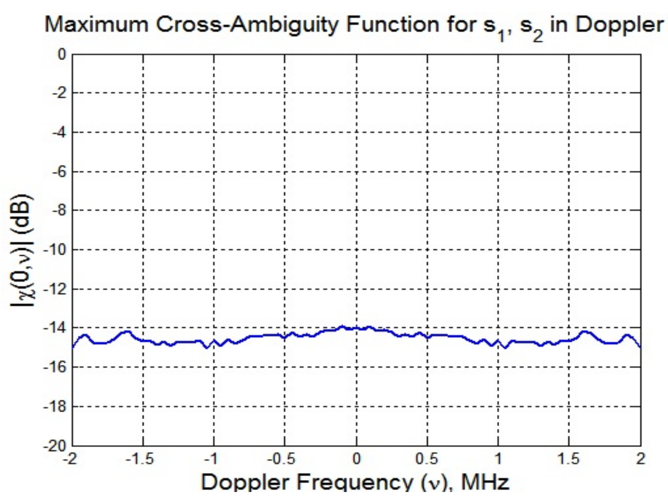

Fig. 3.9. Zero-delay cut (i.e. when $\tau = 0$) of the cross-ambiguity function (CAF) presented in Fig. 3.7 for signals s_1 and s_2.

3.8 Conclusion

The pivot of this chapter is the design of orthogonal (both transmit and receive), Doppler tolerant waveforms for the waveform-agile radar application. We called our orthogonal waveforms "Spread Spectrum Coded LFM (SSCL)" signals. We then present some important properties of the SSCL signals. We adopt cross-ambiguity as a measure to evaluate the orthogonality of two waveforms. We confirmed the empirical understanding that waveforms become more orthogonal as the code length is increased. In the next chapter, we will present high resolution imaging and design considerations for our orthogonal waveforms.

4. ADVANCED PROCESSING AND DESIGN CONSIDERATION FOR OUR WAVEFORMS

4.1 Introduction

Target resolution is a key charateristic of good radar waveforms because it allows the separation of targets into classes based on features. Hence, in designing radar waveforms, engineers must consider the resolution capability of the waveforms. In general, long unmodulated pulse provides poor range resolution. As a result, short pulses are desired for obtaining good range resolution. However, in order to get sufficient energy on target to achieve reasonable detection performance, the radar must transmit waveform at very high peak power, which complicates waveform design. It turns out it is not the transmitted pulse's short duration, but rather its large bandwidth that allows for high range resolution. Thus large bandwidth can be utilized to achieve high target resolution. Often phase and frequency modulations are used to generate high bandwidth, long duration signals.

In this chapter, we will introduce advanced processing capability of our proposed waveforms to resolve targets. We then will describe dual processing of the same received waveforms for ultra-high resolution and Doppler tolerant (low resolution) processing. Finally, we will present biorthogonal code utilization to reduce bandwidth when code length is large.

4.1.1 Contributions and Chapter Organization

The contribution of our research on advanced processing and design of our waveforms are:

1. Usually individual transmit waveforms are designed with fixed bandwidth. For this reason, resolution of these waveforms are also fixed. Our waveforms are designed by combining LFM signals and spread spectrum coding. So, our waveforms contain an LFM signal's bandwidth as well as bandwidth expansion due to spread spectrum coding. As a result, if we process our received waveforms using matched filtering of the spreaded high bandwidth signal, we get extra bandwidth for finer resolution. By contrast, if we process our received waveforms after despreading using matched filtering of the resulting LFM signals, we only get the baseline LFM waveforms bandwidth and resolution capability. Further, when we matched filter two despreaded LFM signals (one could be an up-chirp signal and the other could be a down-chirp signal) with their respective matched filters, it is as if we get two simultaneous non-interfering measurements with each of the LFM signals. This is a unique capability of our proposed waveforms.

2. Our research shows that the orthogonality of our waveforms improve with the length of the spreading code. However, the use of long spreading codes also expands the bandwidth of our waveforms. To mitigate this issue, we investigated biorthogonal codes. We found that biorthogonal code can be used when spreading code is long because it reduces bandwidth expansion by a factor of half without significant increase to the cross-ambiguity.

The rest of the chapter is organized as follows. In the next section, we present the high resolution imaging capability of our waveforms. We demonstrate for some situations that we are not able to resolve the target without the use of bandwidth provided by spread spectrum coding. We present biorthogonal codes in section 4.3. An example has been provided to demonstrate biorthogonal codes generation from orthogonal codes. Finally, in Section 4.3, we present performance (i.e. cross-ambiguity comparison) of biorthogonal codes with Walsh-Hadamard codes.

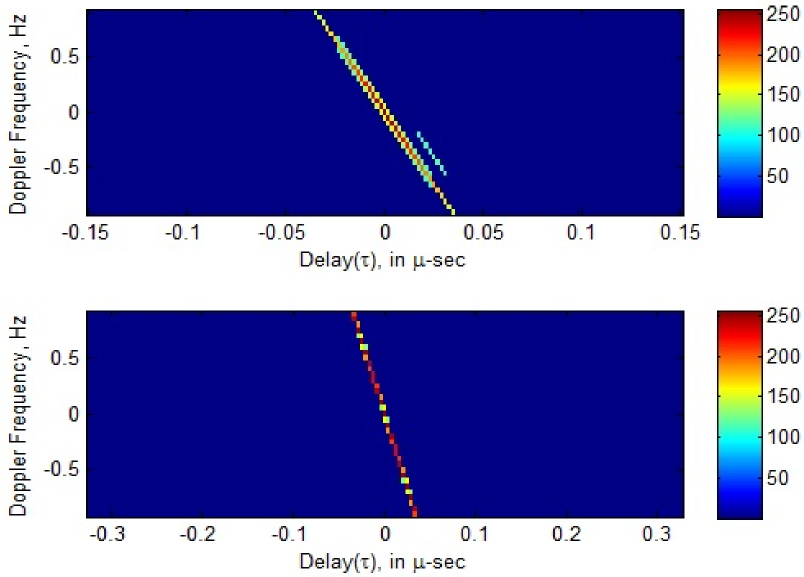

Fig. 4.1. Images of two point targets with a single chirp; strong target is located at the center (0,0) of delay-Doppler plane; the weak target is located at slightly off center. The top image demonstrates that processing the received signals with spread spectrum code on it, we can detect both targets. The bottom image demonstrates that without spread spectrum code, we cannot detect the weak target.

4.2 High Resolution Imaging

One of the merits of our proposed waveforms is high resolution imaging. This waveform allows processing of received signals in two different ways: one approach provides high resolution imaging and the other approach allows Doppler tolerant processing. We observe that because of spread spectrum coded LFM waveforms (that enables high bandwidth), if we process (matched filter) the received signal without despreading, we can obtain high resolution images (i.e. separating a weak target relatively easily that is located very closely to a stronger target). On the other hand, if we despread the received signal and get back our original LFM bandwidth, we will get Doppler tolerant processing but degraded resolution to separate a weak

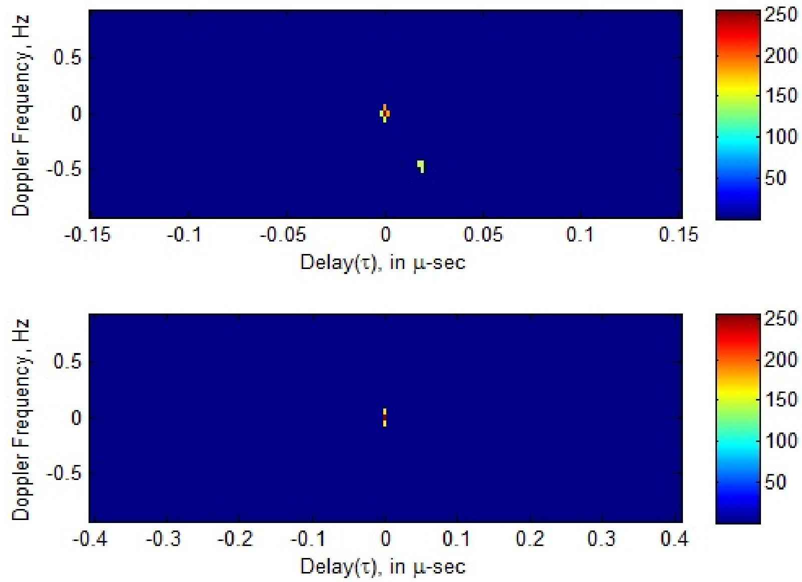

Fig. 4.2. Images of two point targets with two chirps; strong target is located at the center (0,0) of delay-Doppler plane; the weak target is located at slightly off center. The top image demonstrates that processing the received signals with spread spectrum code on it, we can detect both targets. The bottom image demonstrates that without spread spectrum code, we cannot detect the weak target.

target that is close to a strong target. For this experiment, we consider two point targets that are closely spaced. One target (at the center of delay-Doppler plane) is stronger (higher radar cross section) than the other (slightly off center). Our goal is to separate these two targets visually (i.e. distinguishing these targets in the image domain). In Figure 4.1, the top image has been generated with spread spectrum code on it (with bandwidth of about 260MHz). The bottom image has been generated after despreading the received signal (with LFM bandwidth of 30MHz). The top image demonstrates that with certain threshold (without CFAR or other sophisticated processing) we can detect both targets if we process the received signals with spread spectrum code on it. The bottom image demonstrates that with certain threshold we cannot detect both targets just using LFM signal bandwidth.

Figure 4.2 has been generated with waveforms with two chirps (up and down), that provide better interference suppression capability. The top image has been generated with spread spectrum code on it. This waveform provides a bandwidth of about 260MHz. The bottom image has been generated after despreading the receive signal and hence it provides only LFM bandwidth of 30MHz. As shown in Figure 4.1, the top image demonstrates that with certain threshold we can detect both targets if we process the received signals with the spread spectrum code on it. The bottom image demonstrates that with certain threshold we may not detect both targets using just the LFM signal bandwidth.

4.3 Diversity Waveforms Processing for Enhanced Delay-Doppler Resolution

A very important attribute of our proposed waveform is that we can approximate non-interfering measurement and processing when two or more waveforms are employed to discriminate multiple scatters in delay and Doppler. It was reported by Guey and Bell [5] that single radar waveform of constrained time-bandwidth product makes it difficult to distinguish two or more targets closely spaced in both delay and Doppler. It was shown that by using diverse waveforms, enhanced discrimination in delay-Doppler measurements is possible. The key assumption in this investigation was that waveforms should not interfere with each other. In other words, the delay-Doppler imaging system should be able to get several independent non-interfering measurements of the target environment.

When radar system is capable of operating multiple waveforms using several independent channels without any interference, output of each channel has a two-

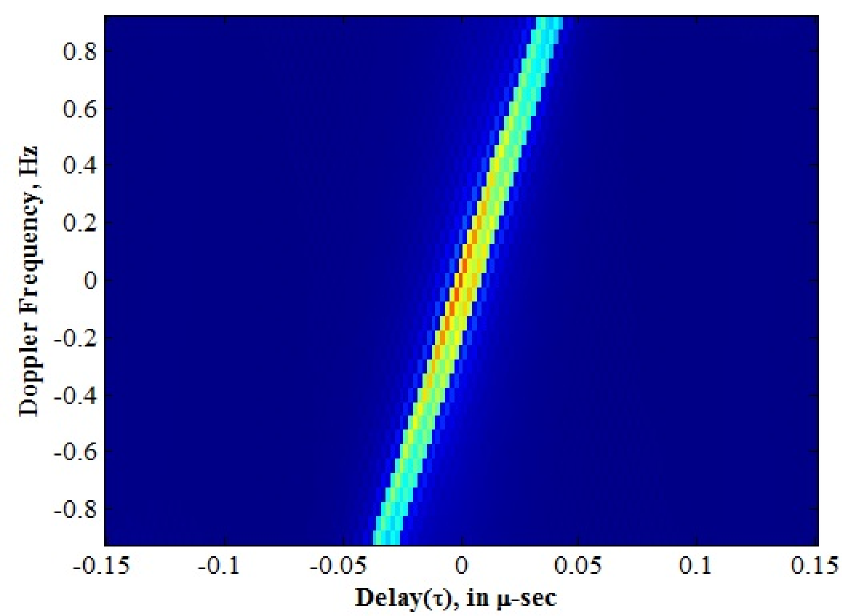

Fig. 4.3. Two targets are closely-spaced in the image scene. Measurement with a single chirp could be difficult to resolve these targets

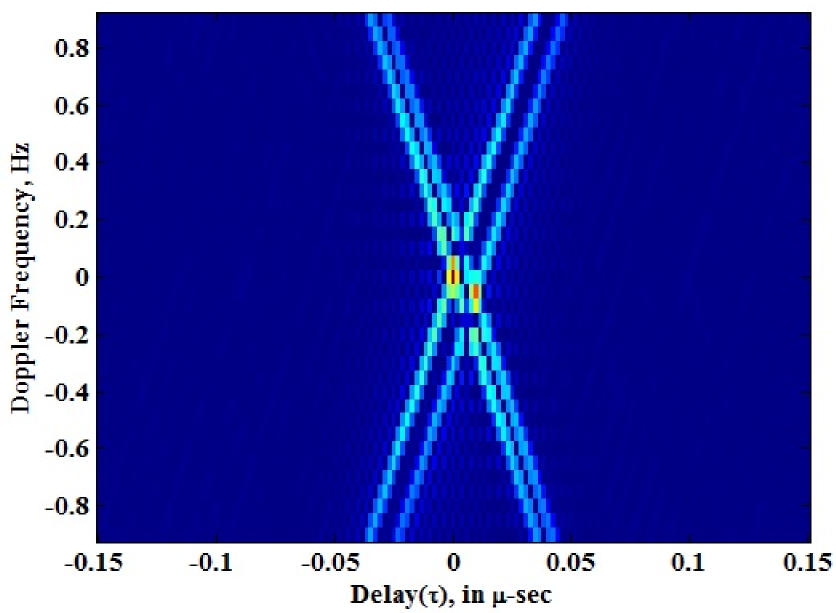

Fig. 4.4. Two targets are closely-spaced in the image scene. By using two waveforms we can resolve these targets. First we make a measuremnet with a coded up-chirp waveform, then with a coded down-chirp waveform. After despreading operation at the receiver, we coherently combine these two waveforms. This provides independent look of the point scatterers by two different waveforms, thus better delay-Doppler resolution

dimensional image of the target environment. For a point target located at $(\tau_0,\ \upsilon_0)$, this can be formulated as

$$\begin{aligned}
\mathrm{O}_T^0(\tau,\upsilon) &= e^{i\phi}e^{-i2\pi(\upsilon-\upsilon_0)\tau_0}\chi_{s_0}(\tau-\tau_0,\upsilon-\upsilon_0)\\
&= \tilde{\chi}_{s_0}(\tau-\tau_0,\upsilon-\upsilon_0)\\
\mathrm{O}_T^1(\tau,\upsilon) &= e^{i\phi}e^{-i2\pi(\upsilon-\upsilon_0)\tau_0}\chi_{s_1}(\tau-\tau_0,\upsilon-\upsilon_0)\\
&= \tilde{\chi}_{s_1}(\tau-\tau_0,\upsilon-\upsilon_0)\\
\vdots\quad &\vdots\\
\mathrm{O}_T^{N-1}(\tau,\upsilon) &= e^{i\phi}e^{-i2\pi(\upsilon-\upsilon_0)\tau_0}\chi_{s_0}(\tau-\tau_0,\upsilon-\upsilon_0)\\
&= \tilde{\chi}_{s_{N-1}}(\tau-\tau_0,\upsilon-\upsilon_0)
\end{aligned}$$

where $\mathrm{O}_T^i(\tau,\upsilon)$ is the image obtained through the i-th channel and $\tilde{\chi}$ denotes complex modulation factor $e^{i\phi}e^{-i2\pi(\upsilon-\upsilon_0)\tau_0}$. By coherently summing the images up, we get the composite image,

$$\mathrm{O}_T^C(\tau,\upsilon) = e^{i\phi}e^{-i2\pi(\upsilon-\upsilon_0)\tau_0}\sum_{i=0}^{N-1}\chi_{s_i}(\tau-\tau_0,\upsilon-\upsilon_0).$$

The above expression can be thought of as an image of a point target generated by a new point-spread function

$$C(\tau,\upsilon) = \sum_{i=0}^{N-1}\chi_{s_i}(\tau,\upsilon)$$

This new point-spread function is known as *Composite Ambiguity Function (CAF)* or *Combined Ambiguity Function* [10].

Now, consider we transmit two (could be more) spread spectrum coded LFM waveforms. One LFM waveform is made up of an up-chirp and the other with a down-chirp. After despreading operation at the receiver, we can get two non-interfering LFM signals. Coherent combination of these two waveforms will provide an independent look of the point scatterers by two different waveforms. This provides better delay-Doppler discrimination to resolve closely-spaced targets. Figure 4.3 and Figure 4.4 illustrate this exploitation capability of our proposed waveform.

4.4 Biorthogonal Codes

In radar waveforms design, various codes such as Barker code, Costas code, Frank code, Polyphase codes have been studied extensively. In digital communication, biorthogonal codes have been used to examine bit error performance. It was reported that biorthogonal codes offer improved bit error performance compare to orthogonal codes [24]. Further, biorthogonal codes require only half the bandwidth of orthogonal codes. However, biorthogonal codes have not been applied to radar waveforms design problems. Hence, we examined biorthogonal codes for our orthogonal waveforms design.

Biorthogonal codes can be obtained from any orthogonal codes. Here we present biorthogonal codes generation from the orthogonal Walsh-Hadamard codes [24]. Biorthogonal codes can be defined by the following equation:

$$B_k = \begin{bmatrix} O_{k-1} \\ \bar{O}_{k-1} \end{bmatrix}, \tag{4.1}$$

where O_{k-1} is the orthogonal codeword of dimension $2^{k-1} \times 2^{k-1}$ and B_k is the biorthogonal codeword of dimension $2^k \times 2^k$

4.4.1 An Example of Biorthogonal Codes Generation:

The Walsh-Hadamard code of length 4 is given by

$$O_2 = \begin{bmatrix} 0 & 0 & 0 & 0 \\ 0 & 1 & 0 & 1 \\ 0 & 0 & 1 & 1 \\ 0 & 1 & 1 & 0 \end{bmatrix} = \begin{bmatrix} O_1 & O_1 \\ O_1 & \overline{O}_1 \end{bmatrix}, \text{ Where } O_1 = \begin{bmatrix} 0 & 0 \\ 0 & 1 \end{bmatrix}$$

Similarly, Walsh-Hadamard code of length 8 is given by:

$$O_3 = \begin{bmatrix} 0 & 0 & 0 & 0 & 0 & 0 & 0 & 0 \\ 0 & 1 & 0 & 1 & 0 & 1 & 0 & 1 \\ 0 & 0 & 1 & 1 & 0 & 0 & 1 & 1 \\ 0 & 1 & 1 & 0 & 0 & 1 & 1 & 0 \\ 0 & 0 & 0 & 0 & 1 & 1 & 1 & 1 \\ 0 & 1 & 0 & 1 & 1 & 0 & 1 & 0 \\ 0 & 0 & 1 & 1 & 1 & 1 & 0 & 0 \\ 0 & 1 & 1 & 0 & 1 & 0 & 0 & 1 \end{bmatrix} = \begin{bmatrix} O_2 & O_2 \\ O_2 & \overline{O}_2 \end{bmatrix}$$

Using equation (4.1), we find biorthogonal codeword from 3-bit data as follows:

$$B_3 = \begin{bmatrix} O_2 \\ \overline{O}_2 \end{bmatrix} = \begin{bmatrix} 0 & 0 & 0 & 0 \\ 0 & 1 & 0 & 1 \\ 0 & 0 & 1 & 1 \\ 0 & 1 & 1 & 0 \\ 1 & 1 & 1 & 1 \\ 1 & 0 & 1 & 0 \\ 1 & 1 & 0 & 0 \\ 1 & 0 & 0 & 1 \end{bmatrix}$$

4.5 Bandwidth Reduction Using Biorthogonal Codes

One important parameter that contributes to cross-ambiguity reduction (i.e. orthogonality of two signals) is the code length. We observe that as the code length increases, cross-ambiguity also decreases (i.e. two signals become more orthogonal). However, longer code also expands total bandwidth of the signal (due to spectrum spreading). In practical applications, a bandwidth of more than one gigahertz increases complexity to the system. To address this issue, we investigated biorthogonal codes for our orthogonal waveforms design.

Table 4.1
Cross-ambiguity comparison between biorthogonal and Walsh-Hadamard codes. We observe that biorthogonal codes generate comparable cross-ambiguity with Walsh-Hadamard codes though code lengths are half.

Code Type	**Code Length**	**Cross-ambiguity (dB)**
Biorthogonal	32	-13.5
Biorthogonal	64	-14.6
Biorthogonal	128	-16.5
Biorthogonal	256	-17.5
Walsh-Hadamard	64	-14.0
Walsh-Hadamard	128	-16.04
Walsh-Hadamard	256	-17.33
Walsh-Hadamard	512	-18.2

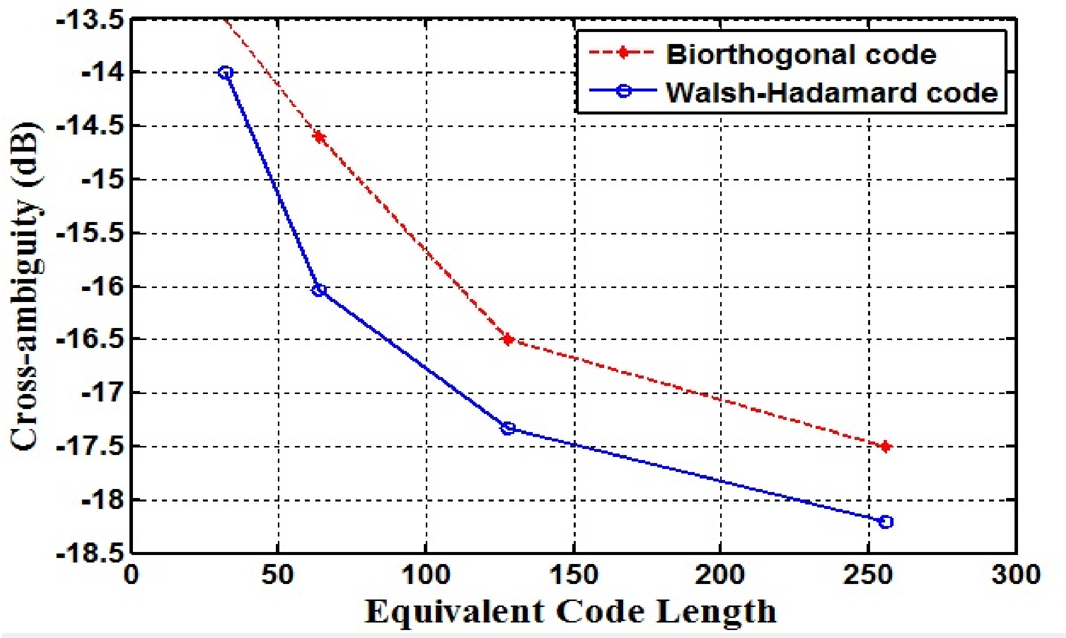

Fig. 4.5. Cross-ambiguity comparison between biorthogonal and Walsh-Hadamard codes. Notice that equivalent length biorthogonal code has been compared with Walsh-Hadamard code. As discussed, performance of biorthogonal code is comparable to Walsh-Hadamard code while biorthogonal codes reduces bandwidth by a factor of half.

Biorthogonal codes are known to provide comparable performance to orthogonal codes but require only half the length of orthogonal codes. Consequently, biorthgonal code may reduce bandwidth requirements by a factor of half. We have generated biorthogonal codes of various lengths (32, 64, 128, 256) from the orthogonal Walash-Hadamard codes of lengths (64, 128, 256, 512) [24] and evaluated cross-ambiguity by applying these codes to our waveforms. Table 4.1 shows comparable performance of biorthogonal codes with Walsh-Hadamard codes though code length is half for the former. We observe that length 256 biorthogonal codes generate comparable (-17.5 vs. -18.2 dB) cross-ambiguity with length 512 Walsh-Hadamard codes. Figure 4.5 also illustrates cross-ambiguity comparison between biorthogonal and Walsh-Hadamard codes. In the plot we use the term "Equivalent Code Length" to show that biorthogonal code length was half (and hence bandwidth is also half) compare to Walsh-Hadamard code.

4.6 Conclusion

In this chapter, we present that our waveforms allow processing of received waveforms in two different ways simultaneously. In the first method, we despread the received waveforms. We recover our baseline LFM signal bandwidth and achieve the resolution capability of a simple LFM signal. In the second method, we process the received signal with the spread spectrum coding. For this case, we achieved extra bandwidth due to spectrum spreading. This allows high resolution capability to separate closely spaced targets. This is a unique capability of our proposed waveform. We also show that we can reduce bandwidth (when code length is large) of our proposed waveforms by using biorthogonal codes without sacrificing cross-ambiguity value significantly.

5. A REVIEW ON RADAR DATA PROCESSING CONCEPT AND SAR SIGNAL THEORY FOR MOVING TARGET

5.1 Introduction

In this chapter, we will review radar data processing concepts. We also discuss Synthetic Aperture Radar (SAR) measurement and signal processing theory. We will introduce a SAR imaging system model and moving target imaging and indication processing. This will help us understand the problem of joint SAR imaging and ground moving target indication (GMTI) processing. In chapter 6, we will present an application of our diverse, orthogonal waveforms to solve joint SAR and GMTI processing.

5.2 An overview of Synthetic Aperture Radar

Synthetic Aperture Radar (SAR), invented by Carl A. Wiley at Goodyear aircraft company, is a mode of radar operation that can interrogate a large ground swath and provide high-resolution images of the illuminated scene. SAR has had huge impact both in civilian and military applications. In the civilian sector, SAR applications include ground mapping for disaster planning, remote sensing for vegetation and crop information, planetary exploration (e.g., the NASA Venus Radar Mapper), oil and mineral exploration, and medical imaging. In the military sector, SAR technology has been used for high resolution imaging surveillance. In SAR-based technology development, computation plays a vital role. In recent years, computation has become very cost effective [25]. Hence, SAR technologies have been evolving and benefitting both civilian and military applications, such as ground mapping by NASA for topographical information.

SAR is a mature technology and hence many well written books and journal articles have been published describing its operation. The book by Curlander and McDonough [26] provides a good overview of basic SAR theory and systems, while the monograph by Soumekh [27] provides a comprehensive treatment of SAR signal processing.

One of the applications of SAR is *moving target indication* (MTI). MTI is a form of radar processing that allows for the detection of moving targets in the presence of stationary clutter. MTI exploits the change in the phase of the returns from a moving target in a sequence of pulses. This results in a Doppler shift in the moving target that is not characteristic of stationary clutter, and this allows the returns from the moving target to be detected in the presence of large stationary clutter.

5.3 Exo-clutter and Endo-clutter GMTI

Consider, v_a be the aircraft velocity, v_r be the radial velocity in a direction of interest, λ be the wavelength of radar waveform, and θ be the angle offset from aircraft velocity vector. Then v_r is defined as

$$v_r = v_a \cos\theta$$

From above expression, the Doppler shift can be calculated as

$$f_d = \frac{2v_r}{\lambda}.$$

The clutter Doppler spectrum ($f_{d\_clutter}$) is then characterized by the spread of the Doppler frequencies that the clutter generates, and this can be defined by

$$f_{d\_\text{clutter}} = \frac{2}{\lambda}\left(v_{r\_\text{clutter\_max}} - v_{r\_\text{clutter\_min}}\right),$$

where $v_{r\_\text{clutter\_max}}$ is the maximum approaching velocity of observable clutter, and $v_{r\_\text{clutter\_min}}$ is the minimum receding velocity of observable clutter.

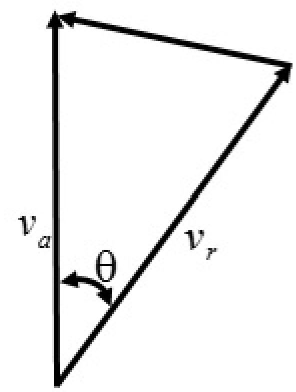

Fig. 5.1. Relationship of aircraft velocity to radial (line of sight) velocity

A radar system usually interrogates a specific angular region at a given time. The signature of the stationary objects located at that angular region will be returned as ground clutter. The ground clutter energy spectrum will be spreaded over a range of velocities depending on the speed of the radar carrying aircraft. In a range-Doppler map, this energy spectrum is known as clutter ridge or clutter band.

Definition 5.3.1 (Exo-clutter Region) *The Doppler region containing no significant clutter energy comparing to the target energy is termed the Exo-clutter region.*

Definition 5.3.2 (Endo-clutter Region) *The Doppler region containing significant clutter energy comparing to the target energy is termed the Endo-clutter region.*

One important point is that even the stationary clutter will exhibit non-uniform relative motion to a GMTI radar if the radar itself is in motion. As a result, stationary clutter will provide energy over a band of Doppler frequencies.

5.4 Displaced Phase Center Antenna Processing

The Displaced phase center antenna (DPCA) processing technique allows suppression of the ground clutter as seen by an airborne radar. Thus it allows detection of moving

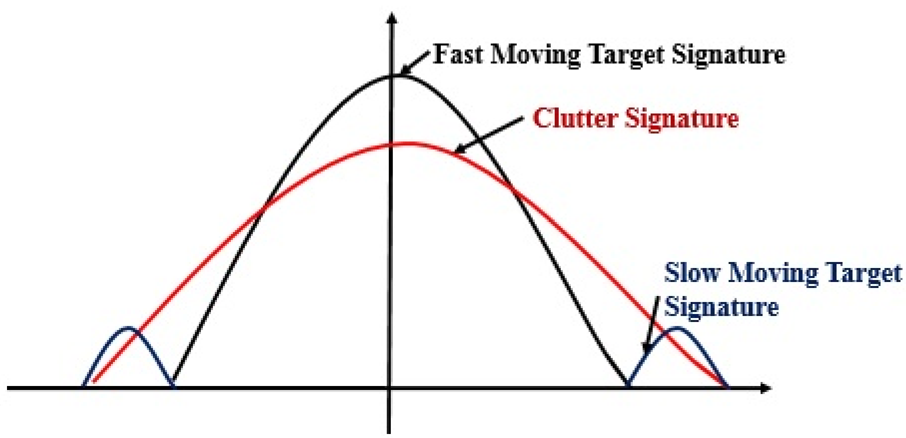

Fig. 5.2. Spectrum of fast moving target, clutter, and slow moving target.

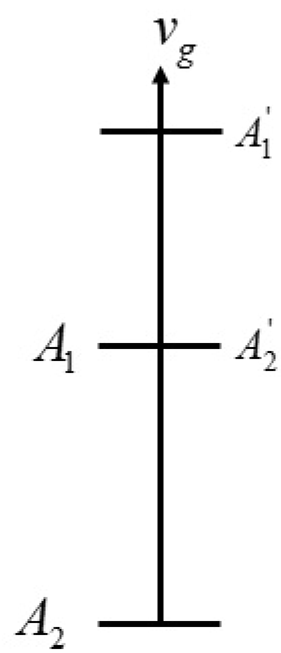

Fig. 5.3. Physical Geometry for Displaced Phase Center Antenna. A_1 and A_2 are the antenna phase centers for pulse 1. A_1' and A_2' are the antenna phase centers for pulse 2. [skolnik]

objects in the scene. In the DPCA technique, two apertures of two side-looking antennas are aligned in parallel with the aircraft's flight path. Their phase centers are separated by the distance, d. If the aircraft is moving at ground speed v_g, then the phase centers move a distance $v_g T_p$, during the pulse repetition interval, T_p.

In Fig. 5.3 the first pulse is transmitted and received by the antenna A_1. The second pulse is transmitted and received by the antenna A_2 during the next interpulse period. If $d = v_g T_p$, the antenna A_2 used on the second pulse will coincide with the antenna A_1 used on the first pulse. Thus signals received at A_1 and A_2 make it appear as if the antennas were stationary. However, a displacement of the transmitters has occurred, while the signal path difference will be the same from pulse to pulse (with negligible range error). The displacement is usually set by the radar carrying aircraft's

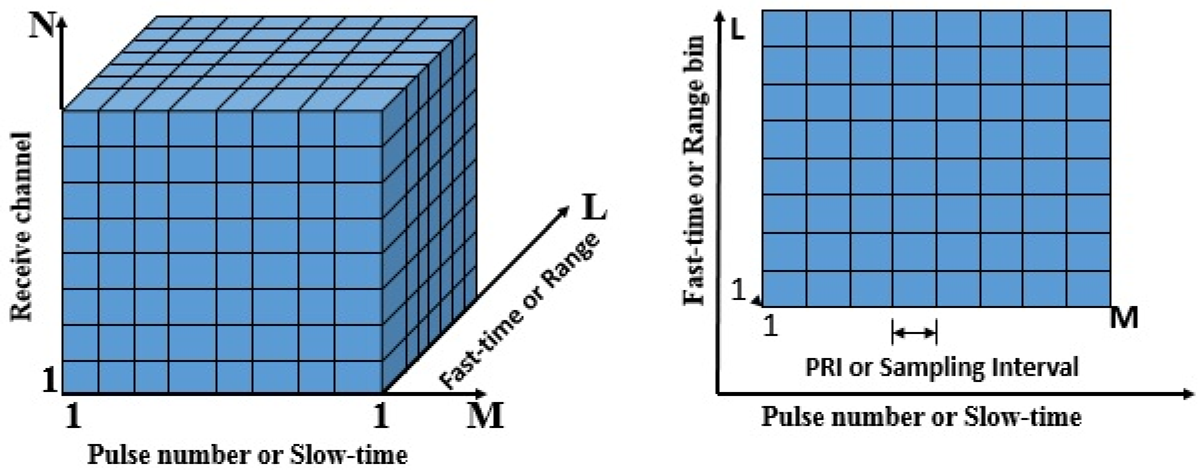

Fig. 5.4. Radar data presentation. Image to the left is the 3D data cube. Image to the right is 2D data matrix from a particular receive channel.

speed and pulse repetition frequency. If d is not equal to $v_g T_p$, then received signal measurement error occurs between A_1 and A_2. This will result in imperfect clutter cancellation.

5.5 Range-Doppler Processing

In radar measurement, a series of echoed radar pulses form a *coherent processing interval* (CPI) or dwell. Each pulse within a CPI is sampled adequately to retrieve meaningful target information. Each sampled point of a pulse is known as range bin, range gate, or resolution cell. Since a radar system samples a pulse as it arrives, the range bin is also known as fast-time sample and the range axis is also known as the fast-time axis. Figure 5.4 shows the 3D data cube and 2D data matrix of a radar measurement.

After sampling the first pulse, the next pulse is sampled and the process continues until the last pulse of the CPI is received. Hence, the pulse axis is known as the slow-

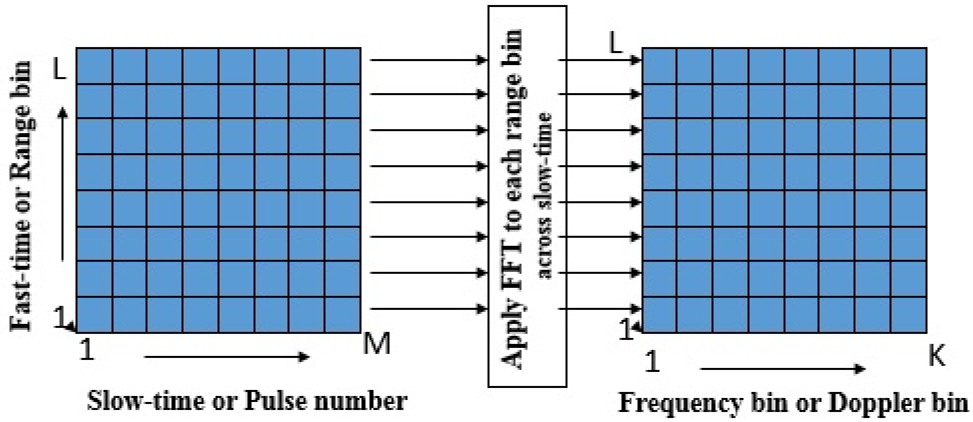

Fig. 5.5. Range-Doppler processing concept.

time axis. In SAR, slow-time is also known as the synthetic aperture axis. Multiple receive channels provide multiple CPI processing and constitute a data cube.

One dimensional filtering or Fourier transform along pulse/slow-time axis is called Doppler processing. Doppler processing provides information about moving targets. Figure 5.5 shows range-Doppler processing concept.

When trying to detect slow moving targets, standard range-Doppler processing may not work. Advanced techniques such as space-time adaptive processing (STAP), displaced phase center antenna (DPCA) based coherent change detection (CCD) must then be used to detect slow moving objects in a high clutter environment. For slow moving target detection, a STAP algorithm may not provide good results [28]. Coherent change detection can be used to detect slow movers.

5.6 SAR Imaging System Model

Figure 5.6 illustrates basic terminology for SAR system. In the SAR imaging geometry, we denote (x, y) as spatial domain coordinate and (k_x, k_y) as spatial frequency domain coordinate. Similarly, $f(x, y)$ is denoted as spatial domain signal and

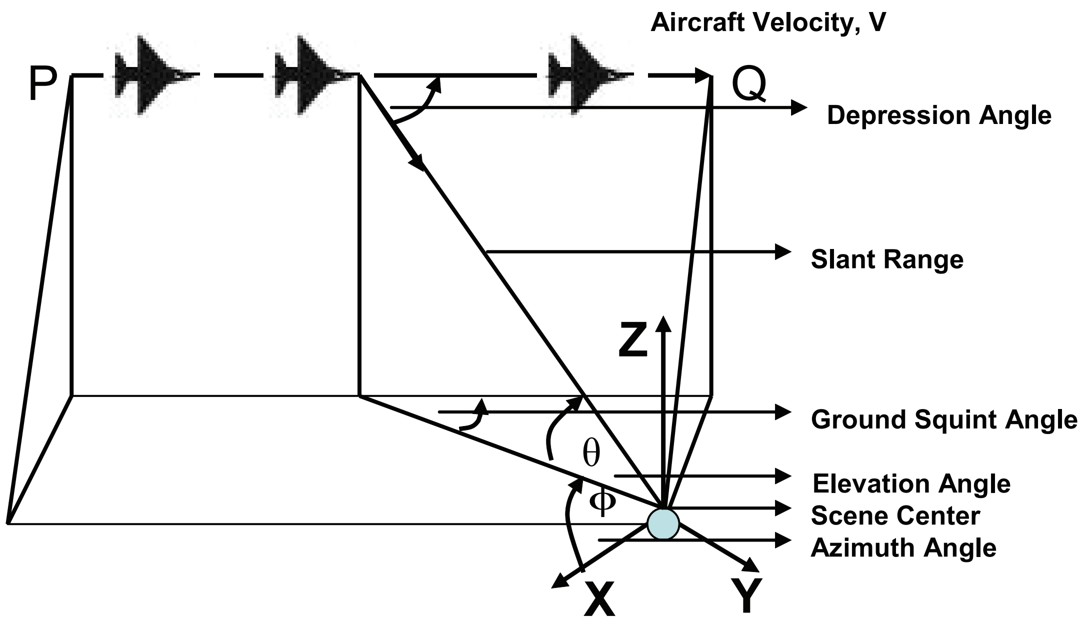

Fig. 5.6. SAR imaging terminology. Azimuth angle ϕ is the angle around the scene center. Elevation angle θ is defined to be the angle measured from the ground plane to the .

$F(k_x, k_y)$ is the spatial Fourier transform of this signal. The wavenumber k is defined as $k = \omega/c$ where ω is the temporal frequency of the radar carrier and c is the speed of light.

Figure 5.7 presents SAR imaging geometry. Consider $f(x, y)$ be the reflectivity function of the target area. A radar located at $(x = X_1, y = Y_1 + u)$ transmits signal $s(t)$ and receives signal $r(t)$. Then, total received signal can be presented as

$$r(u,t) = \iint f(x,y)\, s\left(t - 2\sqrt{\left((X_1 - x)^2 + (Y_1 + u - y)^2\right)}/c\right) dxdy. \tag{5.1}$$

By taking the fast-time / temporal Fourier transform, we get

$$r(u,\omega) = S(\omega) \iint f(x,y) \exp[-i2k\sqrt{\left((X_1 - x)^2 + (Y_1 + u - y)^2\right)}]dxdy, \tag{5.2}$$

where $S(\omega)$ is the Fourier transform of $s(t)$.

By normalizing with $S(\omega)$, we get

$$r(u,\omega) = \iint f(x,y) \exp[-i2k\sqrt{\left((X_1 - x)^2 + (Y_1 + u - y)^2\right)}]dxdy. \tag{5.3}$$

To recover target function $f(x, y)$, we apply an inversion technique. One technique that can be used is Doppler-based inversion [29]. Using this technique (and applying spatial/slow-time Fourier transform), equation (5.3) becomes

$$r(k_u, \omega) = \exp(i\sqrt{4k^2 - k_u^2}X_1 + ik_uY_1)F(\sqrt{4k^2 - k_u^2}, k_u). \tag{5.4}$$

Multiplying both sides by $\exp(-i\sqrt{4k^2 - k_u^2}X_1 - ik_uY_1)$ we get,

$$F(k_x, k_y) = \exp(-i\sqrt{4k^2 - k_u^2}X_1 - ik_uY_1)r(k_u, \omega), \tag{5.5}$$

where $k_x = \sqrt{4k^2 - k_u^2}$, $k_y = k_u$.

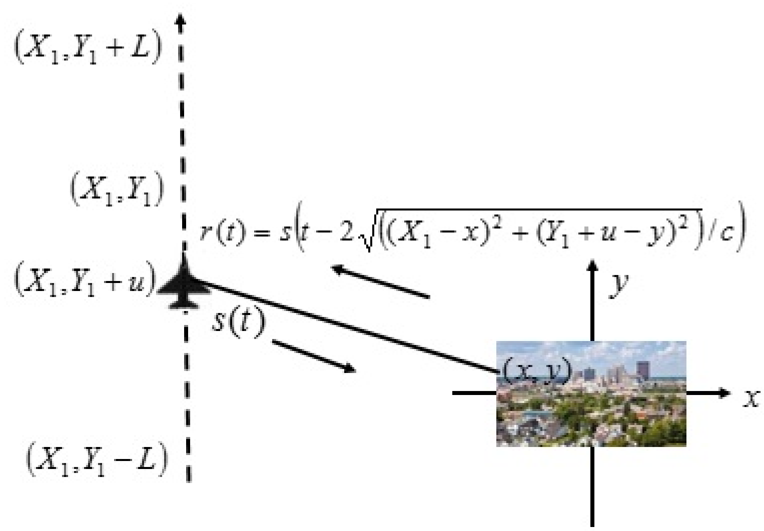

Fig. 5.7. SAR imaging geometry. The Synthetic aperture has length 2L.

5.7 Moving Target Imaging Model

Without proper processing, a moving target's signature (image) smears and is displaced from the true location of the ground scene in a SAR image. This is due to the fact that the SAR imaging scheme assumes both the ground scene and moving objects are stationary. Thus, the phase terms of the components of the received signal (containing both moving and stationary target's) are treated the same. However, the velocities of the moving targets causes their phases to become non-stationary, and inadequate handling of these phases results in inaccurate reconstruction of their images. As a result, to generate focused image of the moving targets, we have to estimate the velocity of a moving target and apply this information to the received signal and then form the images.

Several authors have published solutions to the moving target imaging problem. However, many of these solutions can be traced back to the original work published by Mehrdad Soumekh [29]. Soumekh developed moving target velocity estimation by using subaperture processing. Here we provide a general overview of this algorithm. The details of this algorithm can be found in the book *Fourier Array Imaging* [29]

We denote normalized velocity of the target (v_x, v_y) as ratio of its velocity to the radar's speed. Let $g(x, y)$ be the reflectivity function of the moving target when radar is located at $(X_1, 0)$. Then at location (X_1, u) reflectivity of the target becomes $g\left(x - v_x u,\ y - v_y u\right)$. Figure 5.8 shows imaging system geometry and target's motion path.

At (X_1, u), the fast-time (temporal) Fourier transform of the moving target's signature can be defined as

$$r\left(u, \omega\right) = \iint g\left(x - v_x u, y - v_y u\right) \exp\left[i2k\sqrt{\left(x - X_1\right)^2 + \left(y - u\right)^2}\right] dxdy$$

.

The goal of subaperture processing is to estimate (v_x, v_y) from this signal (and then correct the signal phase before applying image formation technique). Figure 5.9 shows subaperture processing technique.

This algorithm works as follows. For a given synthetic aperture length L, consider we have N consecutive received signals. The algorithm then breaks N received signals into P overlapping subaperture of length M $(M < N)$. For each of these subapertures, calculate the Doppler centroid. The mean of these centroid provides an estimate of

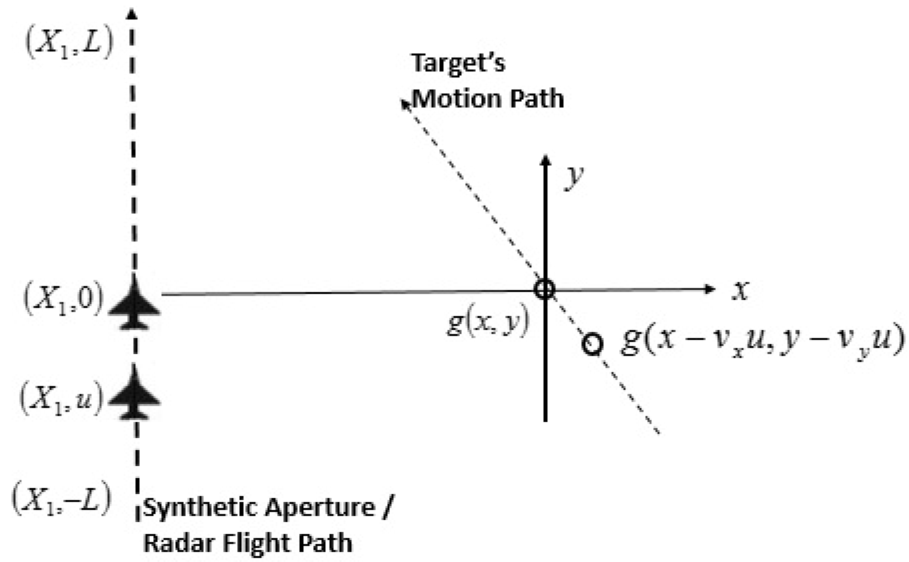

Fig. 5.8. Imaging system geometry and motion path of the moving target.

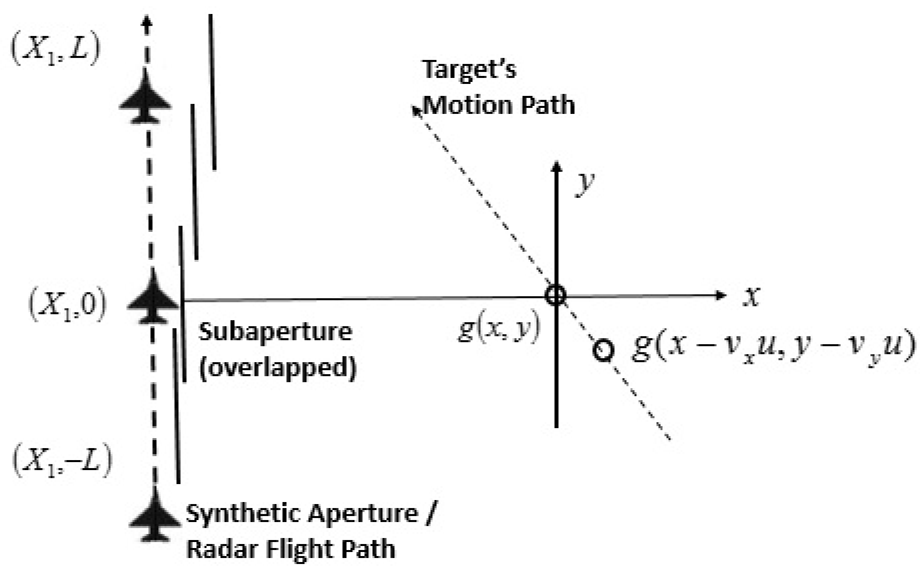

Fig. 5.9. Subaperture processing geometry to form focused image of a moving target.

the velocity vector (v_x, v_y). Figure 5.10 shows a block diagram of the subaperture based moving target velocity estimation.

5.8 Conclusion

In this chapter, we presented radar data processing concepts and an overview of synthetic aperture radar (SAR). We describe SAR imaging system model and signal processing concept. We then develop issues with moving target imaging and discussed subaperture processing to estimate moving target velocity. This estimated velocity can be used to form focused image of a moving target. These results will be used in the next chapter, where we develop an approach to joint SAR and GMTI signaling and processing.

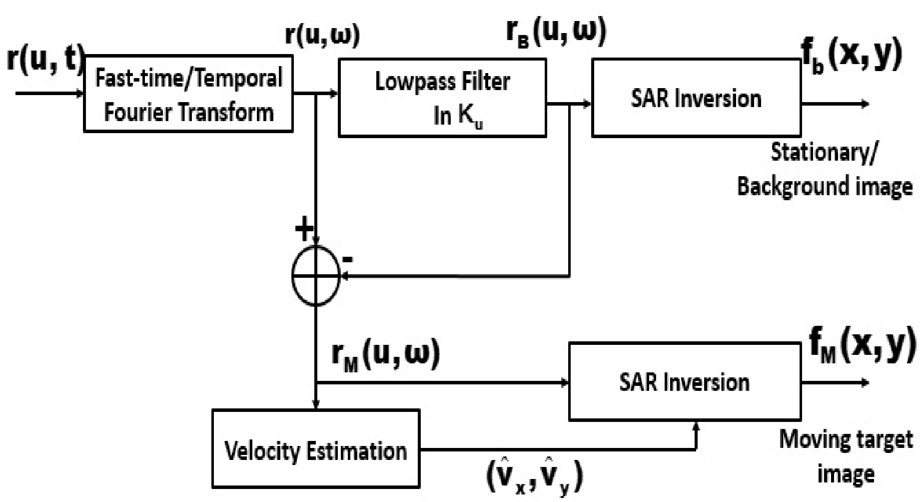

Fig. 5.10. Block diagram for subaperture based moving target velocity estimation

6. JOINT SAR AND GMTI PROCESSING

6.1 Introduction

Joint processing of Synthetic Aperture Radar (SAR) and Ground Moving Target Indication (GMTI) involves accomplishing ground imaging and detecting moving targets simultaneously. In security applications, we are interested in both surveilling and knowing the movement of objects in that particular area. For example, within an area of a football stadium, security experts may be interested in monitoring people's and vehicles' movements. Joint SAR and GMTI processing can be used for this purpose.

Developing technology to process SAR and GMTI concurrently is not straightforward. This is due to the fact that operational parameters for these two modes of radar measurement are quite different. For example, exoclutter GMTI processing (i.e. fast moving target detection) requires a high pulse repetition frequency (PRF), but a high PRF results in increased range ambiguity and an increased processing burden in SAR imaging.

Our motivation for this research is to develop a novel radar signaling and processing scheme to solve this problem efficiently. We propose combining diverse, orthogonal waveforms and introducing corresponding processing techniques to reduce the problems and complexities of joint GMTI and SAR exploitation. For the exoclutter GMTI problem, the necessary high-PRF pulse train will be used to eliminate Doppler aliasing for detecting fast moving objects. For the endoclutter GMTI (i.e. slow moving target detection) and SAR imaging problem, we will transmit low PRF pulses. The goal for using low PRF pulses for endoclutter GMTI and SAR imaging is to ensure that the range ambiguity issue has been addressed.

6.1.1 Contributions and Chapter Organization

Traditionally, radar systems are configured to operate either in GMTI or SAR processing mode, but not both simultaneously because this adds complexity to radar operations. We develop a pragmatic solution to this problem. Our investigation provides a relatively simple approach to joint GMTI and SAR processing that has not been developed before. First of all, by using diverse and orthogonal waveforms, we can employ some waveforms for exoclutter GMTI processing and the others for SAR imaging and endoclutter GMTI processing, simultaneously. Also, we can set a high PRF rate for the waveforms designated for exoclutter GMTI and a low PRF rate for the waveforms for SAR imaging and endoclutter GMTI. Further, since exoclutter GMTI does not require a high bandwidth, we can assign low bandwidth for these waveforms but assign high bandwidth for SAR waveforms. In this manner, we can make more efficient use of bandwidth, which is a scarce resource. Secondly, though we designated some waveforms for SAR and the others for exoclutter GMTI, we can use exoclutter GMTI waveforms for SAR processing to improve SNR. As mentioned earlier, high PRF waveforms introduce range ambiguity for SAR processing. This introduces the research question of how these waveforms can be used for SAR processing? The solution to this problem is that we can exploit the orthogonality of our waveforms to separate them at the receiver and thus solve the range ambiguity issue associated with high PRF waveforms.

In the next section, we present key results reported in the literature for this problem area. In section 6.4, we provide our approach for joint SAR and GMTI processing. Our assumption is that the ground scene has both fast and slow moving targets. Hence, we will require both high and low PRF rate waveforms to detect these targets. Further, we design the SAR waveforms to provide higher bandwidth than the exoclutter waveforms. We provide results of our joint SAR and GMTI processing in section 6.5. We also present an algorithm for focused image formation of moving targets in section 6.6.

6.2 A Short Literature Review on Joint GMTI and SAR Research

As an important research problem, joint GMTI and SAR processing has engaged researchers from both the defense industry [30], [31], [32], and [33] and academia [34]. Many researchers have attempted to solve only the endoclutter GMTI problem (*i.e.*, change detection-based GMTI or STAP-based GMTI). Murthy, Pillai, and Davis [28] presented frequency-jump burst waveforms for simultaneous SAR and GMTI. Davis [35] also presented a common waveform for simultaneous SAR and GMTI. As mentioned earlier, if an object moves slowly and accurate registration of two time-successive SAR images can be performed, endoclutter GMTI provides good detection performance of the slow moving object (assuming range ambiguity is not an issue). However, for faster-moving ground objects, the exoclutter GMTI method will be needed. Consider an operating environment where we can expect both slow and fast moving objects. In this scenario, we may have to run both exoclutter and endoclutter GMTI algorithms. However, PRF requirements for these two methods are different (exoclutter GMTI will require a higher PRF than endoclutter GMTI). Hence, one possible strategy would be to design a radar system to transmit some pulses with high PRF (to detect fast moving targets) and then transmit some pulses with low PRF to detect slow moving target and for SAR image formation. Our proposed approach implements this strategy. Further, our approach can provide additional capabilities such as efficient bandwidth utilization for SAR pulses (higher bandwidth) and GMTI pulses (lower bandwidth).

The merits of using diverse waveforms in pulse-Doppler radar has been studied in the past [10]. Bell and Monrocq [36] outlined a multiplexed-waveform Doppler filter bank concept for diverse waveforms. Majumder, Bell, and Rangaswamy [37] presented LFM-based Doppler tolerant, orthogonal waveform design. Among other papers, these papers motivated our approach to develop a joint GMTI and SAR signal processing architecture.

6.3 Multiplexed Waveform Pulse Doppler Processor

Many radar systems are designed with a single type of transmit waveform. For this reason, a single matched filter is built into the receiver to be matched with the transmit signal. However, when diverse waveforms to be transmitted, the matched filter at the receiver has to be matched with each of the different types of waveforms to provide maximum output. A concept for processing diverse waveforms for delay-Doppler measurement and imaging using a pulse-Doppler processor has been developed by Bell and Monrocq [36]. The authors named this processor the Multiplexed Waveform Pulse-Doppler Processor (MWPDP). We incorporate this processing concept for joint SAR and GMTI processing since we also proposed diverse, orthogonal waveforms for our research. In this section, we highlight the basic constructs of the MWPDP as presented in [36].

First, we will present structure of a simple pulse-Doppler processor that uses identical pulses. This processor will guide us developing a more complex pulse-Doppler processor that uses diverse waveforms.

Consider a pulse train made up of M identical pulses, whose complex baseband is represented by

$$s(t) = \sum_{j=1}^{M} a_j p(t - [j-1]\Delta),$$

where $p(t)$ is the pulse that has been repeatedly transmitted at Δ, interval and a_j is the complex amplitude of each pulse.

In the presence of Gaussian noise with power spectral density $S_{nn}(f)$, it can be shown that matched filter $\tilde{H}_M(f)$ for the pulse train with output sample time $T = M\Delta$ is

$$\tilde{H}_M(f) = \frac{\sum_{j=1}^{M} a_j^* P^*(f) e^{i2\pi f(j-1)\Delta}}{S_{nn}(f)} . e^{-j\pi f M\Delta} = H(f) \sum_{j=1}^{M} a_j^* e^{-i2\pi f(M-j)\Delta}$$

where $H(f) = \frac{P^*(f)}{S_{nn}(f)} e^{-i2\pi f\Delta}$ is the matched filter for a single pulse $p(t)$ yielding the maximum signal-to-noise-ratio when sampled at $t_s = \Delta$. In Figure 6.1, the top image is a block diagram of the pulse train matched filter. It is made up of a matched filter matched to the individual pulse shape.

The output of this matched filter is sampled at the pulse repetition interval with a delay offset corresponding to the particular range cell of interest. The samples are then multiplied by the conjugates of the complex modulation coefficients a_j and coherently summed. Finally, at time $T = M\Delta$ (*i.e.*after all pulses have been processed and summed) the output of the accumulator is sampled. This is the matched filter output for the entire pulse train which can now be processed using a threshold test or more sophisticated detection processing (e.g., Constant False Alarm Rate processing).

When narrowband signals (*i.e.*, for $p(t)$ whose bandwidth is small compared to the radar carrier frequency) are used, one of the most common forms of target induced modulation that is reflected in the a_j is a Doppler frequency shift. For for a Doppler frequency f_d, the coefficients a_j can be represented as

$$a_j = e^{i2\pi f_d j\Delta}$$

The successive phase shift from pulse to pulse corresponds to a phasor rotation of $2\pi f_d\Delta$. Multiplication by a_j^* performs a rotation in the opposite direction, resulting in the matched filter for the Doppler shifted pulse train if f_d is known. In most pulse-Doppler radar systems, processing consists of taking the M samples corresponding to the delay cell being processed and taking the M-point DFT of the sample sequence. This efficiently generates a bank of matched filters corresponding to M-matched filters for Doppler frequencies uniformly distributed over the $1/\Delta$-Hz unambiguous Doppler frequency interval. In Figure 6.1, the bottom image is the block diagram of the pulse-Doppler processor for a coherent pulse train of M identical pulses.

Now consider we have M different pulses represented by a pulse train

$$s(t) = \sum_{j=1}^{M} a_j p_j(t - [j-1]\Delta)$$

where $p_1(t)$, $p_2(t), ..., p_M(t)$ are diverse pulses, a_j is the complex amplitude of the pulses, and Δ is the pulse repetition interval of the pulse train.

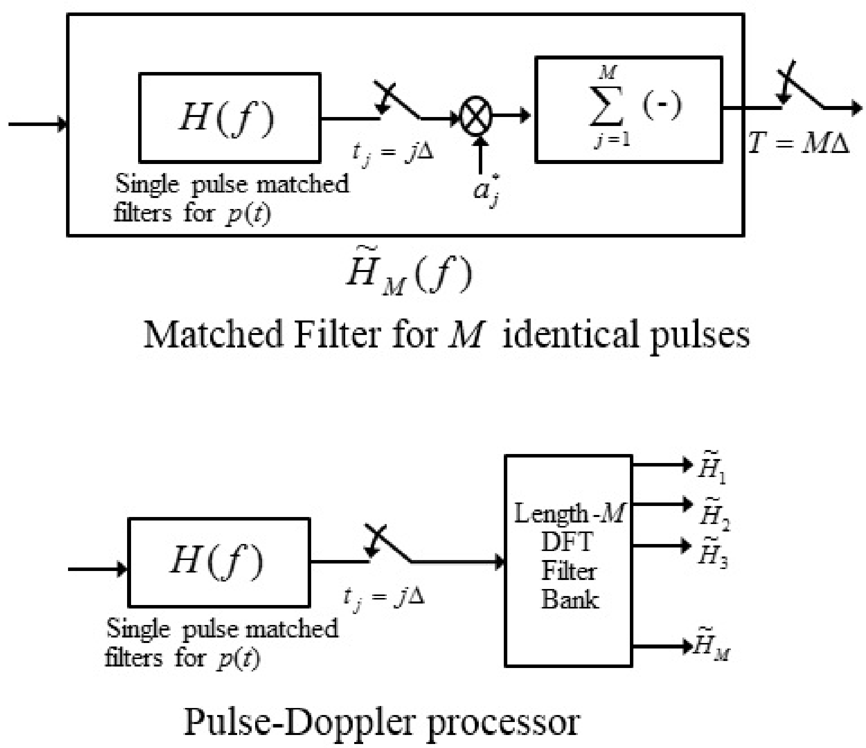

Fig. 6.1. Matched filter and pulse-Doppler processor for M identical pulses

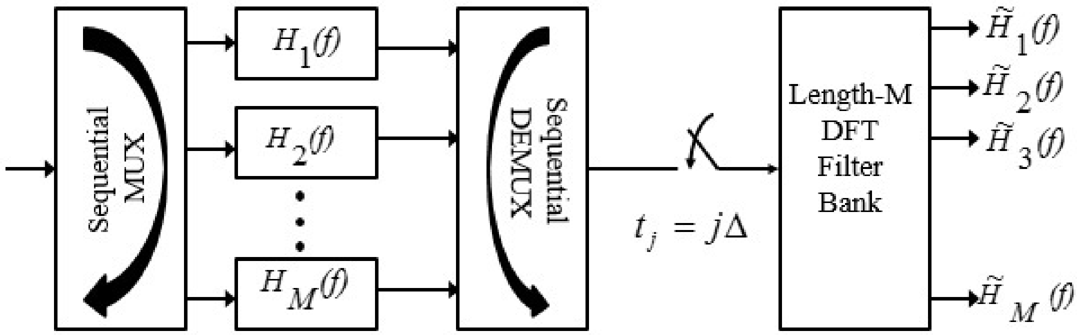

Fig. 6.2. Multiplexed Waveform Pulse-Doppler Processor (MWPDP) for a coherent pulse train of M different pulses

In the Multiplexed Waveform Pulse-Doppler Processor (MWPDP) concept, the front end matched filters are switched in and out in a synchronous manner, cycling through each of the pulse filters sequentially and their outputs before computing the Discrete Fourier Transform (DFT). Figure 6.2 shows a block diagram of the MWPDP processor. As discussed in the paper [36], the interesting thing about Multiplexed Waveform Pulse-Doppler Processor is that the sampled output for a target located in a range cell under test and having a Doppler frequency corresponding exactly to one of the frequencies in the Doppler filter bank is identical to that for the complete matched filter for the diversity pulse train, but the overall delayDoppler response does not have the cross terms present in the ambiguity function of the diversity pulse train. There is a significant cost, however. The resulting Doppler filter band is a time-varying Doppler filter bank.

6.4 Our Approach For Joint GMTI and SAR Processing

We will assume that the ground scene has both fast and slow moving targets. Hence, we will require a high PRF rate for exoclutter GMTI (i.e. to detect the fast moving target from its Doppler) and low PRF rate for SAR imaging and endoclutter GMTI. We will assume that we have two different transmit waveforms (SAR and Exoclutter GMTI) encoded with orthogonal codes. We will design the endoclutter GMTI/SAR waveforms to provide higher bandwidth than the exoclutter waveforms. Endoclutter GMTI/SAR pulses are coded with code C and exoclutter GMTI pulses are coded with code D. We will separate the SAR pulses by despreading it with the code C. More specifically, if a transmit pulse was coded with C, despreading with C will provide the highest auto-ambiguity response; but despreading with D will provide low cross-ambiguity response. In this manner, we can separate the SAR/endoclutter pulses from exoclutter pulses. We used the *Multiplexed Matched Filter* to separate SAR and exoclutter GMTI pulses. Figure 6.3 illustrates our notional joint GMTI and SAR processing concept.

6.4.1 Endoclutter GMTI and SAR Image Processing

Figure 6.5 shows an algorithmic flow diagram for SAR imaging and endoclutter GMTI. For this type of GMTI [38] [39] [40] and SAR imaging, we will assume that a PRF rate of 1500 Hz is too high to detect slow moving targets and will cause unacceptable range ambiguity. Hence, we will have to set the PRF rate for SAR pulses to an appropriate level. In our example, we use a PRF rate of 300 Hz for SAR pulse (pulse/signal 1). To detect a slow moving target, we form two SAR images from two different receivers that are displaced 0.3 meter apart (Displaced Phase Center Antenna, DPCA). Then perform coherent changed detection to detect the moving target. Figure 6.4 shows data recording for SAR imaging and endoclutter GMTI.

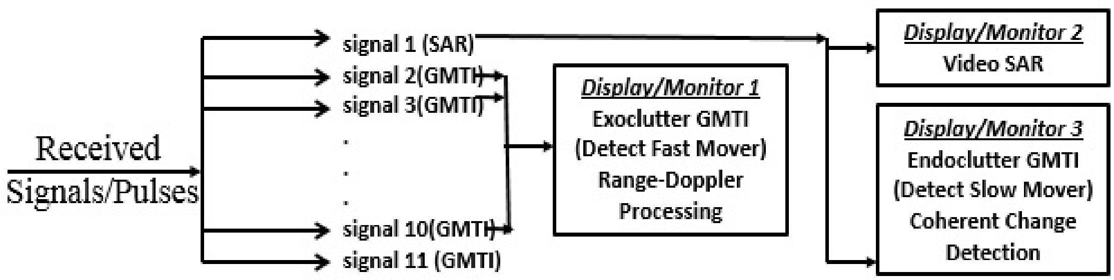

Fig. 6.3. Joint GMTI and SAR processing concept. We will transmit a group of 11 pulses at a time and repeat. Transmit pulse 1 is SAR pulse and coded with C. This waveform provides bandwidth of 600 MHz for high resolution SAR images and coherent change detection for endoclutter GMTI (to detect slow moving targets). PRF rate for SAR pulse is 300Hz. Transmit pulses 2-11 are exoclutter GMTI pulses and coded with D. These waveforms provide bandwidth of 200 MHz and PRF for these pulses is 1500Hz to detect the fast moving targets using Doppler

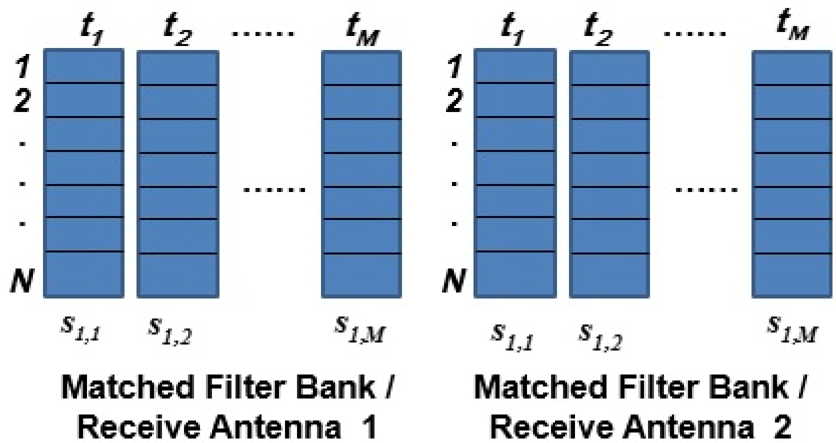

Fig. 6.4. Phase history data recording for endoclutter GMTI algorithm and SAR processing. $s_{1,1}$ is pulse 1 (SAR pulse) at time t_1; similarly, $s_{1,M}$ is pulse 1 at time t_M. We will perform DPCA based coherent change detection to detect the slow moving targets. Hence, we will record phase history in two receive antennas separated at 0.3 meter apart.

6.4.2 Exoclutter GMTI Processing

Figure 6.6 shows an algorithmic flow diagram for exoclutter GMTI. We will assume that a PRF rate of 1500 Hz will be sufficient for exoclutter GMTI. Hence, transmit pulses s_2 through s_{11} were sent at the PRF rate of 1500Hz. Consider a coherent processing interval (CPI) consists of 100 pulses. These 100 pulses can be obtained from 10 repetitions of 11 diverse, orthogonal waveforms. We have designated pulse number 1 (with high bandwidth) for SAR imaging. At the receiver, we will have a multiplexed matched filter to separate 10 (pulses 2 to 11) GMTI pulses and repeat it 10 times to accumulate 100 pulses for a coherent processing interva (CPI). Finally, we apply FFT to develop a range-Doppler map of the moving object. Note that we can use all pulses (s_1 through s_{11}) for exoclutter GMTI to avoid potential issues of coherently combining several blocks of pulses with omitted pulses among them in a CPI.

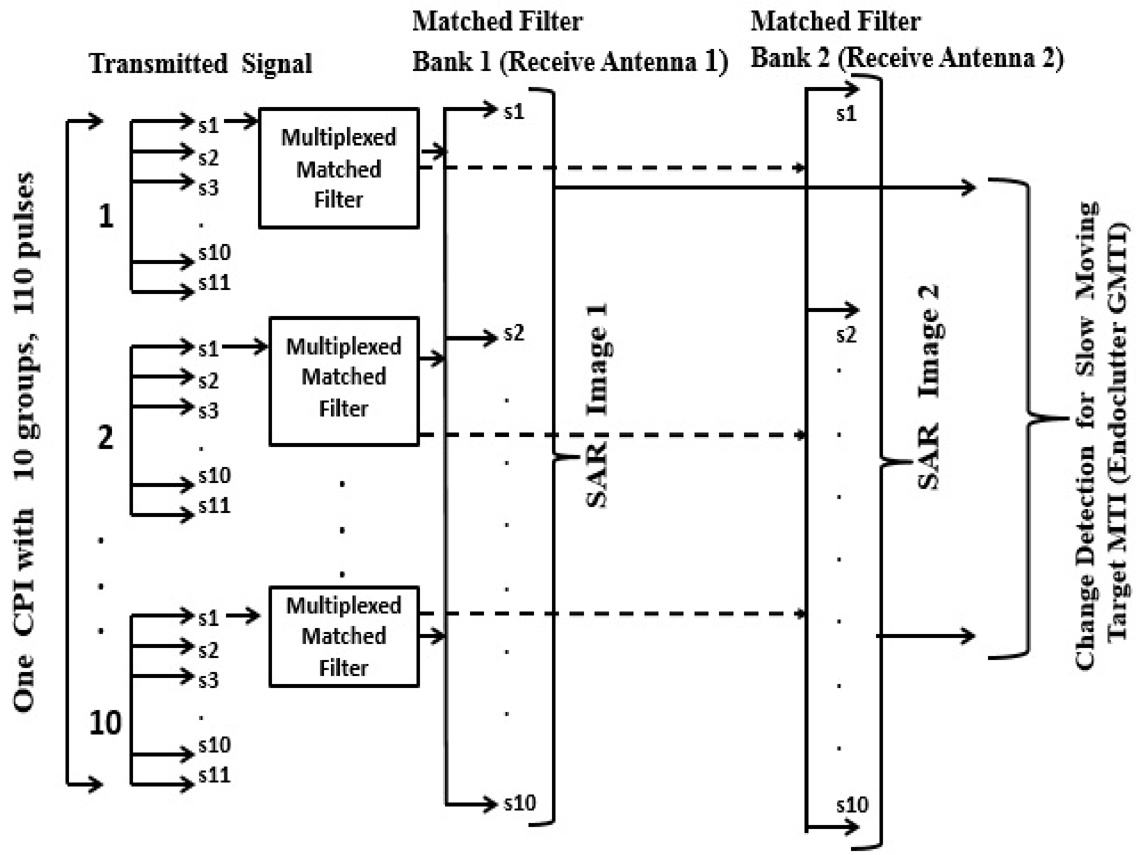

Fig. 6.5. Endoclutter GMTI algorithm and SAR image processing architecture. Out of 110 (10 repititions of 11 pulses) diverse, orthogonal waveforms for a CPI, we can extract 10 pulses (pulse 1 out of 11 pulses) using a multiples matched filter bank. These pulses (phase history data) can be recorded into two receivers at 0.3 meter apart (DPCA). Then form two SAR images from these two receivers and apply coherent change detection to detect the slow moving target

6.5 Results

Based on our discussion on joint GMTI and SAR processing scheme, we develop scenarios to detect slow and fast moving targets simultaneously from an interrogated scene. Detecting slow moving targets (i.e. endoclutter targets) is a complex problem. Space-time adaptive processing and coherent change detection (CCD) are often

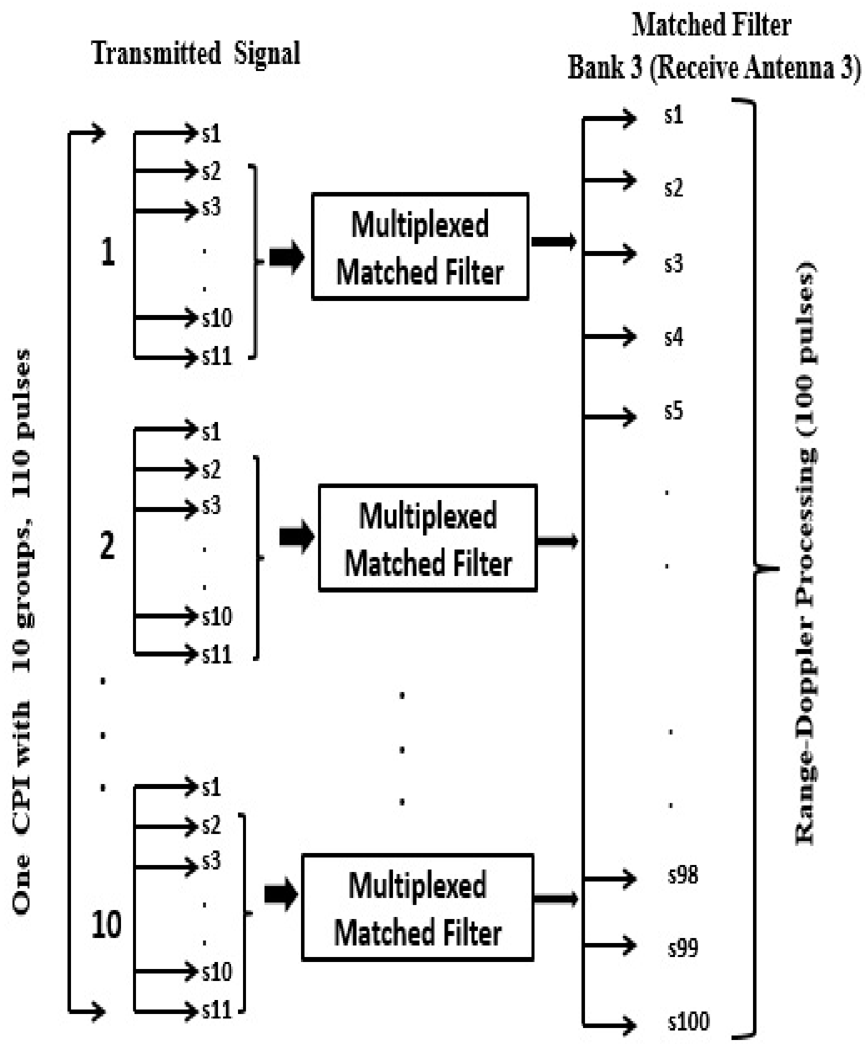

Fig. 6.6. Exoclutter GMTI algorithm concept. Out of 110 (10 repititions of 11 pulses) diverse, orthogonal waveforms for a CPI, we extract 100 pulses (10 repititions of pulses 2-11) at the receiver. Then apply range-Doppler processing.

used to detect slow moving targets. We have used DPCA-based (displaced phased center antenna) coherent changed detection to detect the slow moving targets. After detecting a moving target, the smeared signature of this target can be focused using different algorithms [32], [39], [41], [42].

Table 6.1
Experimental parameters used to model and detect slow moving target (endoclutter GMTI) phenomenology in a SAR system.

Parameters	Values
PRF	300 Hz
Bandwidth	600MHz
Radar Platform Velocity	75 m/sec
Distance Between Two Receivers	0.3 m
Carrier Frequency	16.9 GHz
Target Speed	5 m/sec

Table 6.2
Experimental parameters used to detect fast moving target (Exoclutter GMTI).

Parameters	Values
PRF	1500 Hz
Bandwidth	200MHz
Radar Platform Velocity	75 m/sec
Carrier Frequency	16.9 GHz

6.5.1 Endoclutter GMTI and SAR Processing Results

Table 6.1 presents key parameters used to develop signal processing algorithm for SAR image processing and endoclutter GMTI. The details of modeling targets (both stationary and moving) in synthetic aperture radar system can be found in different books [27] [29] [43]. In this simulation, we have used moving target SAR signal processing theory presented in chapter 8 of the monograph by Soumekh [27]. In our first scenario, we had four stationary targets and one moving target in the scene. We generated SAR phase history data based on Table 6.1 parameters and recorded into two receive antennas separated by 0.3 meter. Two SAR images are generated using backprojection algorithm (from two receive antennas). Because the receive antennas were physically separated, the phase of the moving target signature will be slightly different, but the stationary target's phase will remain constant. Hence, when we perform coherent change detection, the moving targets' signatures will be present, but the stationary targets' signatures will be cancelled. Notice that, non-coherent change detection (amplitude only change detection) will not reveal this phenomenology. Fig-

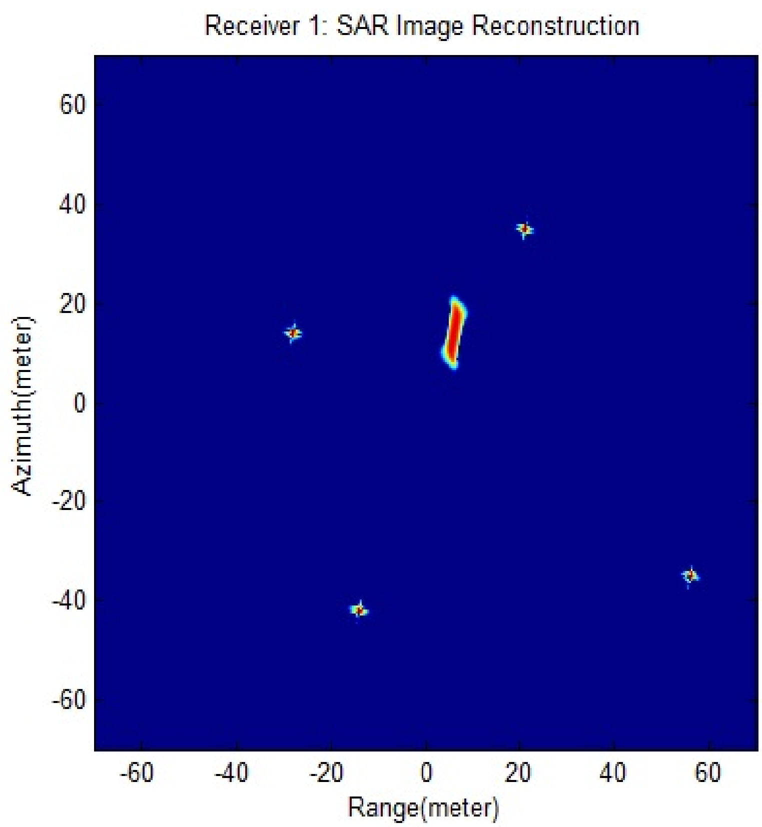

Fig. 6.7. SAR image formation from matched filter bank 1 (receive antenna 1). In this scenario, interrogated scene had 4 stationary point targets and one moving target. Moving target's signature smears in SAR imagery due to it's velocity

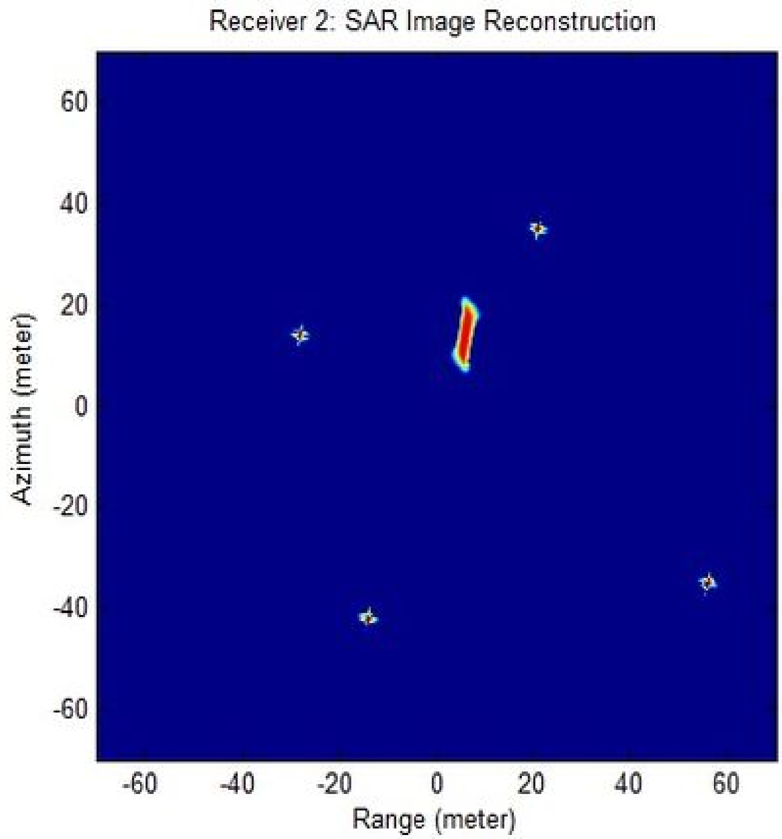

Fig. 6.8. SAR image formation from matched filter bank 2 (receive antenna 2). In this scenario, interrogated scene had 4 stationary point targets and one moving target. Moving target's signature smears in SAR imagery due to it's velocity

ures 6.7 and 6.8 show two SAR images constructed from two receive antennas' phase history data. Figure 6.9 shows detected slow moving target of the interrogated scene. In our second scenario, we have three stationary targets and two moving targets in the scene. Once again, we generated SAR phase history data based on Table 6.1 parameters and recorded it with two receive antennas separated by 0.3 meter. Then two SAR images were generated using the backprojection algorithm (from the two receive antennas). Figures 6.10 and 6.11 show two SAR images constructed from two

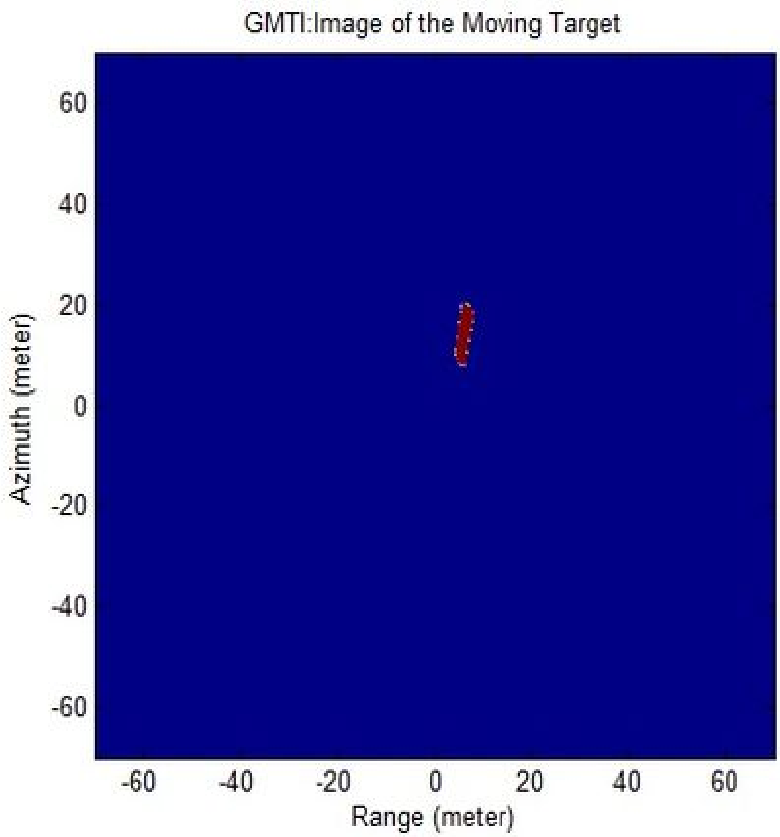

Fig. 6.9. Coherent change detection based on displaced phase center antenna (DPCA) has been used to detect the slow moving target from two SAR images presenetd in Figure 6.7 and Figure 6.8

receive antennas' phase history data. Figure 6.12 shows detected slow moving targets of the interrogated scene.

6.5.2 Exoclutter GMTI Processing Results

Table 6.2 presents key parameters used to develop signal processing algorithm for fast moving target detection (exoclutter GMTI). As mentioned earlier, to detect fast moving targets based on Doppler, a high PRF rate is needed to prevent Doppler aliasing and the resulting Doppler ambiguity. Also, a lower bandwidth is sufficient for

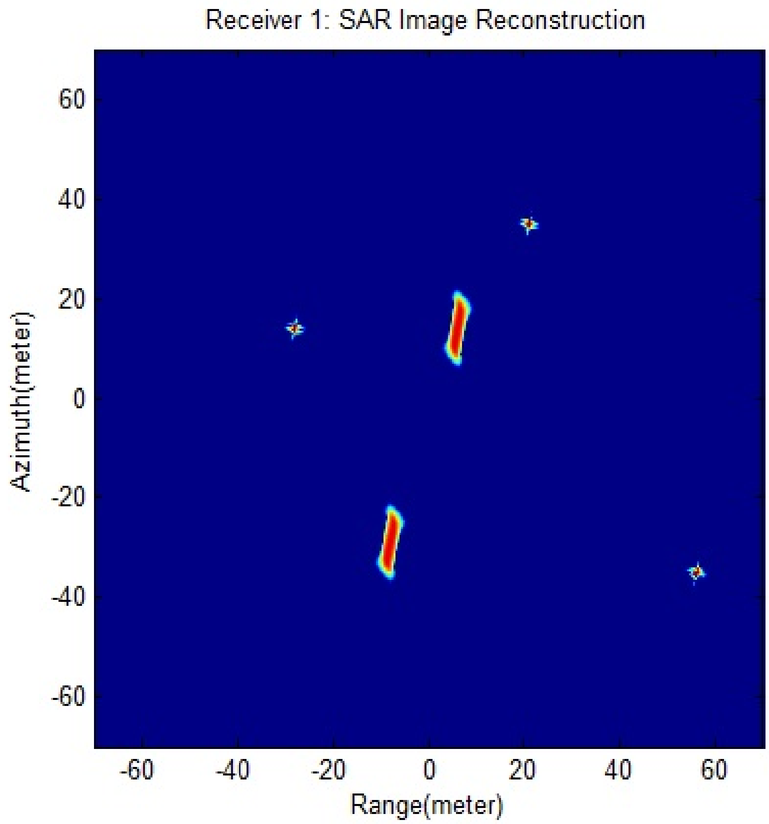

Fig. 6.10. SAR image formation from matched filter bank 1 (receive antenna 1). In this scenario, interrogated scene had 3 stationary point targets and two moving targets. Moving targets' signatures smear in SAR imagery due to their velocity.

exoclutter GMTI. Hence, PRF rate is set to 1500Hz and bandwidth is set to 200MHz to detect the fast moving targets. In our simulation, there were three moving targets in the scene. Two targets have the same velocity but are situated in different locations; one target has different velocity than the other two. Figure 6.13 shows range-Doppler map of these three moving targets.

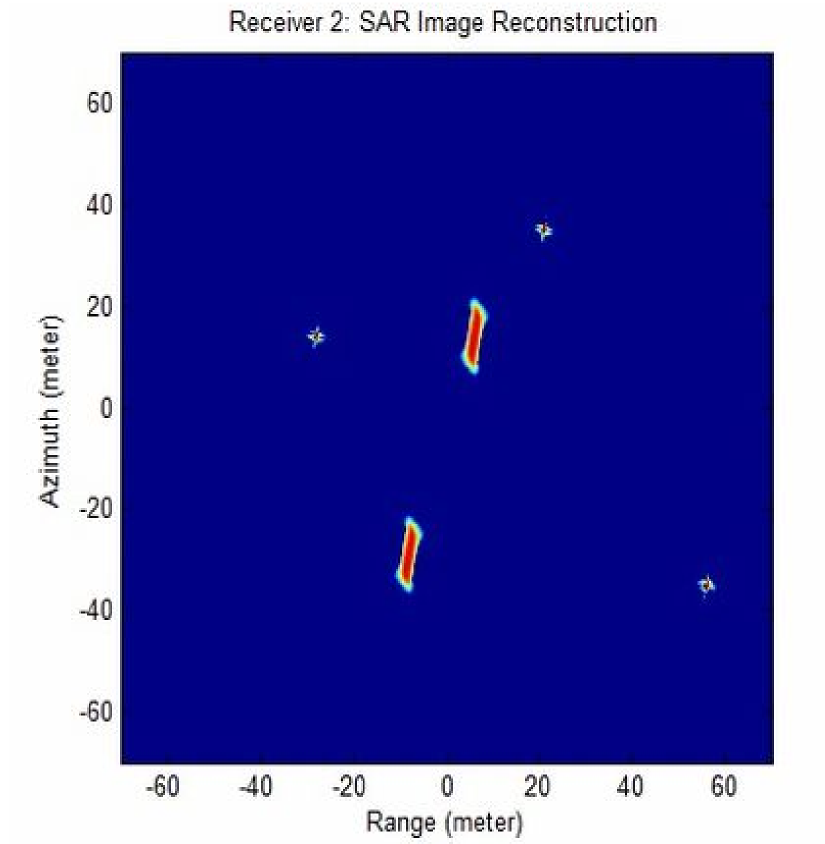

Fig. 6.11. SAR image formation from matched filter bank 2 (receive antenna 2). In this scenario, interrogated scene had 3 stationary point targets and two moving targets.

6.6 Focused Image of a Moving Target

As discussed earlier and in Chapter 5, the signatures of moving targets are smeared and dislocate from their true locations. In order to form a focused image of a moving target, its velocity must be estimated and its phase must be corrected prior to applying the imaging algorithm. We have used subaperture based method (outlined in Chapter 5) to form focused image of a moving target. In Figure 6.14, we see that the ground scene has 4 stationary targets and the images of these targets are focused. No smearing occured. Figure 6.15 shows a smeared, dislocated moving target image

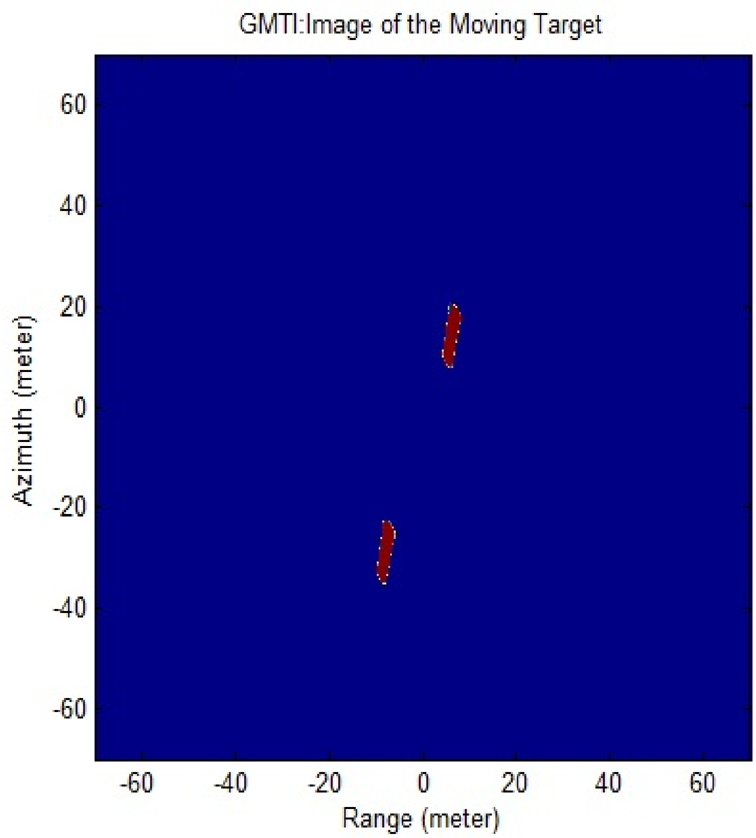

Fig. 6.12. Coherent change detection based on displaced phase center antenna (DPCA) has been used to detect the slow moving targets from two SAR images presenetd in Figure 6.10 and Figure 6.11

(its true location was at the scene center). This is due to the fact that a stationary target image formation algorithm is used to form SAR image of a moving target. Figure. 6.16) shows that the moving target image is focused and properly located at the scene center when moving target focusing algorithm is used. Stationary targets shown in Fig. 6.14 become defocused if the focusing algorithm is applied to these targets. This is shown in Figure 6.17.

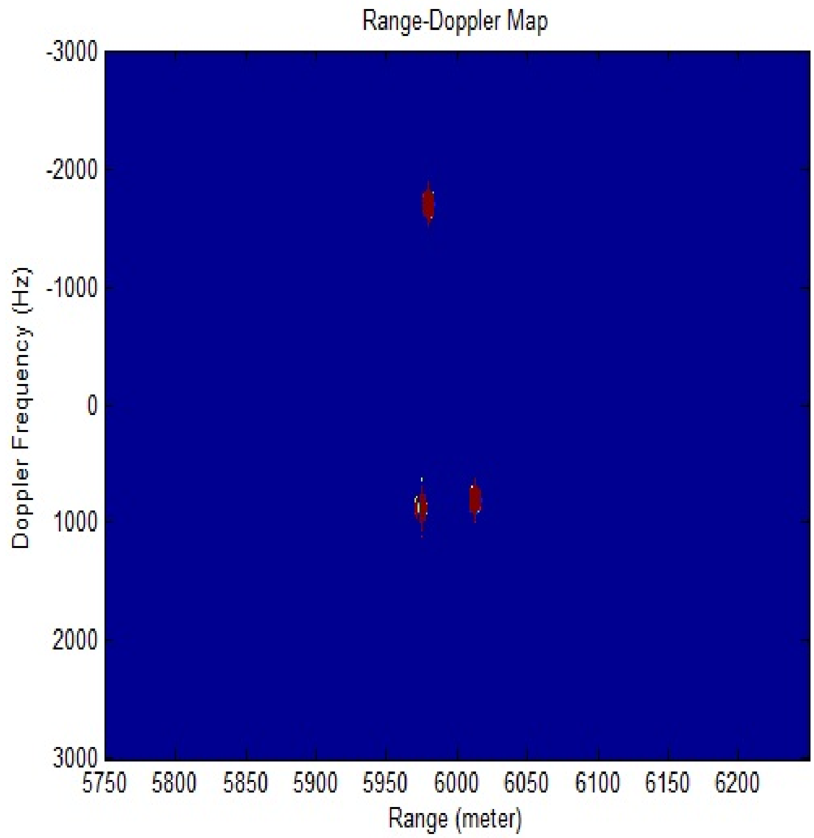

Fig. 6.13. Range-Doppler processing to detect fast moving targets. The interrogated scene has three moving targets. Two targets have same velocity; hence they generated same Doppler frequency.

6.7 Discussion

The signal processing architecture for joint GMTI and SAR processing presented here assumes that transmit signals (endoclutter GMTI/SAR pulses and exoclutter GMTI pulses) are orthogonal and the system can separate them at the receiver (applying multiplex matched filter bank concept). In addition, PRF rate for exoclutter GMTI pulses (1500Hz) are much higher than the endoclutter GMTI / SAR pulses (300Hz) and the system is able to maintain it. Further, endoclutter GMTI pulses were designed to provide higher bandwidth (600MHz) than the exoclutter GMTI pulses

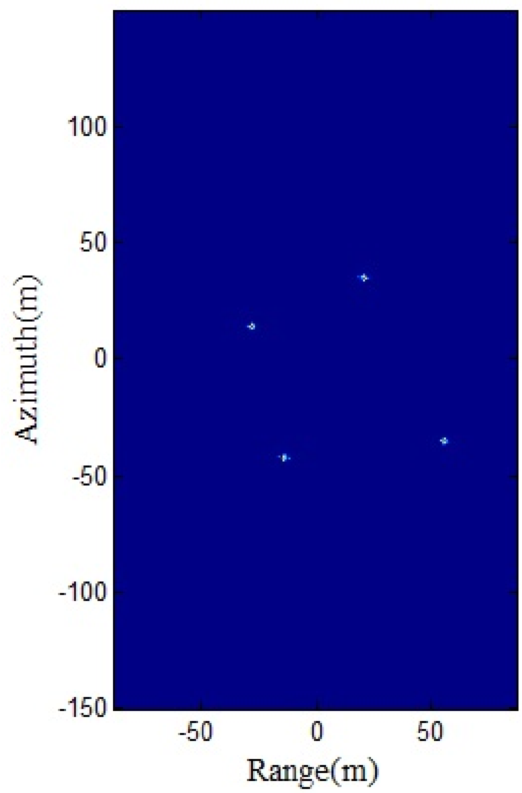

Fig. 6.14. The ground scene has 4 stationary targets and these targets are focused. No smearing occured

(200MHz). Under these assumptions, radar system can process the receive signals to produce three different outputs simultaneously: (1) Video SAR output, (2) Coherent change detection output for the slow moving targets detection (endoclutter GMTI) using low PRF SAR pulses, and (3) range-Doppler processing output for the fast moving target (exoclutter GMTI) using high PRF pulses.

6.8 Conclusion

In this chapter, we established a signal processing framework to accomplish joint GMTI and SAR processing. Our signal processing algorithm reduces complexities

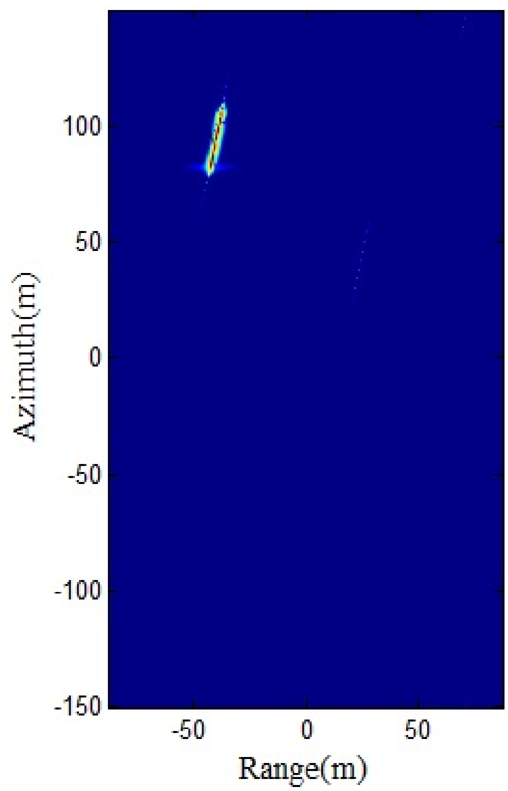

Fig. 6.15. At the center of the ground scene there was a moving target. It's image has been smeared and dislocated

associated with reconfiguring a radar system for the GMTI mode or SAR mode. Our approach allows efficient bandwidth utilization by employing appropriate bandwidths for GMTI pulses and SAR image formation pulses. Further, our approach provides a solution to range ambiguity issue associated with high PRF operation by using orthogonal waveforms to separate individual waveforms at the receiver.

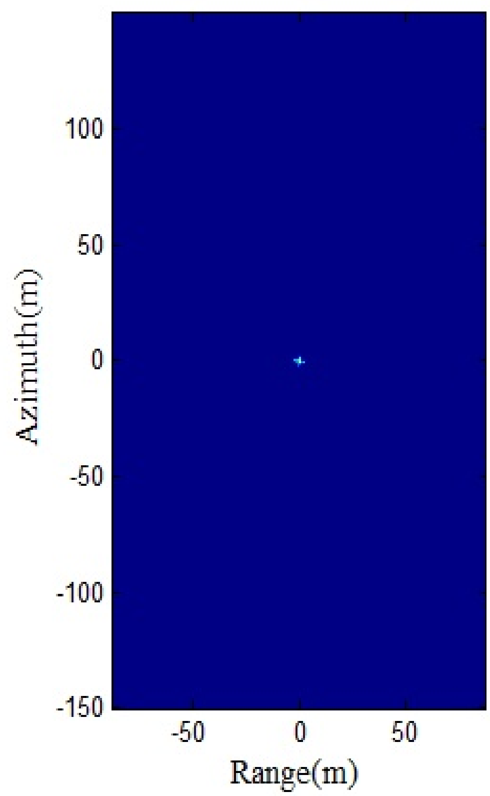

Fig. 6.16. After moving target focusing algorithm has been applied, the target's (in Fig. 6.15) image is now focused and localized. This was done by estimating velocity of the moving target and then correcting the phase

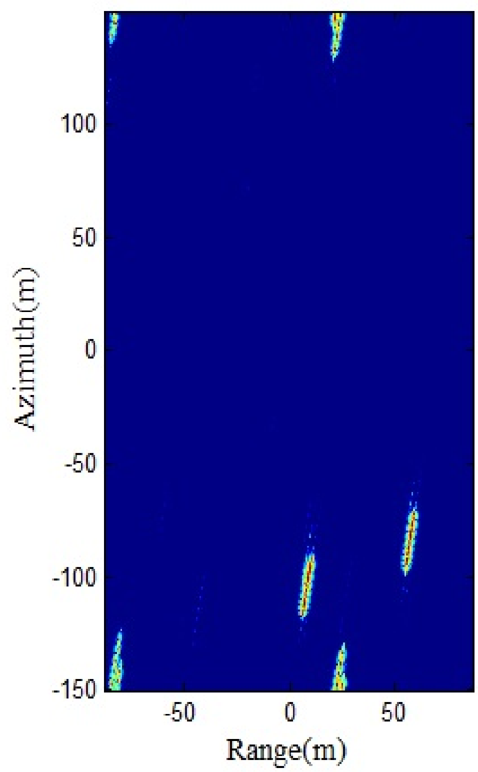

Fig. 6.17. Stationary targets (in Fig. 6.14) become defocused if their phases are corrected by applying moving target's velocity

7. SUMMARY

In this dissertation research, we have investigated two open problems in radar signal processing that have gained significant interest. First, we designed a set of approximately orthogonal (on both transmit and receive), Doppler tolerant waveforms for waveform agile radar (e.g. MIMO radar) application. Secondly, we integrated these waveforms for solving a radar signal processing problem, which is joint processing of SAR and ground moving target indication processing .

In Chapter 3, we presented a solution to our first research problem i.e. design a set of orthogonal, Doppler tolerant waveforms. Our solution incorporated direct sequence spread spectrum (DSSS) coding techniques on linear frequency modulated (LFM) signals. We call this *Spread Spectrum Coded LFM (SSCL)* signal. LFM waveforms satisfy Doppler tolerance criteria and DSSS allows these waveforms to be made orthogonal during transmission. From analytical expressions of the waveforms we have designed and from simulation results, we found that: (a) cross-ambiguity function of two LFM spread spectrum coded waveforms is small for all delays and Dopplers (i.e. transmit and receive signals satisfy the orthogonality constraint), and (b) The length of the spread spectrum code determines the amount of interference suppression (i.e. complete orthogonal or near orthogonal of the received signals).

We presented high resolution imaging capability and design consideration of our proposed waveforms in Chapter 4. Our waveforms allow processing the same received signal in two different ways; one method can provide multiple noninterfering measurements with different ambiguity responses at LFM signal resolutions and the other method can provide ultra-high resolution. This is a unique capability of our proposed waveforms. From the code length property of our waveforms, we found that the length of the codes such as 8, 16, 32 or 512 determine the degree of orthogonality of the received signal. Furthermore, the length of the codes also determine bandwidth expansion of the SSCL signaling and hence increased range resolution (of the coded signal). In practical applications, a bandwidth of more than one gigahertz increases complexity to the radar system, and hence using large code can be unrealistic. To address this issue, we investigated biorthogonal codes. Biorthogonal codes can be used to reduce bandwidth (thus reducing the code length) by a factor of two when code length is large.

An application of our proposed orthogonal waveforms is joint processing of SAR and ground moving target indication (GMTI). Hence, in Chapter 5, we briefly described synthetic aperture radar (SAR) signal processing theory. We illustrated SAR imaging geometry and terminology. We pointed out that moving targets signatures in SAR images smears and shifts to different locations. Therefore, imaging of moving targets in SAR requires additional processing, which involves velocity estimation and modifying the phases of moving targets' signal before applying image processing algorithms. We outlined subaperture based processing algorithm to form focused images of moving targets.

Finally, in Chapter 6, we presented a novel approach for joint SAR and GMTI processing. One important parameter for both SAR imaging and GMTI processing is the pulse repetition frequency (PRF). High PRF rate is essential for detecting fast moving targets (i.e., exoclutter GMTI) using range-Doppler processing. However, low PRF rate is necessary for SAR imaging (also for slow moving target detection/endoclutter GMTI) because a high PRF rate introduces range ambiguity. Hence, to accomplish these two tasks simultaneously, a radar system has to operate either in SAR imaging mode (using low PRF rate) or GMTI mode (using high PRF rate). Then the research statement becomes is there an approach to accomplish both SAR and GMTI processing in a single mode? Our proposed orthogonal waveforms provide a solution to this problem. We have shown that by combining diverse, orthogonal waveforms and introducing corresponding processing techniques, SAR and GMTI processing can be accomplished simultaneously. Our waveforms' orthogonality allows the flexibility to select either the high PRF waveforms or the low PRF waveforms or both depending on application. For the exoclutter GMTI problem, the necessary high-PRF pulse train can be used to achieve unaliased, unambiguous measurement for detecting fast moving objects. For SAR imaging and the endoclutter GMTI problem, we can select the low PRF pulses. Our signal processing concept achieves the following benefits: (1) accomplish GMTI and SAR processing concurrently by eliminating the complexities associated with reconfiguring a radar system, (2) use bandwidth more efficiently by employing appropriate bandwidth for exoclutter GMTI pulses and SAR image formation pulses, and (3) reduce range ambiguity issue associated with high PRF operation.

8. FUTURE RESEARCH

In the orthogonal MIMO radar concept, both transmit and receive waveforms should be orthogonal, and radar systems' performance (such as detection) should be analyzed based on this assumption. However, most of the current MIMO radar research is not based on this assumption. Some researchers define MIMO radar as transmitting orthogonal waveforms. However, received waveforms are non-orthogonal and hence optimize the received signal for performance. Other researchers define MIMO radar as optimizing both transmit and receive waveforms (to maximize detection) while transmitters and receivers are situated at different locations.

In a traditional phased-array radar system, beamforming allows radiating energy to be focused in specific target areas to maximize SNR and target detection. By contrast, in MIMO radar, transmit beamforming is not done. As a result, there is $\sqrt{M}$ fold reduction in transmit power loss and detection can be degraded (M is number of transmitters). Some researchers claim that in the orthogonal MIMO radar concept, this power loss can be mitigated because M orthogonal transmissions can provide enough SNR to detect a target.

Nearly orthogonal waveforms (both transmit and receive) presented in this dissertation research open new research opportunities in the area of multiple-input multiple-output (MIMO) radar. One research project could be comparing target detection performance under orthogonal MIMO and traditional phased-array radar system when transmit beamforming is not performed. A second research project could be analyzing space-time adaptive processing (STAP) under orthogonal MIMO radar and compare it with phased-array radar system processing. Because of multi-look by multiple antenna elements at the same time, under the orthogonal MIMO radar construct, adaptive clutter cancellation could be faster than a traditional beamforming approach. A third research project could be verifying this claim.

LIST OF REFERENCES

LIST OF REFERENCES

[1] J. Li and P. Stoica, *MIMO Radar Signal Processing*. New York, NY: John Wiley and Sons, 1st ed., 2009.

[2] M. Greenspan, "MIMO radar signal processing of space time coded waveforms." IEEE Signal Processing Society Baltimore Chapter Meeting, May 2008.

[3] J. Guerci, *Cognitive Radar: The Knowledge-Aided Fully Adaptive Approach*. Boston, MA: Artech House, 1st ed., 2010.

[4] P. Woodward, *Probability and Information Theory With Applications to Radar*. NEW YORK, NY: McGRAW-HILL BOOK CO., INC, 1st ed., 1953.

[5] J.-C. Guey. and M. Bell, "Diversity waveform sets for delay-doppler imaging," *IEEE TRANSACTIONS ON INFORMATION THEORY*, vol. 44, July 1998.

[6] A. W. Rihaczek, *Principles of high-resolution radar*. New York, NY: McGraw-Hill, 1st ed., 1969.

[7] G. Curry, *Radar System Performance Modeling*. Norwood: Artech House, 1st ed., 2001.

[8] A. Nehorai, F. Gini, M. Greco, A. Papandreou-Suppappola, and M. Rangaswamy, "Introduction to the issue on adaptive waveform design for agile sensing and communication," *IEEE Journal of Selected Topics in Signal Processing*, vol. 1, June 2007.

[9] N. Levanon and E. Mozeson, *Radar Signals*. Harlow, England: Wiley-IEEE Press, 1st ed., 2004.

[10] C. Cook and M.Bernfeld, *Radar Signals: An Introduction to Theory and Application*. New York, NY: Academic Press, 1st ed., 1967.

[11] R. Calderbank, S. Howard, and B. Moran, "Waveform diversity in radar signal processing," *IEEE Signal Processing Magazine*, vol. 26, Jan 2009.

[12] J. J. M. de Wit, W. L. van Rossum, and A. de Jong, "Orthogonal waveforms for FMCW MIMO radar," in *Proceedings of IEEE Radar Conference*, Institute of Electrical and Electronics Engineers (IEEE), May 2011.

[13] S. R. J. Axelsson, "Suppressed ambiguity in range by phase-coded waveforms," in *Proceedings of the IEEE Geoscience and Remote Sensing*, Institute of Electrical and Electronics Engineers (IEEE), 2001.

[14] S. Searle and S. Howard, "Waveform design and processing for multichannel MIMO radar," in *Proceedings of IEEE Radar Conference*, Institute of Electrical and Electronics Engineers (IEEE), May 2009.

[15] C.-F. Chang and M. R. Bell, "Frequency-coded waveforms for enhanced delay-doppler resolutio," *IEEE TRANSACTIONS ON INFORMATION THEORY*, vol. 49, November 2003.

[16] S.D.Howard, A. R. Calderbank, and W. Moran, "A simple signal processing architecture for instantaneous radar polarimetry," *IEEE TRANSACTIONS ON INFORMATION THEORY*, vol. 53, April 2007.

[17] I. Gladkova, "Analysis of stepped-frequency pulse train design," *IEEE Transactions on Aerospace and Electronic Systems*, vol. 45, October 2009.

[18] M. Zoltowski, W. Moran, and et.al., "Unitary design of radar waveform diversity sets," in *Proceedings of Asilomar Conference*, 2008.

[19] S. Sen and A. Nehorai, "OFDM MIMO Radar for low-grazing angle tracking," in *Proceedings of Asilomar Conference*, 2009.

[20] C.-F. Chang and M. Bell, "Frequency division multiplexing technique for composite ambiguity function approximation," *Digital Signal Processing*, vol. 16, September 2006.

[21] D. K. S. Hengstler, "A novel chirp modulation spread spectrum technique for multiple access," in *Proceedings of the IEEE International Symposium on Spread Spectrum Techniques and Applications (ISSSTA 2002)*, vol. 1, Institute of Electrical and Electronics Engineers (IEEE), September 2002.

[22] J. Proakis and M. Salehi, *Communication Systems Engineering*. New Jersey, NJ: Prentice-Hall, Inc, 1st ed., 1994.

[23] M. Simon and J. Omura, *Spread Spectrum Communications*. Maryland, MD: Computer Science Press, 1st ed., 1985.

[24] B. Sklar, *Digital Communications: Fundamentals and Applications*. New Jersey, NJ: Prentice-Hall, Inc, 2nd ed., 2001.

[25] W.Chapman, S. Ranka, S. Sahni, M. Schmalz, U. Majumder, L. Moore, and B. Elton, "Parallel processing techniques for the processing of sar data on gpus," in *IEEE International Symposium on Signal Processing and Information Technology*, Institute of Electrical and Electronics Engineers (IEEE), 2011.

[26] J. C. Curlander and R. N. McDonough, *Synthetic Aperture Radar: Systems and Signal Processing*. New York, NY: John Wiley and Sons, 1991.

[27] M. Soumekh, *Synthetic Aperture Radar Signal Processing*. New York, NY: John Wiley and Sons, 2nd ed., 1999.

[28] V. Murthy, U. Pillai, and M. Davis, "Waveforms for simultaneous sar and gmti," in *Proceedings of IEEE Radar Conference*, Institute of Electrical and Electronics Engineers (IEEE), May 2012.

[29] M. Soumekh, *Fourier Array Imaging*. New Jersey, NJ: Prentice-Hall, Inc, 1st ed., 1994.

[30] M. Minardi and E. Zelnio, "Comparison of SAR based GMTI and standard GMTI in a dense target environment," in *Proc. SPIE 6237, Algorithms for Synthetic Aperture Radar Imagery XIII, 62370X*, The International Society for Optical Engineering (SPIE), May 2006.

[31] R. Perry, R. DiPietro, and R. Fante, "Sar imaging of moving targets," *IEEE Transactions on Aerospace and Electronic Systems*, vol. 35, January 1999.

[32] J. Fienup, "Detection of moving targets in sar imagery by focusing," *IEEE Transactions on Aerospace and Electronic Systems*, vol. 37, July 2001.

[33] M. Pettersson, "Detection of moving targets in wideband sar," *IEEE Transactions on Aerospace and Electronic Systems*, vol. 40, July 2004.

[34] M. Soumekh, "Moving target detection and imaging using x-band along-track monopulse sar," *IEEE Transactions on Aerospace and Electronic Systems*, vol. 38, January 2002.

[35] M. Davis, R. Kapfer, and R. Bozek, "Common waveform for simultaneous sar and gmti," in *Proceedings of IEEE Radar Conference*, Institute of Electrical and Electronics Engineers (IEEE), May 2011.

[36] M.R.Bell and S.Monrocq., "Diversity waveform signal processing for delay-doppler measurement and imaging," *Digital Signal Processing*, vol. 12, no. 2, 2002.

[37] U. Majumder, M. R. Bell, and M. Rangaswamy, "A novel approach for designing diversity radar waveforms that are orthogonal on both transmit and receive," in *Proceedings of IEEE Radar Conference*, Institute of Electrical and Electronics Engineers (IEEE), May 2013.

[38] U. Majumder, M. Soumekh, M. Minardi, and J. Kirk., "Spatially-varying calibration of along-track monopulse synthetic aperture radar imagery for ground moving target indication and tracking," in *Proceedings of IEEE Radar Conference*, Institute of Electrical and Electronics Engineers (IEEE), May 2010.

[39] J. Goldstein, M.L.Picciolo, M. Rangaswamy, and J. Griesbach, "Detection of dismounts uisng synthetic aperture radar," in *Proceedings of IEEE Radar Conference*, Institute of Electrical and Electronics Engineers (IEEE), May 2010.

[40] U. Majumder, M. Soumekh, M. Minardi, and J. Kirk, "Synthetic aperture radar moving target indication processing of along-track monopulse nonlinear gotcha data," in *Proceedings of IEEE Radar Conference*, Institute of Electrical and Electronics Engineers (IEEE), May 2009.

[41] J.Jao, "Theory of synthetic aperture radar imaging of a moving target," *IEEE Geoscience and Remote Sensing*, vol. 39, September 2001.

[42] C. Jakowatz, D. Wahl, and P. Eichel, "Refocus of constant velocity moving targets in synthetic aperture radar imagery," in *Proc. SPIE Defense and Security Conference, Algorithms for Synthetic Aperture Radar Imagery V*, The International Society for Optical Engineering (SPIE), April 1996.

[43] M. Curlander and R. McDonough, *Synthetic Aperture Radar: Systems and Signal Processing.* New York, NY: John Wiley and Sons, 1991.

VITA

VITA

Uttam K. Majumder received Bachelor of Science (BS) degree from the Department of Computer Science, The City College of New York (CCNY) in June 2003 graduating in Summa Cum Laude. He then earned an MS degree from the Department of Electrical Engineering, The Air Force Institute of Technology in March 2007. He also earned an MBA degree from Wright State University in June 2009. He is currently pursuing a Ph.D degree in Electrical Engineering from Purdue University, West Lafayette, Indiana. He has been working with the Air Force Research Laboratory (AFRL) since August 2003. His responsibilities include conducting research on Synthetic Aperture Radar (SAR) algorithm development for surveillance applications, high performance computing for SAR based automatic target recognition (ATR), and project management. He is also an adjunct faculty at The Wright State University, Dayton, Ohio. He developed a graduate level course on SAR Signal and Image Processing and teaches this course. Mr. Majumder published more than 25 technical papers in various professional conferences. His current research interests include radar signal processing, digital image processing, wide-angle SAR imaging, inverse problems and sparse aperture imaging, automatic target recognition, moving target detection, tracking, and geolocation, high performance computing, and innovation and change in project management.